Aus der

Neurologischen Universitätsklinik Tübingen

Hertie Institut für klinische Hirnforschung

Abteilung Neurologie mit Schwerpunkt

Neurodegenerative Erkrankungen

CRISPR/Cas-based gene therapy in Adult-Onset Leukoencephalopathy with axonal spheroids and pigmented glia: designing the optimal guide RNA

Inaugural-Dissertation
zur Erlangung des Doktorgrades
der Medizin

der Medizinischen Fakultät
der Eberhard Karls Universität
zu Tübingen

vorgelegt von

Schmitz, Anne Sophie

2024

Dekan: Professor Dr. Bernd Pichler

1. Berichterstatter: Professor Dr. L. Schöls
2. Berichterstatter: Professor Dr. S. Liebau
3. Berichterstatter: Professorin Dr. K. Lohmann

Tag der Disputation: 28.03.2024

TABLE OF CONTENTS

INDEXES 5

1 INTRODUCTION 9

1.1 Adult-onset leukoencephalopathy with axonal spheroids and pigmented glia 9

1.1.1 Definition and clinical characteristics 9
1.1.2 Pathophysiology 10
1.1.3 Therapy 13

1.2 Genome editing 13

1.3 Disease modeling in induced pluripotent stem cells (iPSC) 17

1.4 Objective of the study 18

2 MATERIAL AND METHODS 20

2.1 Material 20

2.2 Methods 28

2.2.1 Methods Part I: Identification of efficient sgRNAs for knockout of human CSF1R 28
2.2.2 Methods Part II: Generation of homozygous and heterozygous CSF1R iPSC knockout lines 40

3 RESULTS 51

3.1 Testing of sgRNAs in THP-1 cells 51

3.1.1 SgRNA design 51
3.1.2 Selection of a CSF1R expressing cell line and optimization of CSF1R Western Blot 51
3.1.3 Transfection efficiency 53
3.1.4 CSF1R assessment on DNA level 54
3.1.5 CSF1R expression on protein level 59

3.2 Generation of *CSF1R* iPSC knockout lines 62

3.2.1 Cell culture 62
3.2.2 Clone selection 63
3.2.3 Off-target analysis 67
3.2.4 Stem cell characterization 67

4 DISCUSSION 76

4.1 Testing sgRNAs in the THP-1 cell line 76

4.1.1 Cell line selection and optimization of CSF1R Western Blot 76
4.1.2 Transfection efficiency 78
4.1.3 CSF1R assessment on DNA level 78
4.1.4 CSF1R expression on protein level 80

4.2 Establishment of *CSF1R* knockouts in iPSC **83**

4.2.1 Clone selection 83
4.2.2 Off-target analysis 83
4.2.3 Stem cell characterization 84
4.2.4 Summary of objectives and findings 85

5 SUMMARY **86**

6 BIBLIOGRAPHY **90**

7 STATEMENT OF ORIGINALITY **101**

8 PUBLICATIONS **102**

Indexes

Abbreviations

ALSP	adult-onset leukoencephalopathy with axonal spheroids and pigmented glia
AP	alkaline phosphatase
APS	ammonium persulfate
ATP	adenosine triphosphate
BCA	bicinchoninic acid
bp	basepair
Cas9	CRISPR-associated nuclease 9
cDNA	copy DNA
CFD	cutting frequency determination
CNS	central nervous system
CRISPR	clustered regularly interspaced palindromic repeats
crRNA	CRISPR RNA
CSF1	colony stimulating factor 1
CSF1R	colony stimulating factor 1 receptor
CT	computer-assisted tomography
DAPI	4',6-diamidino-2-phenylindole
DMEM-F12	Dulbecco's Modified Eagle Medium F-12
DNA	desoxyribonucleic acid
dNTP	deoxyribonucleoside triphosphate
DSB	double-strand break
DPBS	Dulbecco’s phosphate buffered saline
E8	essential 8
EB	embryoid body
ECL	enhanced chemiluminescence
EDTA	ethylenediaminetetraacetic acid
e.g.	exempli gratia, for example
eGFP	enhanced green fluorescent protein
ESC	embryonic stem cells

FACS	fluorescence activated cell sorting
FCS	fetal calf serum
FL1	fluorescence channel 1
g	gravitational constant
GAPDH	glyceraldehyde-3-phosphate dehydrogenase
HDR	homology directed repair
hESC	human embryonic stem cell
HSCT	hematopoietic stem cell transplantation
i.e.	id est, that is
ICE	inference of CRISPR edits
IL-34	interleukine-34
iPSC	induced pluripotent stem cells
kDa	kilo-Dalton
KO-SR	knockout serum replacement
M, µM	molar, micromolar
MIT	Massachusetts Institute of Technology
MPS	mononuclear phagocyte system
MRI	magnetic resonance imaging
NCBI	National Center for Biotechnology Information
NHEJ	non-homologous end joining
NTC	no template control
P/S	penicilline-streptomycine
PAM	protospacer-adjacent motif
PBS-T	phosphate-buffered saline with Tween20
PCR	polymerase chain reaction
PFA	paraformaldehyde
PSIM	primitive streak induction medium
PVDF	polyvinylidene difluoride
RI	Rho-kinase inhibitor
RIPA	radioimmunoprecipitation assay
RNA	ribonucleic acid
RNP	ribonucleoprotein

RPMI	Roswell Park Memorial Institute
RT-PCR	real time polymerase chain reaction
SDS	sodium dodecyl sulfate
sgRNA	single guide RNA
SMA	smooth muscle antigen
SNP	single-nucleotide polymorphism
TALEN	transcription activator-like effector nucleases
TBS-T	tris-buffered saline with Tween20
TEMED	tetramethylethylenediamine
TGFβ1	transforming growth factor beta 1
tracrRNA	transactivating CRISPR RNA
TUJ	beta-III-tubulin
ZFN	zinc-finger nucleases

Figures

Figure 1: Components of CRISPR/Cas. 16
Figure 2: Experiment plan for testing sgRNAs in THP-1 cells. 28
Figure 3: *CSF1R* gene and sgRNA positions. 29
Figure 4: Standard curve and linear regression formula for THP-1 cells. 31
Figure 5: Set-up of the 24-well plate for the electroporated cells. 33
Figure 6: Positions of the crRNAs used for the CRISPR approach in iPSC. 41
Figure 7: CSF1R Western Blots. 53
Figure 8: eGFP flow cytometry. 54
Figure 9: PCR for sequencing of transfected THP-1 cells. 55
Figure 10: ICE analysis. 56
Figure 11: ICE alignment results from the first electroporation. 58
Figure 12: Mean indel percentages and standard deviation. 59
Figure 13: Ponceau staining. 60
Figure 14: Western Blot data from three independent electroporations. 62
Figure 15: Cell culture images. 63
Figure 16: PCR screening for *CSF1R* of expanded iPSC clones. 64
Figure 17: Sequences and alignments of homozygous knockout clones. 65
Figure 18: Sequences and alignments of heterozygous knockout clones. 66
Figure 19: Off-target sequencing. 67
Figure 20: Alkaline Phosphatase staining. 68
Figure 21: Oct3/4 immunocytochemistry. 69
Figure 22: Tra-1-81 immunocytochemistry. 70
Figure 23: RT-PCR for pluripotency markers. 71
Figure 24: FoxA2 and Sox17 immunocytochemistry. 72
Figure 25: SMA immunocytochemistry. 73
Figure 26: TUJ immunocytochemistry. 74

Figure 27: Karyograms. 75

Tables

Table 1: Reagents and manufacturers 20
Table 2: Buffer and media composition 23
Table 3: Kits and manufacturers 26
Table 4: Laboratory equipment 26
Table 5: Single guide RNAs (sgRNAs) and corresponding sequences 29
Table 6: Composition of sgRNA complexes 34
Table 7: Sequencing primers THP-1 37
Table 8: Composition of the PCR approach 37
Table 9: PCR program 37
Table 10: Composition of the PCR approach 38
Table 11: Sequencing PCR program 39
Table 12: Sequencing primers iPSC 43
Table 13: Predicted off-target loci and corresponding MIT scores 44
Table 14: Sequencing primers off-targets 45
Table 15: RT-PCR primers 48
Table 16: RT-PCR program 49
Table 17: SgRNA efficacy and specificity scores 51

1 Introduction

1.1 Adult-onset leukoencephalopathy with axonal spheroids and pigmented glia

1.1.1 Definition and clinical characteristics

Adult-onset leukoencephalopathy with axonal spheroids and pigmented glia (ALSP) is a rare neurodegenerative disorder caused by autosomal dominant mutations in the gene encoding the colony stimulating factor 1 receptor (CSF1R) (Rademakers et al., 2012).

The clinical hallmark of ALSP is cognitive decline progressing to dementia, which is often accompanied by psychiatric symptoms, such as anxiety, depression and other changes in behavior and personality. Motor impairment, especially gait disturbances due to parkinsonism, paresis or spasticity as well as pyramidal signs and speech disturbances are further common symptoms. In some cases other clinical features, such as epilepsy or sensory disturbances, have also been observed (Konno et al., 2017; Papapetropoulos et al., 2022). Due to the variable symptoms, patients are initially often misdiagnosed with other neurologic or psychiatric disorders, such as Multiple Sclerosis, Parkinson's Disease, Alzheimer's Disease or depression before genetic testing reveals the *CSF1R* mutation (S. I. Kim et al., 2019; Sundal et al., 2012; Terada et al., 2004).

After causing first symptoms at a mean age of 43 years, the disease progresses rapidly and leads to death within approximately six to seven years (Konno et al., 2017). On average, women are affected at a considerably younger age than men, the mean age of onset being 40 years for women and 47 years for men (Konno et al., 2017; Papapetropoulos et al., 2022).

Brain imaging findings include pathological changes in magnetic resonance imaging (MRI) and computer-assisted tomography (CT) scans, and subtle changes are often already present in the pre-symptomatic stage of the disease. Radiological imaging of ALSP patients is characterized by white matter lesions, cortical atrophy resulting in relatively large ventricles, thinning of the corpus callosum and signal changes in the corpus callosum (Bender et al., 2014). In addition, abnormal

signaling in the pyramidal tracts and calcifications in the white matter have been observed in ALSP patients (Konno et al., 2018; Sundal et al., 2012).
Pathological examination of brain biopsies and autopsies shows myelin loss and damaged axons in the brain tissue as well as the spheroidal formations in axons and pigmented glia that ALSP owes its name to (S. I. Kim et al., 2019; Lynch et al., 2016). These biopsy findings were needed to establish the diagnosis before the identification of the causative gene mutation in 2012, which then made it possible to confirm the diagnosis by genetic testing for *CSF1R* mutations (Rademakers et al., 2012).

1.1.2 Pathophysiology

As mentioned above, ALSP is caused by mutations in CSF1R. CSF1R is mainly expressed in cells that are part of the mononuclear phagocyte system (MPS), e.g. monocytes, tissue macrophages and osteoclasts. It functions as a surface receptor for two ligands, colony stimulating factor 1 (CSF1) and interleukine-34 (IL-34). These ligands are essential for the survival, proliferation, differentiation and chemotaxis of the cells that carry the receptor (Stanley & Chitu, 2014; Tushinski & Stanley, 1983; W. Yu et al., 2012).
CSF1R is a class III receptor tyrosine kinase, i.e. a transmembrane receptor comprised of an extracellular, a transmembrane and an intracellular domain containing the tyrosine kinase domain. The intracellular domain also contains an adenosine triphosphate (ATP)-binding site. Binding of a ligand leads to the formation of homodimers and to the activation of the signaling pathway through autophosphorylation (Stanley & Chitu, 2014).
The gene encoding CSF1R consists of 22 exons on chromosome 5 (Papapetropoulos et al., 2022). Most of the approximately 100 known mutations found in ALSP patients are located in the part of the gene that encodes the tyrosine kinase domain, a smaller part is located in the ATP binding domain of the receptor (Papapetropoulos et al., 2022). The disease is inherited in an autosomal-dominant manner. In some cases it is caused by *de novo* mutations (Karle et al., 2013). In their group of 122 patients, Konno et al. found an age-dependent

disease penetrance ranging from 10% at 27 years to 95% at 60 years (Konno et al., 2017).

In overexpression experiments using a murine pro-B cell line and the murine homologue of *CSF1R*, it has been proposed that the disease-causing mutations are loss-of-function mutations (Pridans et al., 2013). This is unusual for autosomal-dominant mutations, as loss of function mutations can usually be compensated by the functioning allele. In the case of ALSP however, heterozygous mutations lead to the disease phenotype as well. This may be explained by a dominant negative effect of the mutant protein in the homodimeric receptors. However, this has not yet been verified through experiments.

In the brain, CSF1R is mainly expressed by microglia, the tissue-resident macrophages of the central nervous system (CNS) (Ginhoux et al., 2010). Expression can also be found on neurons but to a much lower extent (Luo et al., 2013). This suggests that ALSP is caused by microglia malfunction, wherefore the disease is considered to be part of a group of diseases called microgliopathies, also including e.g. Nasu-Hakola Disease and Multiple Sclerosis (Sasaki, 2017). However, the mechanism that connects the microglia malfunction to the disease phenotype in ALSP is not yet known.

In contrast to other glial cells and neurons, which are derived from the neuroectoderm, microglia originate from myeloid tissue (Chan et al., 2007). Their precursors are formed in the course of embryonic hematopoiesis in the yolk sac and populate the brain during prenatal development (Ginhoux et al., 2013).

Microglia seem to be involved in the brain's prenatal development as phagocytes, eliminating cells that undergo apoptosis (Calderó et al., 2009; Frade & Barde, 1998). In the adult brain, microglia form the innate immune system (Nayak et al., 2014) and are involved in neuroinflammation and many CNS pathologies (Benveniste et al., 2001; Boillée & Cleveland, 2008; Hatton & Duncan, 2019). Furthermore, Blinzinger and Kreutzberg were able to show that microglia react to the functional status of synapses and are involved in the process of synaptic stripping (Blinzinger & Kreutzberg, 1968; Graeber & Streit, 2010). Overall, microglia seem to have a neuroprotective effect. However, it is also known that under

certain circumstances, they contribute to autoimmune diseases such as Multiple Sclerosis (Graeber & Streit, 2010).

In an *in vitro* model, Liu et al. showed that overactivation of microglia leads to their degeneration (B. Liu et al., 2001). Degenerated microglia can be found in the adult brain and to a much higher amount in brains of patients suffering from Alzheimer's disease (Graeber & Streit, 2010). These findings suggest that the degeneration of microglia leads to a decrease of their neuroprotective effects and thus promotes neurodegeneration. This thesis would explain earlier studies showing that patients who suffer from seizures early in life have a higher risk for neurological insults during adulthood (Somera-Molina et al., 2009) and that a certain mutation in microglia contributes to the pathogenesis of amyotrophic lateral sclerosis (ALS) (Boillée and Cleveland, 2008; Gowing *et al.*, 2008).

In addition to their role in neurodegenerative diseases, microglia have been attributed a role in the growth of brain tumors, secondary damages after brain trauma and the pathogenesis of neuropathic pain (Graeber & Streit, 2010; Inoue & Tsuda, 2018; Lünemann et al., 2006).

There have been numerous studies about the homeostasis of the brain's microglia population, but it remains a controversial topic. The microglia population increases considerably under pathological conditions, a process called microgliosis. Some authors argue that this expansion results exclusively from the local proliferation of the resident population (Ajami et al., 2007; Ginhoux et al., 2010) whereas other studies suggest that it might additionally be caused by the recruitment of bone marrow derived precursor cells which migrate to the brain and differentiate into microglia (Flgel et al., 2001; Lawson et al., 1992). In order to investigate this, Eglitis et al. transplanted adult mice with genetically marked bone marrow cells from young mice. In this study, they were able to observe that the transplanted cells infiltrated the brain (Eglitis & Mezey, 1997). However, in this case, the mice were irradiated beforehand. Mildner et al. argue that if this is not the case and the blood brain barrier is not damaged due to a CNS disease, migration into the brain is not possible (Mildner et al., 2007).

1.1.3 Therapy

Therapeutic options for ALSP patients are mostly limited to symptomatic treatment, such as physical and occupational therapy, and medication such as antidepressants and antispasmodics. However, as ALSP is a microgliopathy and since monocytes can be recruited from the periphery under pathological condition, hematopoietic stem cell transplantation (HSCT) has been investigated as a new therapeutic approach for ALSP patients. To date, there are 15 reported cases of ALSP patients treated with allogenic HSCT, which led to a stabilization of the disease in most cases (Bergner et al., 2023; Dulski et al., 2022; Eichler et al., 2016; Mochel et al., 2019; Tipton et al., 2021). However, allogenic stem cell therapy is only possible at early stages of the disease, and due to the rapid disease progression, many patients are only diagnosed when already severely affected (Gelfand et al., 2019; Guerreiro et al., 2013; S. I. Kim et al., 2019; Sundal et al., 2012; Terada et al., 2004). In addition, a suitable donor is necessary and the treatment, which requires an immune ablative therapy prior to transplantation, is associated with severe complications and initial worsening of the symptoms (Barriga et al., 2012; Gelfand et al., 2019; Loiseau et al., 2007; Mochel et al., 2019). Side effects such as Graft-versus-Host-Disease and the risk for infections due to the required immunosuppression after transplantation are further obstacles of the treatment (Barriga et al., 2012; Sahin et al., 2016). Clearly, new and safer therapies are required to treat ALSP.

1.2 Genome editing

Genome editing technologies allow the addition, deletion and alteration of genes (Maeder & Gersbach, 2016). These technologies are already applied in various fields, such as producing genetically modified plants for more efficient agriculture or creating disease models for medical research (Carroll, 2017; Im et al., 2016). In addition to these applications, genome editing can also be used for therapeutic purposes by correcting disease-causing mutations, introducing therapeutic genes or deleting harmful ones in patient cells (Maeder & Gersbach, 2016). This approach of gene therapy has already been applied in clinical trials in the form of *ex vivo* as well as *in vivo* gene therapy (Naldini, 2015). For instance, there have

been clinical trials for *ex vivo* gene therapy in patients suffering from β-thalassemia (Naldini, 2015; Thompson et al., 2018). β-thalassemia is a disease caused by mutations in the β-globin gene that can lead to chronic hemolysis and profound anemia (Galanello & Origa, 2010). In their clinical trial, Thompson et al. obtained hematopoietic stem cells from patients with severe β-thalassemia, transfected these cells with the correct β-globin gene using a lentivirus outside of the patient's body, and transplanted the gene-modified cells back into the patients (Thompson et al., 2018). With this approach, they were able to reduce or eliminate the need for long-term red blood cell transfusion in all included patients (Thompson et al., 2018). *In vivo* gene therapy has been applied for instance in clinical trials to treat patients with hemophilia B (Manno et al., 2006; Naldini, 2015). These patients have a lack of factor IX due to mutations in the corresponding gene (Manno et al., 2006). For an *in vivo* approach, the cells are treated within the patient's body. In the mentioned trial, Manno et al. infused patients with a recombinant adeno-associated viral vector expressing human factor IX through the hepatic artery (Manno et al., 2006).

Some of the approaches used for genome editing are based on innate repair mechanisms that cells possess to repair double-strand breaks (DSB) in the DNA (Carroll, 2017). When such a DSB is detected by the cell, it can be repaired by so-called non-homologous end joining (NHEJ) or by homology directed repair (HDR) (Carroll, 2017; Chapman et al., 2012). NHEJ is a repair mechanism in which the break in the DNA is relegated by a combination of nucleases, ligases and polymerases (Lieber et al., 2003). This mechanism is error-prone and often leads to the formation of insertions or deletions, so-called indels, which can cause frameshifts in the gene (Chapman et al., 2012; Lieber, 2010). This can lead to loss of function of the encoded protein by disrupting the correct reading frame, i.e. a knockout of the target gene (Maeder & Gersbach, 2016). If the reading frame was incorrect before, the indel can also recover the correct reading frame and thus restore the protein's expression (Maeder & Gersbach, 2016; Ousterout et al., 2013).

In order to make more specific alterations, HDR can be used (Maeder & Gersbach, 2016). This repair mechanism corrects DSBs by copying a template,

usually the sister chromatid, and inserting this sequence at the location of the break (Chapman et al., 2012; Maeder & Gersbach, 2016). However, it is also possible to introduce an exogenous template of the desired DNA sequence or whole gene into the cell which then serves as DNA repair template (Perrin et al., 1995). Thus, this approach allows not only the correction but also the insertion of sequences or genes into the genome (Maeder & Gersbach, 2016). However, HDR approaches are limited by low editing efficiency (Cox et al., 2015).

There are different methods to induce DSBs in the DNA that make it possible to manipulate genes: zinc-finger nucleases (ZFN), transcription activator-like effector nucleases (TALEN) and clustered regularly interspaced palindromic repeats/CRISPR-associated nuclease (CRISPR/Cas) (Maeder & Gersbach, 2016). Compared to the other two methods, CRISPR/Cas is relatively easy to design, has a low cytotoxicity and is available at lower costs (Im et al., 2016).

The presence of repeated sequences separated by spacer sequences, later identified as the CRISPR/Cas system, was first described in 1987 in prokaryotes and 1993 in archaea (Ishino et al., 1987; Lino et al., 2018; Mojica et al., 1995). The system received its name in 2002 (Jansen et al., 2002). CRISPR stands for “clustered regularly interspaced palindromic repeats”, Cas is the CRISPR-associated nuclease. In 2005, Mojica et al. discovered that the spacer sequences between the repeats were excerpts from the DNA of bacteriophages, i.e. viruses that infect bacteria, and thus concluded that CRISPR/Cas is part of the bacteria’s adaptive immune system (Mojica et al., 2005). Barrangou et al. confirmed this conclusion by analyzing the DNA sequences of several Streptococcus thermophilus strains before and after infection with different bacteriophages (Barrangou et al., 2007). They found that after the infection, new spacers were found in CRISPR loci and that the inserted sequences were identical to sequences of the phage’s genome (Barrangou et al., 2007). Furthermore, they were able to observe that bacteria that possessed such a spacer corresponding to a sequence from a phage’s genome showed higher resistance to this phage (Barrangou et al., 2007).

Transcription of the CRISPR loci leads to the formation of so-called CRISPR RNAs (crRNAs) (Brouns et al., 2008). These crRNAs guide the complex to the genomic target sequence, the sequence identical to the respective spacer

(Brouns et al., 2008). Subsequently, a double strand break is induced by CRISPR-associated (Cas) enzyme (Jinek et al., 2012). The crRNAs are annealed in a duplex molecule with transactivating CRISPR RNA (tracrRNA) that is necessary for the crRNA-Cas interaction (Jinek et al., 2012). For CRISPR experiments, crRNA and tracrRNA can be connected to form a complex called single guide RNA (sgRNA) (Cui et al., 2018). Figure 1 shows the components of the CRISPR/Cas system.

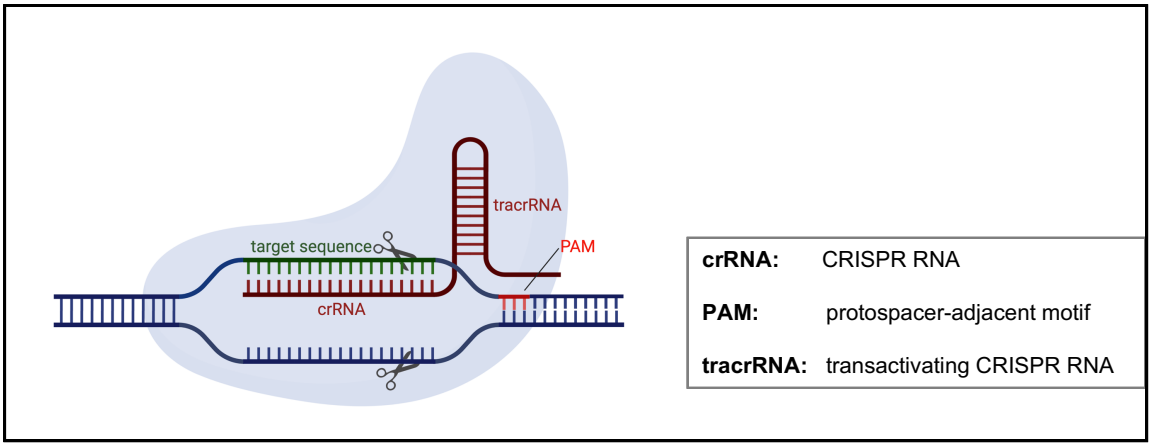

Figure 1: Components of CRISPR/Cas. CRISPR RNAs (crRNAs) guide the complex to the target sequence. A double strand break is then induced by the CRISPR-associated enzyme (Cas) three basepairs upstream of the protospacer-adjacent motif (PAM). The transactivating CRISPR RNA (tracrRNA) annealed with the crRNA enables interaction between crRNA and Cas. CrRNA and tracrRNA can be connected in a complex called single guide RNA (sgRNA).

There is a large diversity of different classes and types of Cas proteins, the most common for genome editing experiments being Streptococcus pyogenes Cas9 (SpCas9) (Nakade et al., 2017). The Cas9 protein introduces the cleavage three basepairs (bp) upstream of a site called the protospacer-adjacent motif (PAM) (Zhang et al., 2016, see Figure 1). This motif can be found directly downstream of the target on the complementary strand and is specific to the Cas protein that is used. The PAM for SpCas 9 is “NGG” with “N” standing for any nucleotide (Zhang et al., 2016). As the PAM only exists in the genome of the invading virus but not in the bacterial one, this avoids cleavage of the bacterial CRISPR locus by Cas9.

For gene editing purposes, the CRISPR/Cas complex can be delivered to the cells in a viral, plasmid, mRNA or protein format (Luther, D.C. et al., 2018). Delivering the complex in the form of a protein has the advantage of a lower insertional mutagenesis in comparison to viral or plasmid approaches (Luther, D.C. et

al., 2018). Furthermore, the protein format leads to less off-target effects and a lower immunogenicity than all other approaches (Luther, D.C. et al., 2018).
One important challenge for the development of CRISPR/Cas-based therapies is to avoid off-target activity that can lead to accidental side effects by reducing the genomic stability and disrupting functioning genes (X. H. Zhang et al., 2015).

1.3 Disease modeling in induced pluripotent stem cells (iPSC)

Disease models are an important tool to improve our understanding of a disease's pathomechanism, which is essential for the development of therapeutic strategies and methods for early disease detection. Furthermore, they can be used for drug screening purposes, as they allow to assess the efficiency as well as the toxicity of a new compound (Elitt et al., 2018; Patil et al., 2019).
There are different types of disease models which all have advantages as well as limitations. *In vivo* animal models provide the possibility to investigate a disease in a complex organ system with its interactions. However, they are not only relatively difficult to maintain but also limited by species differences between animals and humans, so that findings from these models cannot always be reproduced in a human system (Andersen & Winter, 2019; Uhl & Warner, 2015).
While human primary cells might provide a more appropriate disease model in that case, they are often difficult to obtain, as is the case with brain cells such as microglia (Y. Shi et al., 2017). Therefore, *in vitro* models are often based on immortalized cell lines which are easy to obtain and to expand because of their high proliferation rate (Kaur & Dufour, 2012). However, as these cells are often derived from cancer cells, they contain genomic aberrations that primary cells do not have (Elitt et al., 2018; Landry et al., 2013; Maqsood et al., 2013). Embryonic stem cells (ESC) can be used for disease modeling as well in order to avoid the limitations described above, but their acquisition poses ethical concerns (Volarevic et al., 2018). Therefore, the establishment of induced pluripotent stem cells (iPSC) by Takahasi et al. in 2006 was an important progress in *in vitro* disease modeling (Takahashi & Yamanaka, 2006).
The first iPSC were generated from mouse fibroblasts by introducing transcription factors *OCT3/4, SOX2, c-MYC* and *KLF4* into the cells via retroviral delivery

(Takahashi & Yamanaka, 2006). One year later, the same authors were able to use the same method to create human iPSC from human dermal fibroblasts (Takahashi et al., 2007). These human iPSC had the same characteristics as human ESC concerning their morphology, proliferation, expression of ESC markers, and ability to differentiate into cells from all three germ layers (Takahashi et al., 2007). Since the generation of these first human iPSC, the method has been improved by developing transgene-free delivery methods and optimizing the combination of transcription factors used for reprogramming (Okita et al., 2011; J. Yu et al., 2009). Using delivery methods such as episomal plasmids that do not need viral packaging, has the advantage that the vector does not integrate into the genome, thus avoiding insertional mutations that might have an effect on the functionality of the iPSC (Y. Shi et al., 2017). The fact that iPSC can be derived from peripheral cells such as dermal fibroblasts makes them more accessible than primary cells. Nonetheless, they are human cells that are able to differentiate into all somatic cell types so that they can be used for all sorts of disease models (Y. Shi et al., 2017). Another advantage is their expandability (Y. Shi et al., 2017). Furthermore, patient-specific iPSC can be created, as has been done for ALSP (Hayer et al., 2018).

1.4 Objective of the study

Therapeutic options for ALSP patients are very limited at present; at the same time, ALSP is a severe and rapidly progressing disease with a poor prognosis. Clearly, new therapeutic approaches are urgently needed. Promising therapeutic strategies for monogenetic diseases are CRISPR/Cas-based gene therapies. ALSP is a monogenetic disease, and cells of the hematopoietic system are mediating disease pathology in this disease. Therefore, an intriguing approach to ALSP gene therapy is *ex vivo* correction of *CSF1R* mutations in hematopoietic stem cells, i.e. an autologous hematopoietic stem cell transplantation with *ex vivo* gene therapy.

In this case, the patient's own stem cells would be extracted and treated *ex vivo* to knock out or replace the mutated *CSF1R* gene using the CRISPR/Cas system. Then, the stem cells with the edited gene would be reimplanted. In that case, no

immunosuppression would be necessary, so that the treatment is expected to have less side effects than allogenic HSCT. A knockout of the patient's *CSF1R* mutated allele might already be therapeutic if there is indeed a dominant negative mechanism involved in the pathophysiology. Otherwise, the knockout could be combined with the introduction of the correct gene, e.g. via virus-based overexpression. This approach would make it possible to develop one treatment for all patients, regardless of the mutation they carry, instead of having to develop a specific guide RNA for each mutation. Since there are approximately 100 different disease-causing mutations for ALSP, this is an important factor.

In order to establish this new therapy, the first part of the project focused on the design and testing of an optimal guide RNA. The most important features of guide RNAs in gene therapy are high efficiency and high specificity. High efficiency is particularly important in the case of ALSP, as *CSF1R* mutations found in this disease are likely to have a dominant-negative effect, and expression of the mutated gene should be decreased as much as possible. High specificity to the target gene is required to avoid off-target effects that might lead to clinical side effects.

In the second part of the project, the best guide RNAs should be used to generate homozygous and heterozygous *CSF1R* iPSC knockout lines. These knockout iPSC lines will be a helpful tool for future studies further examining the pathophysiology of ALSP. A better understanding of the disease mechanism might help develop methods to diagnose patients earlier in the disease and to identify further therapeutic strategies.

Taken together, the main goal of this project is to provide the basis for CRISPR/Cas-based gene replacement therapy in ALSP patients. The study focuses on the generation of sgRNAs and the evaluation of the sgRNAs' efficiency, and provides an application of these sgRNAs in an iPSC-based *in vitro* system.

The project is divided into two main parts:

I. Identification of efficient sgRNAs for knockout of human *CSF1R*
II. Generation of homozygous and heterozygous *CSF1R* iPSC knockout lines

2 Material and methods

2.1 Material

Table 1: Reagents and manufacturers

Name	Manufacturer
α-thioglycerol	Sigma Aldrich
β-mercaptoethanol	Sigma Aldrich
Accutase	Sigma Aldrich
Acrylamide solution (40%)	AppliChem
Activin A (100 ng/µl)	Peprotech
Alt-R® Cas9 Electroporation Enhancer	Integrated DNA Technologies
Ammoniumperoxidesulfate (APS)	Sigma Aldrich
Anti-adherence rinsing solution	STEMCELL Technologies
Anti-β-Actin antibody (mouse)	Thermo Fisher Scientific
Anti-CSF1R antibody	Abcam
Anti-GAPDH antibody	Meridian Life Science
Atto 550 fluorescent dye	Integrated DNA Technologies, custom production
Atto 647 fluorescent dye	Integrated DNA Technologies, custom production
B27 supplement	Gibco
Bis (2-hydroxyethyl)amino-tris (hydroxymethyl)methan (BIS-TRIS)	VWR
Boric acid	Carl Roth
Bovine serum albumin (BSA)	Sigma Aldrich
Buffer TE CRISPRevolution	Synthego
CHIR-99021 (3 mM)	Tocris
CrRNAs	Integrated DNA Technologies, custom production
4′,6-diamidino-2-phenylindole	Thermo Scientific

(DAPI)	
DMEM-F12	Sigma Aldrich
DMEM high glucose	Life Technologies
Dimethyl sulfoxide (DMSO)	Sigma Aldrich
DNTP Mix	Fermentas
Dulbecco's Phosphate Buffered Saline (DPBS)	Sigma Aldrich
Ethanol	VWR
Ethylenediaminetetraacetic acid (EDTA)	Carl Roth
Fast Red	Sigma Aldrich
Fetal calf serum (FCS)	Merck
Fibroblast growth factor (FGF2)	Peprotech
Fluorescence mounting medium	Dako
Formamide	Applied Biosystems
Gelatine	Sigma Aldrich
Gene Ruler DNA Ladder Mix	Thermo Scientific
GlutaMAX (100X) supplement	Gibco
GoTaq DNA Polymerase	Promega
Heparin	Sigma Aldrich
Immunocytochemistry antibodies	
Primary antibodies	
Goat anti-Sox17	R&D Systems
Mouse anti-SMA	Dako
Mouse anti-Tra1-81	Millipore
Mouse anti-TUJ	Sigma Aldrich
Rabbit anti-Fox-A2	Millipore
Rabbit anti-Oct3/4	Proteintech
Secondary antibodies	
Alexa Fluor 488 Goat anti-rabbit IgG	Life Technologies
Alexa Fluor 488 Goat anti-mouse IgG	Life Technologies
Alexa Fluor 647 Donkey anti-goat IgG	Life Technologies

Insulin	Sigma Aldrich
ITS-supplement 100X	Gibco
Knockout Serum Replacement (KO-SR)	Gibco
L-ascorbic acid-2-phosphate magnesium	Sigma Aldrich
LDN-193189	Geyer
LE Agarose	Lonza
Matrigel	Corning Bioscience
Midori Green Advance DNA Stain	Nippon Genetics Europe GmbH
Naphtol AS-MX-phosphate	Sigma Aldrich
Neurobasal medium	Gibco
Non-essential amino-acid solution (NEAA)	Sigma Aldrich
nonfat dried milk powder	Applichem
Nucleofection supplement	Lonza
Nucleofection solution	Lonza
NuPAGE™ MOPS SDS running buffer	Life technologies
Paraformaldehyde (PFA)	Merck
Penicillin-streptomycine (P/S)	Sigma Aldrich
Pink buffer	Thermo Scientific
Ponceau solution	Sigma Aldrich
Precision Plus Protein Standard Dual Color	BioRad
Progesterone	Sigma Aldrich
Protease inhibitor	Roche
Putrescine	Sigma Aldrich
Rho-kinase inhibitor (RI) Y-27632	Abcam
RIPA buffer	Sigma Aldrich
RNAse A	Thermo Scientific
RNP Cas9	Integrated DNA Technologies
RPMI 1640	Sigma Aldrich

RPMI 1640, advanced	Thermo Scientific
RPMI 1640, HEPES	Thermo Scientific
SB431542	Lonza
SgRNAs	Integrated DNA Technologies, custom production
Sodium acetate	Carl Roth
Sodium azide	Sigma Aldrich
Sodium selenite	Sigma Aldrich
SYBR™ Select Master Mix	Applied Biosystems
Tetramethylethylenediamine (TEMED)	Thermo Scientific
Transforming growth factor beta 1 (TGFβ1)	Peprotech
Transferrin	Sigma Aldrich
Tris base	Applichem
Trypan blue	Sigma Aldrich
Western Blocking Reagent	Roche

Table 2: Buffer and media composition

Name	**Content**
3.5 x Tris buffer	52,32 g Bis-TRIS 200 ml water to pH = 6,5-6,8
3N medium	250 ml N2 medium 250 ml Neurobasal medium 5 ml B27 2.5 ml GlutaMAX 2.5 ml non-essential amino acid solution 0.5 ml β-mercaptoethanol 5 ml P/S 5 ml glucose (160 mg/ml)

E8 medium	500 ml DMEM-F12 + HEPES 1 ml L-ascorbic acid-2-phosphate magnesium 5 ml ITS-supplement 100X 5 µl FGF2 (10 µg/l) 10 µl TGFβ1 (2 µg/µl) 0.5 µl Heparin (100 ng/µl)
EB medium	77 ml DMEM-F12 20 ml KO-SR 1 ml Non-essential amino-acid solution 1 ml P/S 1 ml GlutaMAX 3.5 µl β-mercaptoethanol (50µM)
Electrophoresis buffer	108 g tris base 55 g boric acid 40 ml EDTA solution (0.5 M, pH 8) to 1 l with water
Endoderm induction medium (EIM)	50 ml RPMI 1640 advanced 1 ml B27 0.5 ml P/S 100 µl FCS 25 c Activin A
FACS buffer	DPBS 0.5% BSA 2mM EDTA
Freezing medium	25 ml E8 medium 20 ml KO-SR 5 ml DMSO 10 µM RI
Mesoderm medium	DMEM high glucose 20 ml FCS 1 ml P/S

	1 ml non-essential amino-acid solution 100 µl β-mercaptoethanol 4 µl α-thioglycerol
N2 medium	500 ml DMEM-F12 5 ml transferrin (10 mg/ml) 1.25 ml insulin (10 mg/ml) 0.5 ml progesterone (2 mM) 0.5 ml putrescine (100 mM) 30 µl sodium selenite (500 µM)
Primitive streak induction medium (PSIM)	20 ml RPMI 1640 advanced 0.4 ml B27 0.2 ml P/S 40 µl FCS 13.3 µl CHIR-99021 10 µl Activin A
TBE buffer, 10X	108 g tris base 55 g boric acid 40 ml EDTA (0.5 M)
Tris-buffered saline (TBS), 10X	151.42 g tris base 219.15 g sodium chloride to 2.5 l with water
Tris-buffered saline with Tween20 (TBS-T)	2.5 l TBS 2.5 ml Tween20
THP-1 medium	RPMI 1640 medium 10 % FCS 1 % GlutaMAX 1 % P/S

Table 3: Kits and manufacturers

Name	Manufacturer
Enhanced chemiluminescence (ECL) substrate: Immobilon Western HRP Substrate	Merck
Gene Jet Genomic DNA Purification Kit	Thermo Scientific
QUIAquick Gel Extraction Kit	Qiagen
QuickExtract™ DNA Extraction Solution	Lucigen
Neon™ Transfection System 10 µL Kit	Invitrogen™
Pierce BCA Protein Assay Kit	Thermo Scientific
Revert Aid First Strand cDNA Synthesis Kit	Roche
RNeasy Mini Kit	Qiagen

Table 4: Laboratory equipment

Name	Manufacturer
24-well-plate	Greiner Bio-One
6-well-plate	Greiner Bio-One
96-well PCR plate	Applied Biosystems
Aggrewell plate	STEMCELL Technologies
Cell culture flask	Corning
Centrifuge 5810R	Eppendorf
Coverslips	VWR
CryoTube™ Vials	Thermo Scientific
FACSCalibur	BD Biosciences
Falcon tubes	Corning
HERAcell™ VIOS 160i CO2-Inkubator	Thermo Scientific
Microcentrifuge tubes	Eppendorf
Mini-Protean® Tetra Cell Casting Module	Bio-Rad
Mini-PROTEAN® Tetra electrophoresis system	Bio-Rad
Molecular Imager GelDoc™ XR+	BioRad

NanoDrop	Thermo Scientific
Neon™ transfection system	Thermo Scientific
Neubauer chamber	Karl Hecht
Nitrocellulose membrane	GE Healthcare Life Sciences
Nucleofector™ 2b	Lonza
Petridish	Corning
Pipet tips	Biozym
Polyvinylidene difluoride (PVDF) membrane	Merck
RH basic magnetic stirrer	IKA
Thermal cycler	Thermo Scientific
Thermo Mixer C	Eppendorf
Viia 7 Real-Time PCR System	Thermo Scientific
Vortex mixer Vortex Genie-2	Carl Roth
Waterbath	Sigma Aldrich

2.2 Methods

2.2.1 Methods Part I: Identification of efficient sgRNAs for knockout of human CSF1R

Figure 2 provides an overview over the experiments that were performed to achieve the first objective of this study: the identification of efficient sgRNAs for *CSF1R* knockout in an established cell line.

First, sgRNAs were designed by means of online tools. In parallel, CSF1R protein expression was assessed by Western Blot in K-562 cells and in THP-1 cells in order to select an appropriate cell line for further experiments. Both of these cell lines were chosen because they were expected to express CSF1R due to their origin in myelogenous leukemia cells, as described in more detail in 2.2.1.2. Subsequently, the selected cell line was electroporated with the CRISPR/Cas9 system using the previously designed sgRNAs. Finally, CSF1R expression in the electroporated cells was assessed on DNA and protein level.

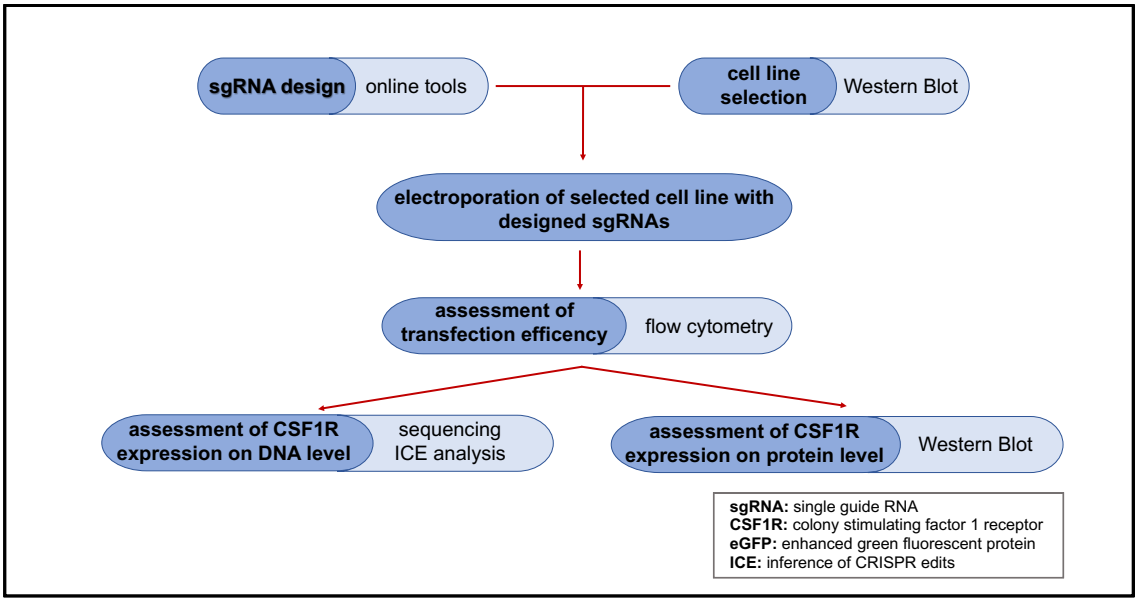

Figure 2: Experiment plan for testing sgRNAs in THP-1 cells. Overview of the steps involved in the testing of sgRNAs in a cell line and the methods used for each step.

2.2.1.1 sgRNA design

SgRNAs for *CSF1R* were designed using the following tools: chopchop, Broad Institute GPP sgRNA designer, CRISPOR and Dharmacon Horizon Discovery CRISPR Design Tool. In a first step, only exon 2 of the *CSF1R* gene was used

as target as it is the exon that contains the ATG region, i.e. the start codon which is necessary for protein translation. Four sgRNAs were chosen for this region. Second, the whole gene was indicated as target in order to choose another sgRNA.

In total, five sgRNAs with high efficiencies, low self-complementarity, and a high number of mismatches in other parts of the genome were selected. SgRNAs that were designed by more than one tool were preferred.

The positions of the sgRNAs' targets in the *CSF1R* gene are depicted in Figure 3. The sequences of the sgRNAs are presented in Table 5.

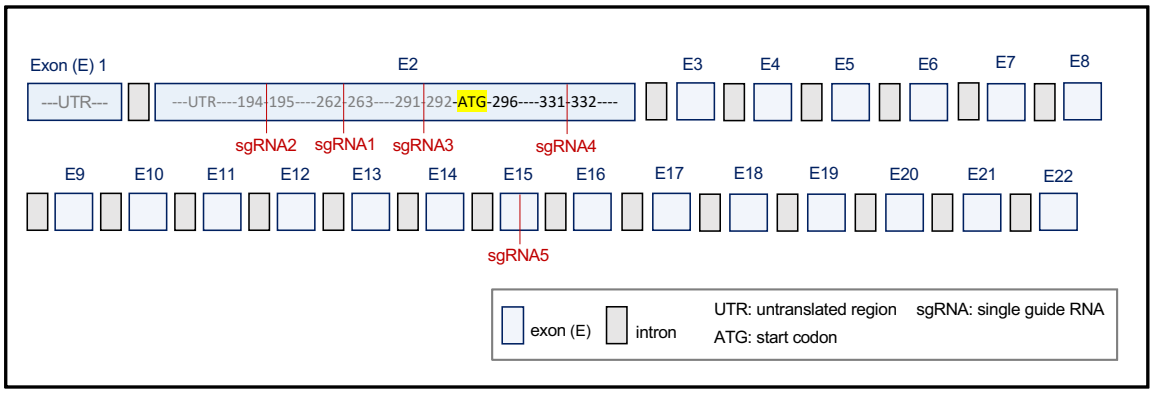

Figure 3: *CSF1R* gene and sgRNA positions. Visualization of the *CSF1R* gene and cutting sites for the 5 designed sgRNAs. SgRNAs 1-4 are located in exon 2 which contains the start codon and is therefore important for translation. SgRNA 5 is located in exon 15. The sizes of the intron and exon symbols are not true to scale.

Table 5: Single guide RNAs (sgRNAs) and corresponding sequences

Name	Sequence
sgRNA 1	TCGGTGGGGAAGTGGCAGGCAGG
sgRNA 2	CTCCGCAGGGATCGGGACACTGG
sgRNA 3	CACTTCCCCACCGAGGCCATGGG
sgRNA 4	TCCTGCTGGTGGCCACAGCTTGG
sgRNA 5	ACTCCGTGATGACCAGTACAGGG

2.2.1.2 Selection of a cell line and optimization of CSF1R Western Blot

In order to select an appropriate cell line for testing the designed sgRNAs, Western Blots for CSF1R were performed in K562 and THP-1 cells. Both are monocytic cell lines derived from patients suffering from chronic (K562) or acute (THP-

1) myelogenous leukemia (Lozzio & Lozzio, 1975; Tsuchiya et al., 1980). Therefore, both cell lines are expected to express CSF1R.

The cells were cultured in cell culture flasks with THP-1 medium (see 2.1, Table 2) at 37 °C. Medium was changed every other day.

For the assessment of CSF1R expression in these cell lines, Western Blots were performed. Different amounts of protein (20 µg, 40 µg and 60 µg) as well as different antibody dilutions and membrane types (nitrocellulose and polyvinylidene difluoride (PVDF)) were tested.

In order to isolate protein from the cells, approximately 8 million cells of each cell line were transferred from the culture flask to a microcentrifuge tube. The cells were counted by adding 90 µl of trypan blue to 10 µl of the cell suspension using a Neubauer chamber and the following formula:

Number of cells / ml = (number of cells in 4 squares / 4) x 10 x 1000

The cells were then centrifuged at 400 *g* for 1 min and washed once with 200 µl of Dulbecco's phosphate buffered saline (DPBS). After another centrifugation at 400 *g* for 1 min, the supernatant was removed and the cells were resuspended in 50 µl of RIPA buffer and 2 µl of protease inhibitor. This mix was placed in a rotator at 4 °C for 45 min and then centrifuged at 13000 *g*, at a temperature of 4°C for 30 min. Subsequently, the supernatant containing the protein was aliquoted and kept at -80 °C until further use, the pellet was discarded. The protein concentration was assessed by a bicinchoninic acid (BCA) assay using the Pierce BCA Protein Assay Kit following the manufacturer's instructions: the BCA working reagents A and B were mixed at a ratio of 50:1. Nine Albumin dilutions from 0 µg / ml to 2000 µg / µl were used as standards, the 0 µg / ml dilution served as a blank. The CSF1R protein samples were diluted 1:10. 10 µl of the sample dilution and the standards, respectively, were added to one well of a 96-well-plate. Duplicates were made for each sample and standard. Then, 80 µl of the prepared working reagent were added to each well. After incubating the plate at 37 °C for 30 min, the absorbance was measured in a plate reader (SpectraMax M/Molecular Devices). To calculate the protein concentration, the mean absorbance from the duplicates was calculated and the absorbance value of the blank was subtracted from the other absorbances. A standard curve and the formula

for the linear regression were created using Microsoft Excel (X=(Y-b)/m, Y=absorbance, b=intercept, m=slope). This formula was used to calculate the protein concentration of the samples. An exemplary standard curve and linear regression formula with the data from the BCA for the THP-1 cells can be seen in Figure 3.

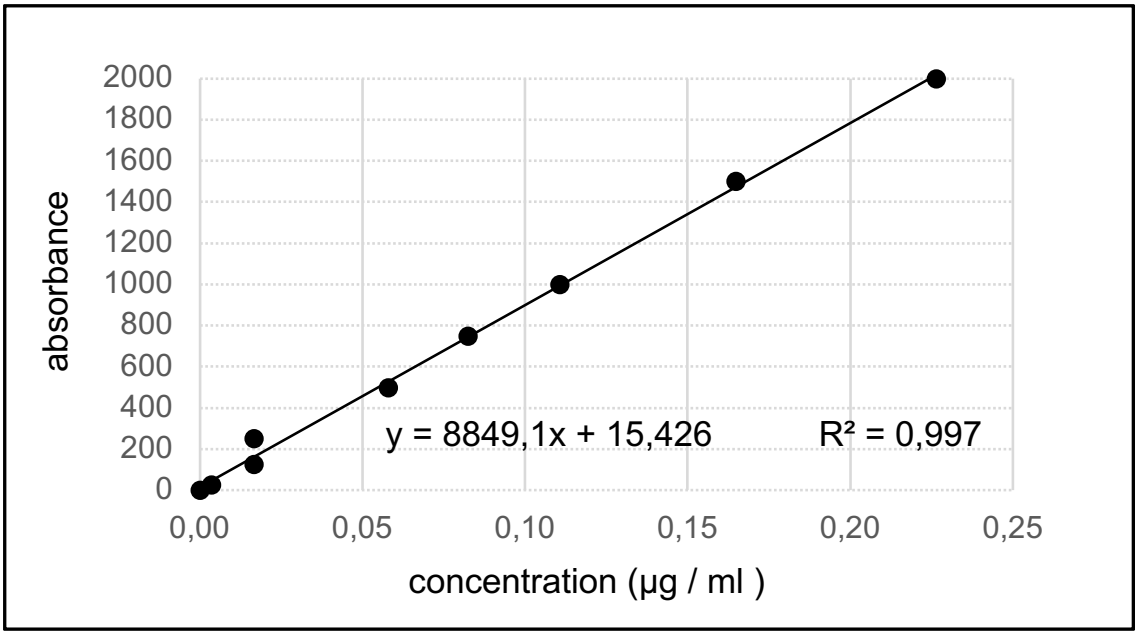

Figure 4: Standard curve and linear regression formula for THP-1 cells. A standard curve was created based on the standards' absorbance. The formula for linear regression was calculated using Microsoft Excel.

In preparation for the Western Blot, a separating and a stacking sodium dodecyl sulfate (SDS) gel were poured in the Mini-Protean® Tetra Cell Casting Module and SDS gel electrophoresis was performed in the Mini-PROTEAN® Tetra electrophoresis system. SDS gel electrophoresis is used to separate the proteins contained in the sample by size. For the separating gel, 1.71 ml of 3.5 x Tris-buffer, 1.5 ml of 40 % acrylamide, 2.73 ml of water, 60 µl of 10 % ammonium persulfate (APS) and 6 µl of tetramethylethylenediamine (TEMED) were added to a falcon and mixed briefly by turning the falcon upside down. The gel was pipetted into the cassettes and overlayed with 100 % isopropanol to avoid bubbles. After 45 min of polymerization, the stacking gels consisting of 0.57 ml of 3.5 x Tris-buffer, 0.2 ml of 40 % acrylamide, 1.21 ml of water, 20 µl of 10 % APS and 2 µl of TEMED was prepared and pipetted into the cassette in the same way. A 12-well comb was inserted. During the 30 min of polymerization the samples were prepared.

20, 40 and 60 µg of the protein samples of K562 and THP-1 cells, respectively, were diluted in RIPA buffer with 4 % protease inhibitor to a volume of 20 µl, followed by addition of 5 µl of Pink Buffer. The samples were denaturized at 95 °C for 5 min, cooled down to 4 °C and kept on ice until loading.

The electrophoresis chamber was filled with running buffer and the electrophoresis module including the gel cassettes was assembled. The comb was removed and the wells were rinsed with running buffer. Subsequently, 5 µl of the protein standard and 20 µl of the sample were loaded. The electrophoresis was started at 80 V for the first 10 min, then the voltage was increased to 120 V for a total running time of approximately 2 h.

For the transfer, the gel was placed into a gel holder cassette with a PVDF membrane between fiber paper and fiber pads. The cassette was placed in the chamber which was filled with transfer buffer. A cool pad and stir bar were added, then the transfer was performed overnight at 20 V and 4 °C. The next day, the voltage was increased to 100 V for 60 min.

The transfer was checked by washing the membranes shortly in distilled water and then placing them in a tray with Ponceau solution for 5 min. If bands were detected, the membranes were labeled with antibodies. The membranes were cut so that the upper part contained the CSF1R protein and the lower part glyceraldehyde-3-phosphate dehydrogenase (GAPDH). They were then washed once with distilled water and three times with tris-buffered saline with Tween20 (TBS-T) for 10 min each.

Next, the blocking reagent consisting of TBS-T and 5 % skimmed milk was prepared. The membranes were put into falcons and 5 ml of the blocking reagent were added. The falcons were put on a roll mixer at room temperature for 2 h.

Meanwhile the primary antibodies were diluted in 5 % Roche Block in TBS-T with 1 % sodium azide. For CSF1R a 1:50, 1:100, 1:250, 1:500 and 1:1000 dilution were tested. GAPDH was diluted 1:100000.

5 ml of this dilution were added to the falcons containing the respective membranes and the membranes were incubated overnight at 4 °C on a shaker.

The next day, the membranes were washed with TBS-T three times, for 10 min each.

Subsequently, the secondary antibody (anti-mouse for all primary antibodies used) was diluted 1:5000 in TBS-T with 1 % skimmed milk. The membranes were incubated with 5 ml of the secondary antibody at room temperature for 1 h. Finally, the membranes were washed another three times with TBS-T.
For the evaluation, a detection solution was prepared. 750 µl each of enhanced chemiluminescence (ECL) compound A and B were mixed in a microcentrifuge tube. 350 µl of this solution were added to each half of a membrane immediately before imaging it using the Bio Rad Gel Reader.

2.2.1.3 Electroporation of THP-1 cells with CRISPR/Cas

Electroporation was used to introduce the CRISPR/Cas complex containing the designed sgRNAs into the cells. In this transfection method the permeability of the cell membrane is increased by the application of an electric field. The electric pulses create pores in the membrane through which molecules can be introduced into the cell.
A 24-well-plate was prepared with 1 ml THP-1 medium without penicillin-streptomycine (P/S) per well for three wells per sgRNA, three wells for a negative control without an sgRNA, and three wells for an eGFP control for assessment of transfection efficiency. The set-up is shown in Figure 5.

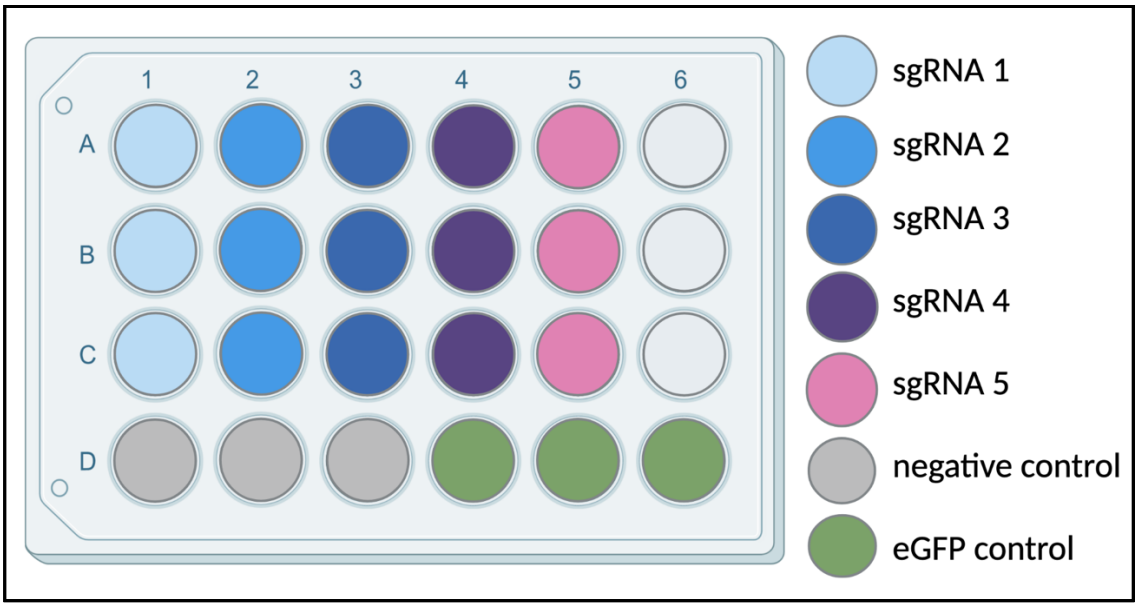

Figure 5: Set-up of the 24-well plate for the electroporated cells. The 24-well plate contains three wells for each sgRNA that cells are transfected with. Additionally, it contains triplicates of an untreated negative control and an eGFP control for assessment of transfection efficiency.

Using the CRISPRevolution Synthetic sgRNA kit, the sgRNAs were resuspended in Buffer TE and diluted to 100 pmol/µl, then vortexed for 30 s and spun down. Complexes for each sgRNA were prepared in 1.5 ml Eppendorf tubes by adding the reagents listed in Table 6 in the indicated order.

Table 6: Composition of sgRNA complexes

Reagent	Volume
1. Buffer R (without causing bubbles)	10.08 µl
2. ribonucleoprotein (RNP) Cas9	2.22 µl
3. sgRNA	2.70 µl

Each complex was then vortexed for one second, spun down and incubated at room temperature for 15 min. Afterwards, it was stored on ice.

During the incubation time the THP-1 cells were prepared. The cells were counted and aliquoted in 7 Eppendorf tubes (one for each sgRNA, one for the negative control and one for the eGFP) containing 300000 cells per tube. The tubes were then centrifuged at 400 *g* for 1 min and the supernatant was removed. Then, 200 µl DPBS were added for washing and the cells were again centrifuged at 400 *g* for 1 min, the supernatant was removed. Next, 180 µl DPBS were added to each tube except the one for the negative control in which 150 µl medium were added from the 24 well plate (50 µl from each control well). The negative control was then redistributed to these 3 wells.

For the actual electroporation, the Neon Transfection System Kit was used. 3 ml Electrolytic Buffer E were added into the Neon tube. Before electroporation, the respective tube containing the cells was centrifuged at 400 *g* for 1 min, the supernatant was removed except for approximately 5 µl. The pellet was resuspended in 20 µl Resuspension Buffer R and then added to the prepared complex without mixing. The cells were mixed with the complex by pipetting up and down with the Neon pipette. Then, 10 µl of the mix were taken up into the pipette which was put into the Neon tube without touching the tube's walls with the pipette. The electroporation was conducted at 1450 V for 10 ms with 3 pulses. After that, the electroporated content was added to the prepared wells.

For the eGFP control, the cells were also centrifuged at 400 *g* for 1 min, the supernatant was removed. 40 µl of Buffer R and 1 ng of eGFP mRNA were added. As with the other samples, the solution was mixed by pipetting up and down with the Neon pipette and then electroporated three times. The content was then added to three wells.

The cells were cultured at 37 °C with medium changes every other day. Cells were harvested for DNA isolation five days after electroporation and for protein isolation when the wells were full with cells again, which took approximately 2 weeks. To harvest the cells, pellets were made from 500 µl of the wells' contents by centrifuging for 1 min at 400 *g*. The cells were then washed once with 200 µl DPBS, centrifuged in the same way again and the supernatant was removed. The cells were kept at - 80 °C until further use.

2.2.1.4 Assessment of transfection efficiency by flow cytometry

The transfection efficiency was assessed by flow cytometry analysis of the eGFP control the day after the electroporation. EGFP is a fluorescent protein so that its presence in the cells after electroporation with eGFP mRNA can be measured by flow cytometry. This way, the efficiency of the uptake of molecules into the cells during electroporation can be evaluated.

For this purpose, the content from the eGFP wells was transferred to one Eppendorf tube each, for the negative control one third of the content of each well was added to one tube. The cells were centrifuged at 400 *g* for 1 min and, after removing the supernatant, resuspended in 200 µl DPBS. For the flow cytometry analysis the cells were transferred to FACS tubes.

Flow cytometry was performed using the BD FACSCalibur™ and analyzed with the BD FlowJo software.

2.2.1.5 Assessment of CSF1R expression on DNA level

DNA was isolated from the cells harvested after electroporation. The DNA was then used for sequencing and inference of CRISPR edits (ICE) analysis.

2.2.1.5.1 DNA isolation

DNA was isolated from the harvested cells using the Gene JET Genomic DNA Purification Kit following the manufacturer's Cultured Mammalian Cells Genomic DNA Purification Protocol. The frozen cells were thawed and suspended in 200 µl DPBS, then 200 µl of Lysis Solution and 20 µl of Proteinase K Solution were added. After incubating at 56 °C for 10 min on a rocket platform, 400 µl of ethanol were added. The sample was transferred to the Purification Column in a collection tube and then centrifuged at 6000 *g* for 1 min. After discarding the flow-through, the sample was washed with 500 µl of Wash Buffer I and centrifuged at 6000 *g* for 1 min. This was repeated with 500 µl of Wash Buffer II, centrifuging the column at maximum speed for 3 min. After emptying the collection tube, the column was spun again for 1 min to dry the membrane. The column was then transferred to a sterile 1,5 ml microcentrifuge tube. 50 µl of Elution Buffer were added and after an incubation time of 2 min at room temperature the sample was centrifuged at 8000 *g* for 1 min. Finally, the purification column was discarded and the DNA concentration in the sample was measured using the Nano Drop spectrophotometer.

2.2.1.5.2 Sequencing

In order to sequence the DNA isolated from the THP-1 cells, two PCRs were performed, the first one in order to amplify the targeted region and the second one to fluorescently label the DNA for the actual sequencing process. Both PCRs were followed by a purification of the DNA product.

Primers were designed using the National Center for Biotechnology Information (NCBI) Primer Blast tool and tested with DNA from unedited K562 cells with the approach described below. Different annealing temperatures (55 °C, 57 °C and 59 °C) were tested and the primer and annealing temperature that led to the strongest bands were chosen for further sequencing. The chosen primers and their sequences are shown in Table 7. Primer pair CSF1R_Seq1 was used for cells treated with sgRNA 1 – 4 which all target exon 2. Primer pair CSF1R_Seq4 for cells treated with sgRNA 5 which targets exon 15. The approach for the first PCR is shown in Table 8. It was prepared in microcentrifuge tubes placed on ice.

The samples were placed in a thermocycler and PCR was performed using the program shown in Table 9.

Table 7: Sequencing primers THP-1

Name	Sequence forward primer Sequence reverse primer
Primer CSF1R_Seq1	GGCTTTAGAAGGGCCCCAAA AAGCAGATACCCACAAGCCT
Primer CSF1R_Seq4	GCTCACAGAGCCGAGGTTAG CATGAGCCATCCAACCCTGA

Table 8: Composition of the PCR approach

Reagent	Amount
5x buffer	10 µl
DNTP	1 µl
Forward primer (5µM)	5 µl
Reverse primer (5µM)	5 µl
Gotaq G2 taq polymerase	0.25 µl
Template DNA	100 µl
H_2O	to 50 µl total

Table 9: PCR program

Temperature	Duration	Cycles
95°C	1 min	1x
95°C	15 s	
57°C	15 s	35x
72°C	30 s	
72°C	7 min	1x
4°C	forever	

The result of the PCR was assessed through electrophoresis on a 1.5% agarose gel containing 20 ml 10X TBE buffer, 180 ml water, 3 g agarose and 8 µl of Midori

Green. 10 µl of the PCR product, as well as 5 µl of the Gene Ruler were loaded to the gel. The electrophoresis was run at 120 V for approximately 60 min. Subsequently, it was assessed through imaging in the Molecular Imager GelDoc™ XR+. If bands could be seen for all samples, the next steps were performed.

For purification of the PCR product, 40 µl of a sodium acetate/ethanol mix (4% 3M sodium acetate in ethanol) were added to a microcentrifuge tube containing 20 µl of the PCR approach from the PCR described above. The samples were then centrifuged for at least 45 min at 3220 *g* at room temperature. Afterwards, the supernatant was discarded by covering the tubes with a cellulose cloth, turning them upside down and swinging them up and down. This was followed by a washing step with 100 µl 70 % ethanol that was added to the samples. They were then centrifuged at 3220 *g* at room temperature for 10 min. Subsequently, the supernatant was discarded in the same way as before. This washing step was repeated using the same amount of ethanol and the same centrifugation parameters. For the next centrifugation step the tubes were not closed and put upside down on a cellulose cloth. The samples were then centrifuged at 23 °C, 600 *g* for 1 min. Finally, 15 µl of Merck ultrapure water were added to the samples. The samples were then attached to a vortex mixer and mixed gently for 30 min.

A sequencing PCR was conducted in order to mark the PCR product. The approach for the sequencing PCR containing the reagents listed in Table 10 was prepared in microcentrifuge tubes placed on ice. The approach was prepared twice for each sample, once with the forward primer and once with the reverse primer. The samples were placed in a thermocycler with the program shown in Table 11.

Table 10: Composition of the PCR approach

Reagent	Amount
Purified PCR product	6 µl
Water	2.65 µl
White 5x buffer	1.65 µl
Sequencing primer (10 µM)	1 µl
BigDye v3.1	0.7 µl

Table 11: Sequencing PCR program

Temperature	Duration	Cycles
94 °C	1 min	1x
94 °C	10 s	
50 °C	5 s	30x
60 °C	4 min	
10 °C	forever	1x

The PCR product from the sequencing PCR was purified in the same manner as the product from the first PCR. The only difference was that only one washing step was performed.

For sequencing, 7 µl of the purified product from the sequencing PCR were added to the wells of a sequencing plate. Then, 15 µl of formamide were added. The samples were sequenced in a 3100 Genetic Analyzer.

The sequencing data was uploaded to the Synthego ICE tool.

2.2.1.6 Assessment of CSF1R expression on protein level

In order to isolate protein from the electroporated cells, the cell pellets were thawed and resuspended in 50 µl of RIPA buffer and 2 µl of protease inhibitor per pellet. Protein was isolated and the concentration was assessed by a BCA assay as described above.

CSF1R expression on protein level in the edited THP-1 cells was examined by Western Blotting. Western Blots were performed as described above with 40 µg of protein. As the protein concentration in the pellets from the second and third electroporation was considerably lower than the first one, only 20 µg of protein were used for these. For the transfer, PVDF membranes were used. The membranes were stained with 1:500 anti-CSF1R antibody solution and 1:50000 anti-GAPDH or anti-β-Actin respectively.

2.2.2 Methods Part II: Generation of homozygous and heterozygous CSF1R *iPSC knockout lines*

Ethical approval for the experiments conducted in iPSC was obtained from the ethics committee of the University Hospital Tübingen (project number 701/2019BO2).

2.2.2.1 iPSC cell culture

2.2.2.1.1 Thawing of iPSC

In preparation, the wells of a 6-well-plate were coated with 0.8 ml each of Matrigel diluted 1:60 in Dulbecco's Modified Eagle Medium F-12 (DMEM-F12). The plate was then incubated at 37 °C for 30 - 90 min. All media needed later on were warmed in the water bath at 37 °C.

The cryotubes containing the frozen iPSC were heated in the water bath at 37 °C until the content was slightly thawed. Subsequently, 1 - 2 ml of DMEM-F12 were added in small drops. The cells were cautiously resuspended and transferred to a 15 ml falcon containing 8 ml Essential 8 (E8) medium supplemented with 1:1 000 Rho-kinase inhibitor (RI). Cells were washed by carefully inverting the tube 3 times and then centrifuged at 300 *g* for 5 min.

Meanwhile, the Matrigel solution was removed from the plate and 1 ml of E8 medium supplemented with 1:1 000 RI) was added to each well. The supernatant was removed from the centrifuged falcons, the cells were resuspended in 1 ml E8 with 1:1000 RI and finally transferred to the prepared wells.

2.2.2.1.2 Cultivation and passaging of iPSC

IPSC were cultivated at 37 °C with medium changes every day. The morphology of the iPSC was evaluated by microscopy. Cells were passaged at a ratio of 1:8 to 1:12 when they reached a confluency of 70 - 80 %.

In order to passage the iPSC, they were first washed with 2 ml of DPBS per well. Subsequently, 1 ml of DPBS/EDTA was added to each well, followed by an incubation period at 37°C for 4 - 8 minutes. In the meantime, Matrigel-coated plates were prepared with 2 ml E8 and 1:1000 RI per well.

Once the beginning detachment of the cells was detected under the microscope, DPBS/EDTA was removed, 1 ml of pre-warmed E8 medium was added and the cell suspension was carefully pipetted up and down 3 - 5 times in order to break the colonies. Depending on the colony density, 1/8 to 1/12 of the cell solution was transferred to the new well.

Before freezing the iPSC, the cells were detached and centrifuged in the same way they were prepared for passaging. Subsequently, cells were centrifuged at 300 g for 5 min and the pellet was then resuspended in 2 ml of freezing medium and transferred to cryotubes. The tubes were then placed in a freezing container at – 80 °C overnight and transferred to the liquid nitrogen tank the next day for long term storage.

2.2.2.2 CRISPR approach

iPSC were edited by using two crRNAs to cut out a part of the *CSF1R* gene, which makes it possible to screen for homozygous and heterozygous knockout clones via PCR. The crRNAs used for this approach correspond with sgRNAs 2 and 4 (Figure 6). The two cutting sites are separated by 136 bp, i. e. a fragment of this size is removed from the *CSF1R* allele in case of successful CRISPR cutting at both sites.

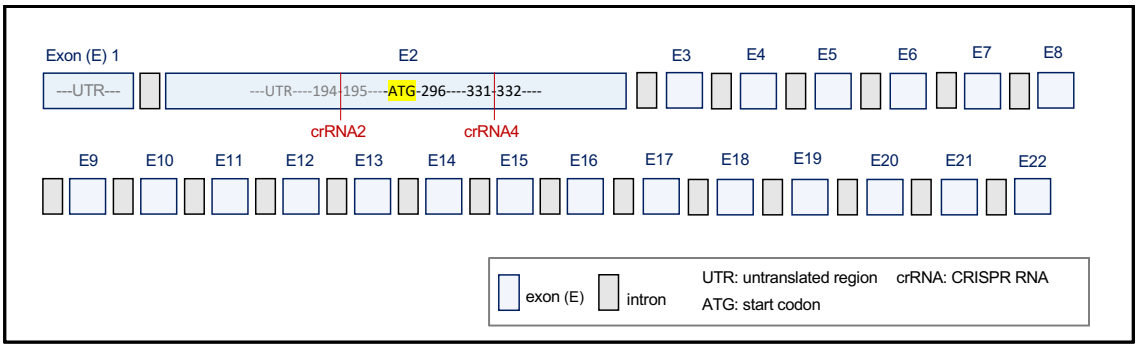

Figure 6: Positions of the crRNAs used for the CRISPR approach in iPSC. Both crRNAs are in exon 2, before and after the ATG, so that the start codon will be cut out when both cuts are made, thus preventing translation. The sizes of the intron and exon symbols are not true to scale.

In preparation for the transfection, the crRNAs were diluted to 50 µM. A solution was prepared containing 82 µl of the Lonza Nucleofection solution and 18 µl of Nucleofection supplement.

First, duplexes were prepared by adding 2.8 µl of a tracrRNA marked with the fluorophore ATTO 550 (50 µM) to 2.8 µl of crRNA2 and 2.8 µl of a tracrRNA

marked with the fluorophore ATTO 647 (50 µM) to crRNA7. These duplexes were incubated at 95 °C for 5 min and then cooled down to room temperature. Then, 1.7 µl of RNP Cas9 were added to each duplex. These complexes were incubated at room temperature for 20 min.
Meanwhile the cells were prepared. iPSC were washed once with 1 ml DPBS and detached by adding 1 ml Accutase. After 15 min of incubation at 37°C, the detachment was stopped by adding 1 ml of E8 medium. The cells were counted and the volume containing 900000 cells was centrifuged at 300 *g* for 5 min. The supernatant was removed and the cells were resuspended in the prepared solution. Both complexes as well as 2.9 µl of the Cas9 Electroporation Enhancer were added to the cells. The mix was transferred to a nucleofection cuvette and electroporation was performed using a Nucleofector 2b, program B16. Afterwards, the cells were transferred to a falcon with prewarmed E8 medium.
FACS was used to sort for cells positive for both fluorescent markers and thus containing both crRNAs. For this purpose, the cells were centrifuged at 100 *g* for 5 min and the pellet was resuspended in 200 µl of iPSC FACS buffer. The cells that screened double-positive in the FACS analysis were collected in 15 ml falcons containing E8 supplemented with 1 % P/S and 0,1 % RI and then transferred to a 10 cm Petri dish with the same medium. Approximately 20000 cells were plated per dish.

2.2.2.3 Selection of CSF1R *knockout clones*

When colonies had formed in the Petri dish, cells from each of these colonies were picked and transferred to one well of a Matrigel-coated 24-well-plate with E8 medium supplemented with 1 % P/S. Medium was changed every day until the cells were confluent.
For PCR-screening to detect the allele(s) shortened by removal of the DNA fragment between the two crRNA cutting sites, DNA was isolated using the Lucigen QuickExtract™ DNA Extraction Solution.
PCR was performed using the same protocol as for the PCR described in 3.3.4.2. with primer pair CSF1R_Seq7 and an annealing temperature of 59 °C. The se-

quences of the primers are shown in Table 12. DNA fragment sizes corresponding to wildtype or edited *CSF1R*, respectively, were analyzed using gel electrophoresis. This screening allowed to differentiate between wildtype clones with only one band corresponding to the original length of *CSF1R,* homozygous knockouts with only the band corresponding to the shortened version and heterozygous knockout with both bands.

Table 12: Sequencing primers iPSC

Name	**Sequence forward primer** **Sequence reverse primer**
Primer CSF1R_Seq7	TCTTCTCCCAAGACCCCTTGA GTCTAGTCTATCACTGTCCCCC

All clones that were screened positive for either homozygous or heterozygous knockout were expanded before the knockout state was confirmed by Sanger sequencing. To harvest the cells for DNA isolation, they were detached with DPBS/EDTA as described above (see 2.2.2.1.2.) and transferred to a 15 ml falcon. They were centrifuged at 300 *g* for 5 min and the supernatant was removed. DNA was isolated from the resulting pellet using the Gene JET Genomic DNA Purification Kit according to the manufacturer's protocol and as described above for THP-1 cells. Sequencing was then performed following the same protocol as for the sequencing of THP-1 cells with primers CSF1R_Seq7_F and CSF1R_Seq7_R. For the heterozygous clones, DNA from the two differently sized bands was extracted from the PCR gel using the QIAquick Gel Extraction Kit and treated separately for the rest of the sequencing. For this purpose, after the PCR that is performed as the first step of sequencing, the bands were separately cut out of the electrophoresis gel with a scalpel. Then, each gel slice was transferred to a microcentrifuge tube and 100 µl of Buffer QG per 100 µg sample were added. The samples were incubated at 50 °C with intermittent vortexing until the slice had dissolved. Depending on the colour of the mix, 3 M sodium acetate was added until the sample turned yellow. Subsequently, 100 µl isopro-

panol per 100 µg gel were added to the mixture. The samples were then centrifuged for 1 min at 17 900 *g* in a spin column with a collection tube, the flow-through was discarded. Next, 500 µl Buffer QG were added and the centrifugation step was repeated in the same way as before. 750 µl of Buffer PE were added and after an incubation time of 5 min at room temperature, the samples were again centrifuged at 17 900 *g* for 1 min. The flow-through was discarded and the spin column was placed in a new microcentrifuge tube. Finally, 50 µl Buffer EB were pipetted directly onto the spin column's membrane. After incubation for 4 min at room temperature, the tube was centrifuged for 1 min at 17900 *g*. Following this extraction, the samples were treated in the same way as the other DNA samples.

2.2.2.4 Off-target analysis

In order to evaluate off-target effects of the CRISPR/Cas9 system, the most probable off-targets were identified by the CRISPOR web tool. The off-targets identified this way as well as the respective Massachusetts Institute of Technology (MIT) off-target scores are listed in Table 13.

Table 13: Predicted off-target loci and corresponding MIT scores

off-target locus	MIT off-target score
crRNA 2	
RP11-393I2.4/ZNF292 (chromosome 6)	0.34
SLC43A1 (chromosome 11)	0.28
CYTH2 (chromosome 19)	0.25
AC068134.8/ALPP (chromosome 2)	0.12
MINK1 (chromosome 17)	0.11
crRNA 4	
PLD4 (chromosome 14)	1.49
ZNF407 (chromosome 18)	1.47
MATK (chromosome 19)	0.65
ANKDD1B (chromosome 5)	0.64
BBS7 (chromosome 4)	0.47

The top 5 exonic off-targets according to the MIT off-target score for each of the two sgRNAs were sequenced using specific primers. The primers were designed using the primer3 tool and NCBI Primer Blast. The primer sequences are listed in Table 14. Sequencing was performed in the same way as for the confirmation of the knockout status as described above.

Table 14: Sequencing primers off-targets

off-target	**forward primer** **reverse primer**
RP11-393I2.4/ZNF292	AAGTGGATAGGGAGAGAGCC AGAAGGGTGCAGAGTTTCCA
SLC43A1	GGCTTGCTGATGATTCCCAG ACTTCTGGTTTTCAAGCTCAGG
CYTH2	TGCATGCACGTGAACAAATG CCCATGTGCCTTTGGTGAAA
AC068134.8/ ALPP	TTCAGGTTCAGCTGTTTTGC GCTACTCGGGAGGCTGAAG
MINK1	AGGGAATTGGGAAGTTGGGA TTGGGACTACAGGCATGCA
PLD4	ACGCCATTACTTGCCATTGT GTCCTCTGCAAGCATCACAG
ZNF407	ACCTAGCAAGTCTACCCAGC CTGATCCTCCCTGCACTACC
MATK	CAGGCGCCTAGAGTCCTTAG GACCGAGAGAGTGGAGAGTG
ANKDD1B	CCCCTGACCACTCCACTATG CGTCCTTCCTTACCTCTCTCC
BBS7	GATGGCACCTTGAACTACTGT GAAGGGCAGACTCACGAATTT

2.2.2.5 Characterization of CSF1R *knockout iPSC clones*

In order to verify the pluripotent status of the iPSC after the genetic modifications, the cells were assessed for their expression of the surface protein alkaline phosphatase (AP) and pluripotency markers Oct3/4 and Tra1-81 on protein level, the transcriptional expression of pluripotency markers *OCT4*, *SOX2*, *KLF4*, *NANOG* and *TDGF1*, and their ability to spontaneously differentiate into all three germ layers. Furthermore, whole genome single nucleotide polymorphism (SNP) genotyping was performed by Life & Brain GENOMICS.

2.2.2.5.1 Expression of alkaline phosphatase (AP)

Alkaline phosphatase (AP) is an enzyme that is highly expressed in pluripotent stem cells (Stefkova et al., 2015). Naphtol AS-MX phosphate was used as a substrate for AP and the enzyme's activity was visualized by adding Fast Red.
For the evaluation of AP activity, iPSC were cultured on Matrigel-coated 24-well-plates. First, the cells were washed with 1 ml of DPBS and fixed with 4 % paraformaldehyde (PFA) at room temperature for 1 min. 60 µl of Naphtol AS-MX phosphate were mixed with 1 ml of Fast Red and 0.5 ml of the mixture were added to each well of iPSC. Following an incubation period of 15 - 30 min in the dark, the red staining was assessed visually.

2.2.2.5.2 Immunostaining for pluripotency markers

The iPSC clones were stained for pluripotency markers Tra1-81 and Oct3/4. 4',6-diamidino-2-phenylindole (DAPI) was used to stain nuclear DNA.
For immunostaining, the iPSC were cultured on Matrigel-coated coverslips in 24-well-plates. After fixation with 4 % PFA for 15 min at 37 °C, the cells were washed with DPBS three times. Subsequently, 500 µl of DPBS-T supplemented with 5 % FCS were added to each well for blocking and permeabilization. Following an incubation period of 45 min, the fluid was removed. The primary antibodies were diluted 1:50 (Oct3/4) or 1:500 (Tra1-81) in DPBS-T with 5 % FCS. 70 µl of the respective antibody dilution were pipetted onto each coverslip. The coverslips were then left to incubate overnight at 4 °C in a moist chamber. The next day, the coverslips were again transferred to the 24-well-plate and washed three times

with PBS by adding 0.5 ml of DPBS to each well and removing it after 5 min. Then, 70 µl of a 1:1000 dilution of the secondary antibody in DPBS-T were pipetted onto the coverslips. From that moment on, the coverslips were kept in the dark. After an incubation period of 45 min at room temperature the coverslips were again washed three times with DPBS for 5 min each time as described above.

Subsequently, the coverslips were incubated first with another 70 µl of the primary antibody solution for 1 h at 37 °C and secondly with 70 µl of the secondary antibody dilution for 1 h at room temperature. After each of the incubation periods, three washing steps of 5 min each followed. Finally, 0.5 ml of PBS-T with 1:10 000 DAPI and 1:250 RNAse A were added to each well containing a coverslip. 15 min later, the coverslips were washed three times with DPBS and mounted on the slides using one drop of mounting medium per coverslip.

2.2.2.5.3 Evaluation of transcriptional expression of pluripotency markers by real time polymerase chain reaction (RT-PCR)

The expression of the transcripts of pluripotency genes *OCT4, SOX2, NANOG*, *TDGF1* and *DNMT3B* as well as oncogenes *KLF4* and *cMYC* in the iPSC clones was assessed on RNA level by means of RT-PCR and compared to the expression pattern of an untreated iPSC line, two human embryonic stem cell (hESC) lines and a fibroblast control.

RNA was isolated using the RNeasy Mini Kit according to the manufacturer's instructions. The iPSC were first washed with 2 ml of DPBS and then lysed by adding 350 µl of Buffer RLT per well. The contents of the well were transferred to a 1.5 ml microcentrifuge tube to which 350 µl of 70 % ethanol were added. The sample was transferred to a spin column in a collection tube and centrifuged for 15 s at 12 000 *g*. In the next steps first 700 µl of Buffer RW1 and then 500 µl of Buffer RPE were added to the column, each followed by a 15 s centrifugation step at 12 000 *g*. Subsequently, another 500 µl of Buffer RPE were added and the sample was centrifuged for 2 min at 12 000 *g*. In order to completely dry the membrane, the column was again centrifuged for 1 min at 12 000 *g*. After placing the column in a new collection tube, 30 µl of RNAse-free water was pipetted onto

the column membrane and the tube was centrifuged for 1 min at 12 000 *g*. RNA concentration was measured using the Nano Drop spectrophotometer.

Subsequently, RNA was reverse transcribed to copy DNA (cDNA) using the Revert Aid First Strand cDNA Synthesis Kit according to the manufacturer's instructions. All the reagents were kept on ice during the whole process except for the incubation times. First, water was added to 250 ng of the isolated RNA and 1 µl of Oligo $(dT)_{18}$ primer for a total volume of 12 µl. The mixture was incubated at 65 °C for 5 min and spun down. 4 µl of 5X Reaction Buffer, 1 µl of RNAse Inhibitor, 2 µl of dNTP Mix and 1 µl of Reverse Transcriptase were added to the vial. The contents were mixed carefully by pipetting up and down and spun down. Finally, the samples were incubated for 60 min at 42 °C and then for 5 min at 70 °C. The cDNA was stored at - 20 °C until being used for the RT-PCR.

The RT-PCR was performed in triplicates of each of the assessed genes for the knockout iPSC clones, the iPSC control, a fibroblast control and two hESC lines. A master mix containing 125 µl of SYBR Select Master Mix and 1 µl each of the forward and reverse primer diluted to 2 µM was prepared for each of the targets and transferred to the wells of a 96-well-plate. 3 µl of 1.25 ng/µl cDNA of the respective sample were added to the well. The primers and corresponding sequences are listed in Table 15. The RT-PCR was conducted with the program shown in Table 16. The CT values were normalized to hESC H9 as reference and GAPDH as housekeeping gene using the Quant Studio software.

Table 15: RT-PCR primers

Name	**forward primer** **reverse primer**
OCT4	GGAAGGTATTCAGCCAAACG CTCCAGGTTGCCTCTCACTC
SOX2	AGCTCGCAGACCTACATGAA CCGGGGAGATACATGCTGAT
KLF4	CCCCAAGATCAAGCAGGAGG GGGCAGGAAGGATGGGTAAT
NANOG	CAAAGGCAAACAACCCACTT

	TGCGTCACACCATTGCTATT
TDGF1	GGTCTGTGCCCCATGACA
	AGTTCTGGAGTCCTGGAAGC
DNMT3B	GAGATCAGGATGGGAAGGA
	ATAGCCTGTCGCTTGGA
cMYC	GACTCTGAGGAGGAACAAGA
	TGATCCAGACTCTGACCTTT

Table 16: RT-PCR program

Temperature	Duration	Cycles
50 °C	2 min	1 x
95 °C	2 min	
95 °C	1 sec	
60 °C	30 sec	40x
72 °C	5 sec	
95 °C	15 sec	
60 °C	1 min	1x
95 °C	15 sec	

2.2.2.5.4 Spontaneous differentiation into all three germ layers

Pluripotent stem cells are able to differentiate into all thee germ layers, therefore spontaneous differentiation into these layers was used to further evaluate the pluripotency of the iPSC clones. The differentiation was confirmed by immunostaining for specific markers: FoxA2 and Sox17 for endodermal differentiation, smooth muscle antigen (SMA) for mesodermal differentiation and βIII-tubulin (TUJ) for ectodermal differentiation.

For the endodermal differentiation, 200000 cells per well for each clone were plated on coverslips in 4 wells of a 24-well-plate and cultured in E8 medium with 1:1000 RI for one day. The next day, the medium was changed to primitive streak induction medium (see 2.1, Table 2). Subsequently, for 4 days, medium changes were performed every day with endoderm induction medium (see 2.1, Table 2).

The following day, the cells were washed with DPBS, fixed with 4 % PFA for 15 min at 37 °C and stored at 4 °C until being stained.

For meso- and ectodermal differentiation, iPSC were cultured in Aggrewell plates with embroid body (EB) medium (see 2.1, Table 2) for mesodermal differentiation and EB medium supplemented with SB431542 and LDN-193189 for ectodermal differentiation. The plates were pre-treated with Anti-Adherence solution according to the manufacturer's instructions and 1.2 million cells per well were seeded for each line and for each of the two conditions. ½ of the medium was changed every day and the formation of EBs was examined under the microscope. After 2 – 3 days, when EBs had formed, they were collected and incubated as free-floating conglomerates in an uncoated petri dish for 5 hours at 37 °C. Subsequently, 10 - 12 EBs were plated onto 0.1 % gelatin coated coverslips for mesodermal condition and 1:30 Matrigel coated coverslips for ectodermal condition. For the following two weeks medium changes were performed with mesoderm medium or 3N (ectodermal differentiation) (see 2.1, Table 2) every other day. Afterwards, they were washed, fixed and stored in the same way as the cells from the endodermal differentiation.

Finally, cells from all three spontaneous differentiation were immunostained according to the protocol described in chapter 3.4.4.2. The primary antibody solutions used for the staining were 1:300 FoxA2 and 1:250 Sox17 for endodermal differentiation, 1:100 SMA for mesodermal and 1:1000 TUJ for ectodermal differentiation.

2.2.2.5.5 Whole genome single-nucleotide polymorphism (SNP) genotyping

DNA from all iPSC clones and the unedited control was sent to Life & Brain for whole genome single-nucleotide polymorphism (SNP) genotyping.

3 Results

3.1 Testing of sgRNAs in THP-1 cells

3.1.1 SgRNA design

Several online tools with different ranking algorithms were used to design five sgRNAs. The most important factors for the ranking in each tool were the efficiency and specificity of the guide RNA. Selected efficiency and specificity scores for the chosen sgRNAs are shown in Table 17. The Doench ’16 efficiency score (Doench et al., 2016) is indicated in the results of both, the CRISPOR and the chopchop tool (Concordet & Haeussler, 2018; Labun et al., 2019). The Moreno-Mateos score (Moreno-Mateos et al., 2016) as well as both, the MIT and cutting frequency determination (CFD) specificity score (Doench et al., 2016; Haeussler et al., 2016; Hsu et al., 2013) are shown on the CRISPOR website. All the listed scores rank the guide RNA on a scale from 0 – 100, with 100 being the best score that can be obtained. The first selection criterion was the highest possible specificity score, followed by the highest possible efficacy score.

Table 17: SgRNA efficacy and specificity scores

	efficacy scores		**specificity scores**	
	Doench ‘16	**Moreno-Mateos**	**MIT**	**CFD**
sgRNA 1	47	73	44	72
sgRNA 2	47	49	84	93
sgRNA 3	49	59	82	89
sgRNA 4	34	45	49	75
sgRNA 5	70	35	91	94

3.1.2 Selection of a CSF1R expressing cell line and optimization of CSF1R Western Blot

To optimize CSF1R Western Blot, a cell line robustly expressing CSF1R protein was selected. Two cell lines, THP-1 and K562, were tested. As both of these are monocytic cell lines, they were expected to express CSF1R (see 2.2.1.2). Figure

7 shows the results of the performed Western Blots in THP-1 cells and K562 cells, with THP-1 cells showing a reliable, concentration-dependent expression of CSF1R protein. For the optimization of the Western Blot protocol, different antibody concentrations, membrane types, and protein amounts were tested.

For antibody concentration, 1:500 was found to be the optimal dilution for the anti-CSF1R antibody (Figure 7). In Western Blots using a lower anti-CSF1R antibody concentration, no bands could be detected, whereas the results with higher concentrations were comparable to those depicted below (Figure 6/data not shown).

For the selection of a suitable Western Blot membrane, PVDF and Nitrocellulose were tested. Figure 7 A shows the Western Blot performed with a PVDF membrane, Figure 7 B the one performed with a Nitrocellulose membrane. The housekeeping protein GAPDH was used as a positive control. GAPDH band intensity did not reliably correlate with the loaded protein amount (20 µg, 40 µg or 60 µg) on neither membrane type, with the exception of the western blot performed with protein extracted from THP-1 cells and blotted on nitrocellulose membrane (Figure 7 A and B). However, on both membranes, GAPDH was detected at the expected protein size of 37 kDa in all samples. The missing correlation of protein amount and band intensity is likely a result of antibody saturation due to the high abundance of the housekeeping protein GAPDH. CSF1R protein could only be detected on the PVDF membrane, but not on the Nitrocellulose membrane.

Regarding the two cells lines tested for CSF1R protein expression, bands for CSF1R could only be seen in THP-1 samples (100 kDa and approximately 125 kDa), but not in protein isolated from K562 cells. Concerning the protein concentration, there was a clear dose-dependent difference in the intensity of the CSF1R bands that correlated with the protein amount: the 60 µg sample showed the strongest band whereas the 20 µg sample was the faintest.

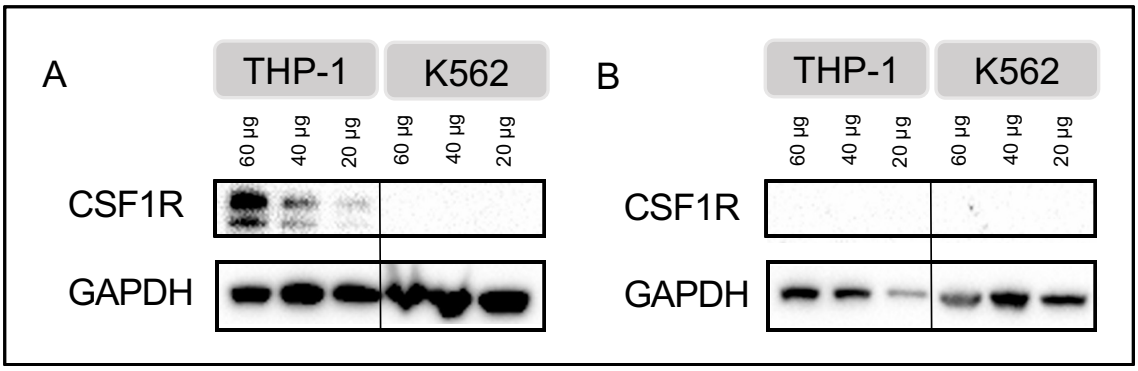

Figure 7: CSF1R Western Blots. Western Blots of CSF1R protein in THP-1 and K562 were performed with a PVDF membrane (A) and a nitrocellulose membrane (B) using an antibody dilution of 1:500 for CSF1R and 1:100000 for GAPDH as a housekeeping control. Protein samples with different amounts of protein ranging from 20 µg to 60 µg were used.

3.1.3 Transfection efficiency

As a first step towards optimizing the CRISPR/Cas9 system for *CSF1R* knockout, the transfection efficiency via electroporation was evaluated by electroporating cells with DNA encoding eGFP. Efficiency was then determined by measuring the green fluorescence of cells transfected with eGFP using flow cytometry.

Figure 8 shows the flow cytometry data of cells transfected with eGFP in triplicates from all three electroporations as well as the negative control. Electroporation settings are described in section 2.2.1.3. EGFP was detected in channel FL1. The transfection efficiency was determined by calculating the difference between eGFP positive cells (Q2 and Q3) in transfected cells compared to control cells. The transfection efficiency was on average 99.12 ± 0.21 % (mean ± standard deviation (SD)) in the first run (95% confidence interval (CI) 98.89-99.36 %), 98.86 ± 0.62 % in the second run (95% CI 98.23-99.48 %) and 97.27 ± 3.77 % in the third run (95% CI 90.25-97.78 %). The mean transfection of all three runs was 98.42 ± 3.25 %.

The applied electroporation settings were used for all further experiments.

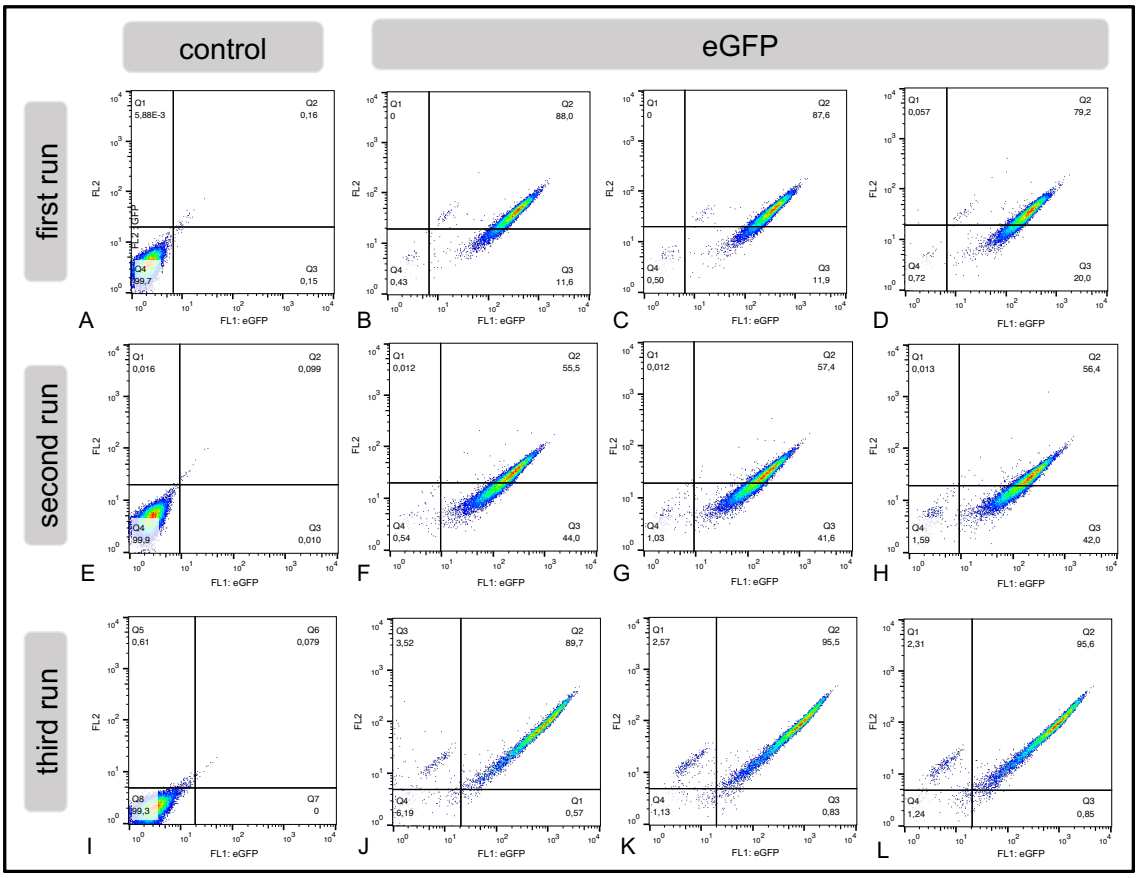

Figure 8: eGFP flow cytometry. Green fluorescence was measured in negative control (A, E, I) and in triplicates of THP-1 cells transfected with eGFP (B-D, F-H, J-L) from three electroporation runs by flow cytometry. The green fluorescence signal is detected in the FL1 channel.

3.1.4 CSF1R *assessment on DNA level*

In order to evaluate the efficiency of the designed sgRNAs, THP-1 cells were electroporated with a complex of Cas9 and one of the five sgRNAs as described in the Method section 2.2.1.3. After cell proliferation and DNA isolation, *CSF1R* DNA was sequenced to determine the indel frequency as a measure for the sgRNA/Cas9 complex cutting efficiency.

Figure 9 shows a representative image of the PCR performed as the first step of the sequencing protocol. For all cells treated with sgRNAs a well as the negative control, DNA from each triplicate was PCR-amplified. The successful performance of the first step of the sequencing PCR was confirmed by gel electrophoresis, which showed a strong band at the expected band size of 522 bp in all samples treated with primer pair CSF1R_Seq1 and at the expected size of 389 bp in samples treated with primer pair CSF1R_Seq4.

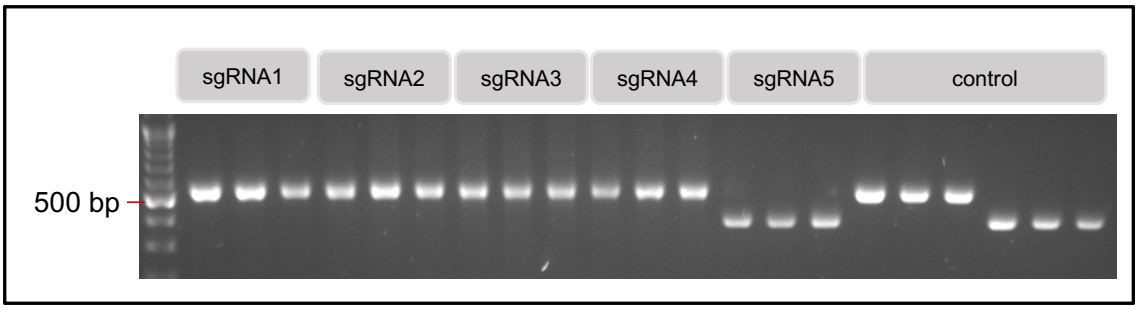

Figure 9: PCR for sequencing of transfected THP-1 cells. DNA for the PCR was isolated from each triplicate treated with different sgRNAs as well as from untreated control cells. The targets for sgRNA 1 - 4 are all in the same exon so that the same primer was used. SgRNA 5 targets a different exon so that a different primer was used. The control DNA was sequenced with both primer sets.

Sequencing was then completed as described in 2.2.1.5.2. The sequencing data was uploaded to the Synthego ICE tool in order to analyze indels in *CSF1R* induced by the CRISPR/Cas complex containing the different sgRNAs.

Figure 10 shows exemplary results from ICE analysis for cells treated with sgRNA1 in the first run. Graph A depicts the frequency of indels by indel size. Negative values on the x-axis correspond to deletions, positive values to insertions. The exact insertions and deletions found in the DNA are depicted in Figure 10 B as well as the percentage of DNA that had this specific insertion or deletion. These two figures show that in 86 % of the sequenced DNA insertions or deletions could be found, whereas in 9 % of the DNA there were no changes to the DNA sequence in comparison to the unedited negative control. In Figure 10 C, the sequence is visualized, the upper sequence depicts the sequence of the DNA isolated from cells treated with sgRNA1. The lower sequence is the one from the negative control.

The sequence visualized in Figure 10 C shows that before the predicted cutting site, the sequence is very clear and matches the one of the untreated negative control. Starting at the cutting site however, the peaks in the DNA from the edited cells are much lower and the sequence is much less clear, there are often several peaks at the same place. Furthermore, the bases with the highest peaks do not match the control sequence anymore. This corresponds with the insertions and deletions presented in Figure 10 B.

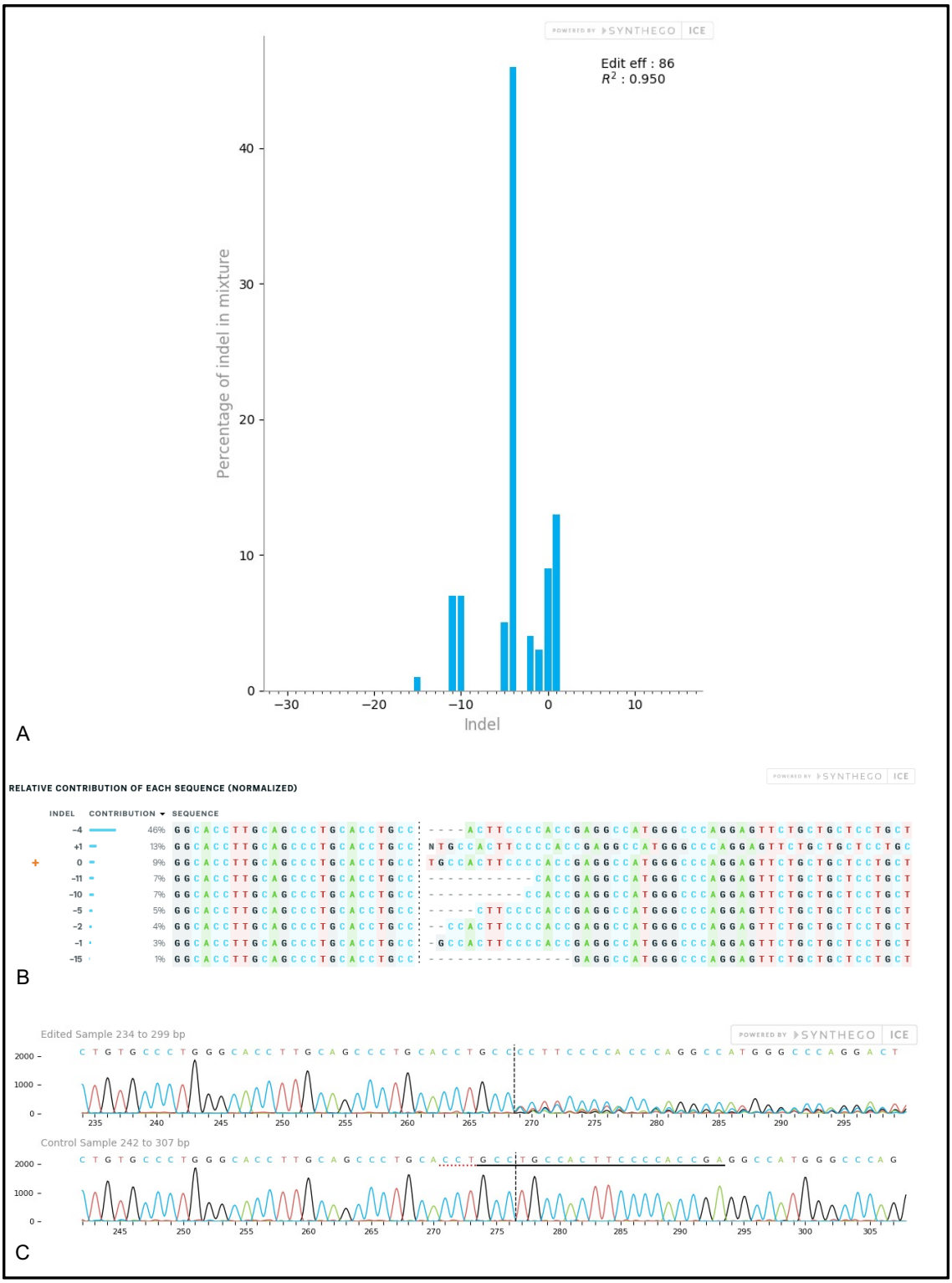

Figure 10: ICE analysis. Exemplary results from ICE analysis from one triplicate of cells treated with sgRNA1 in the first electroporation. Graph A shows the indel sizes found in the sequence on the x-axis, the frequency of these indel sizes is shown on the y-axis. The sequences of these indels are depicted in B, again with percentage of DNA that they were found in. The pooled sequence is shown in C, the upper sequence is from the edited cells, the lower one from the negative control. The letters over the sequence mark the base with the highest peak. The underlined sequence in the control marks the sgRNA's target, the NGG is underlined in red. The vertical dotted line marks the predicted cutting site.

In Figure 11 the sequence alignments for THP-1 cells treated with each of the sgRNAs in the first electroporation are shown. Similarly to the sequence of cells treated with sgRNA 1 described above, in THP-1 transfected with sgRNA 2 (Figure 11 B), 3 (Figure 11 C) and 4 (Figure 11 D), indels were detected in the sequencing data. In contrast, no such change was observed in the DNA from cells edited with sgRNA 5 (Figure 11 E). These sequences remained clear, the peaks remained high and the sequence still corresponded to the negative control even after the sgRNA's cutting site.

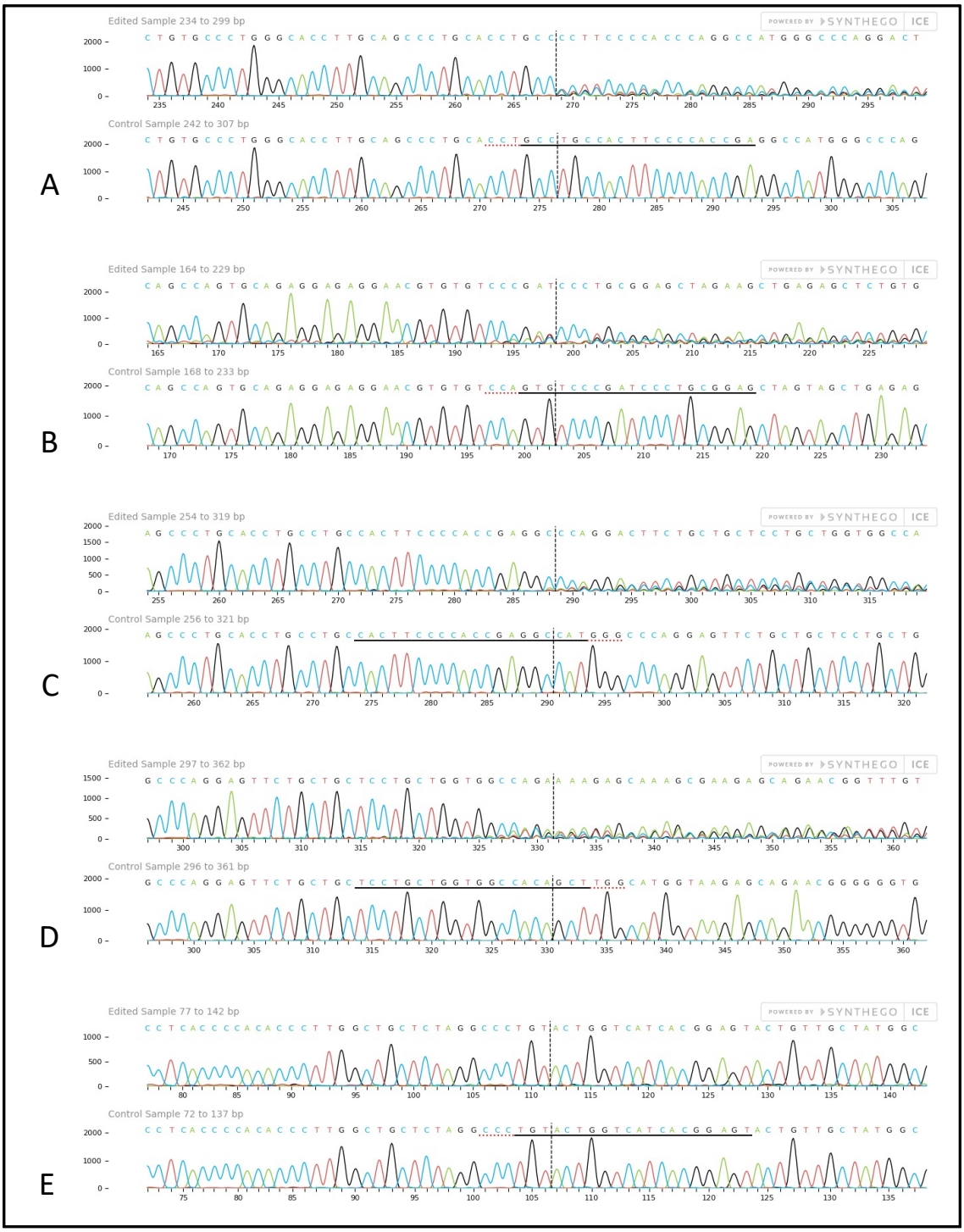

Figure 11: ICE alignment results from the first electroporation. Sequences from cells edited with sgRNA 1 (A), 2 (B), 3 (C), 4 (D) and 5 (E) in the first electroporation were aligned with the sequence from untreated control cells. The upper sequence is from the edited cells, the lower one from the negative control. The underlined sequence in the control marks the sgRNA's target, the NGG is underlined in red. The vertical dotted line marks the predicted cutting site.

Figure 12 shows the indel score calculated by the ICE tool which corresponds to the percentage of the analyzed DNA that contained insertions or deletions. The

indel scores confirmed the results from the visualized sequences on a quantitative level: sgRNAs 1, 2, 3 and 4 had high indel scores in all three electroporation whereas sgRNA 5 did not have an effect on the DNA.

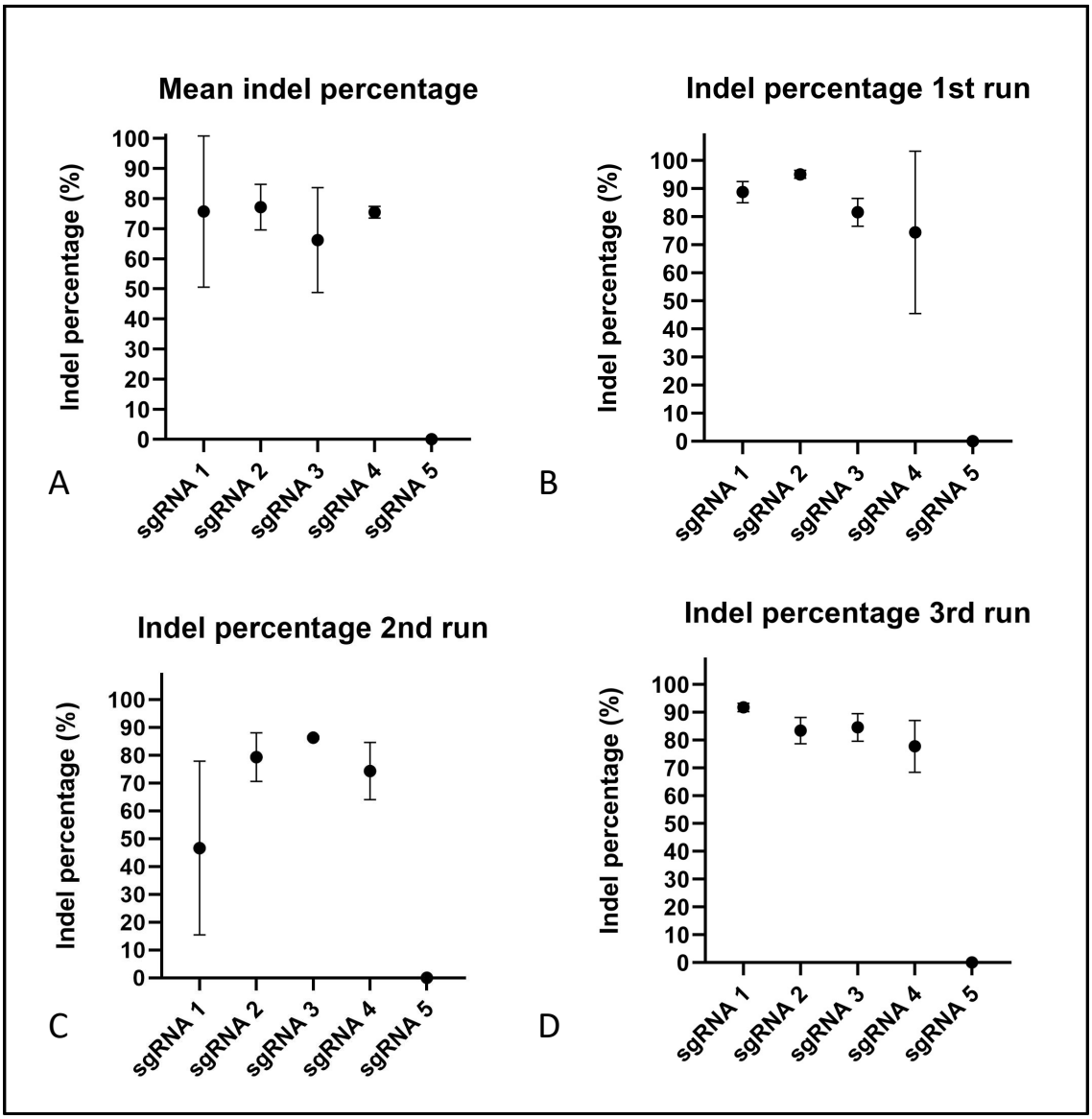

Figure 12: Mean indel percentages and standard deviation. Mean indel percentages were calculated for all three runs (A) and the runs separately (B-D). Indel percentages were taken from the ICE analysis of DNA sequences of edited THP-1 cells with sgRNA 1-5. The graphs show the percentage of insertions and deletions that were found in the DNA of cells treated with the respective sgRNA.

3.1.5 CSF1R expression on protein level

In order to evaluate the effect the observed DNA changes had on protein expression of CSF1R, Western Blots were performed with protein isolated from electroporated cells and the negative control. The optimized Western Blot protocol was used as described in 2.2.1.2 and 2.2.1.6. GAPDH and β-Actin were used as

housekeeping controls. As expected, CSF1R was detected in the negative control as well as in the cells treated with sgRNA 5 which did not induce any changes on DNA level (see 3.1.4). CSF1R was not expressed in cells treated with sgRNA 3 and 4 but could still be detected in cells treated with sgRNA 1 and 2.

Figure 13 shows one of the membranes from the second electroporation after staining with Ponceau solution. The protein standard on the left side of the membrane was used to estimate the size of the proteins blotted on the membrane. On the membrane shown here, protein was detected in the Ponceau staining for all samples, although there were differences in intensity. The first triplicate of sgRNA4 and the second triplicate of the control showed fainter bands than the other samples. Furthermore, the intensity of the bands varied depending on the size of the proteins, the strongest bands were observed between 75 kDa and 25 kDa.

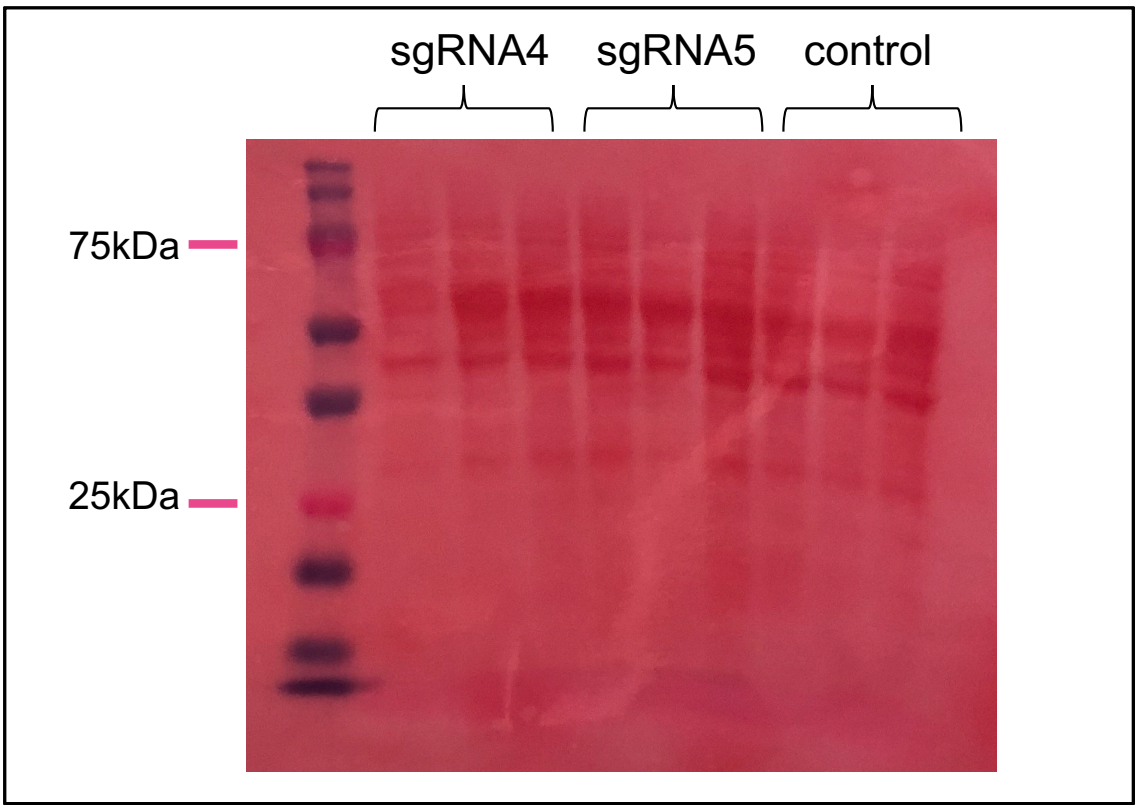

Figure 13: Ponceau staining. Representative picture of a membrane after staining with Ponceau solution. This membrane was used in the second electroporation and contains the protein samples from the THP-1 cells electroporated with sgRNA 4, sgRNA 5 and the negative control as well as protein standard on the left side. All samples were analysed in triplicates.

The data from the Western Blot itself is shown in Figure 14. When compared to the protein standard, the bands for CSF1R and GAPDH respectively were found at the expected protein sizes (CSF1R: double band, 100 kDa and approximately 125 kDa; GAPDH: 37 kDa). The band for β-Actin in the Western Blot with the samples from the third electroporation was detected at the expected height corresponding to its molecular weight of 42 kDa.

The Western Blot data showed irregular bands for GAPDH, which was used as positive control in the first two runs. These differences are likely either due to variations in protein concentration, irregularities during the blotting process or insufficient binding of the GAPDH antibody, or a combination hereof (see also Discussion). Due to this variation, β-Actin was used as a control in the third Western Blot. Though some variation in band intensity was detectable for this housekeeping protein as well, the bands were stronger and clearly discernible.

CSF1R protein was only detectable in some of the samples treated with sgRNA, while it was clearly discernible in the control cells of all three Western Blots.

In samples from the cells treated with sgRNAs 1, 2 and 5, CSF1R was also detectable in all samples, although with varying intensity: there was almost no reduction in protein amount in cells treated with sgRNA 1 and 5, and a moderate reduction in cells treated with sgRNA 2. In contrast to that, in cells treated with sgRNA 3 and 4, CSF1R could not be detected in any of the samples in either of the runs, even when the same samples showed very distinct bands for GAPDH or β-Actin.

In summary, efficiency of CSF1R knockdown on protein levels was highest for sgRNA 3 and 4, and moderate for sgRNA 2.

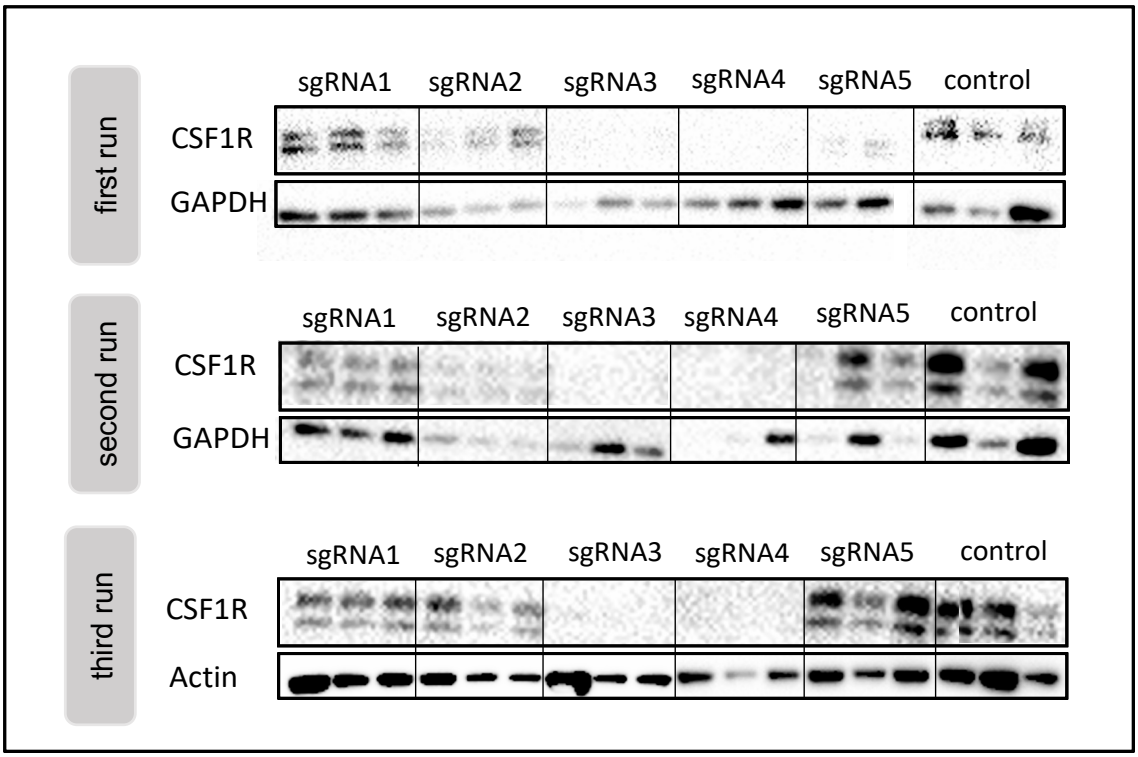

Figure 14: Western Blot data from three independent electroporations. Protein samples were taken from triplicates treated with sgRNA1 - 5 respectively as well as an untreated negative control. Membranes were stained for CSF1R and for GAPDH or Actin as housekeeping gene.

3.2 Generation of CSF1R iPSC knockout lines

3.2.1 Cell culture

For the generation of homozygous and heterozygous *CSF1R* iPSC knockout lines, iPSC were cultured as described in 2.2.2.1.2.

The iPSC exhibited the characteristic phenotype of pluripotent stem cells, growing in regularly shaped colonies with defined edges. Exemplary pictures of iPSCs derived from Clone 40 and Clone 75 are shown in Figure 15. In both pictures the formation of colonies was visible. In the sample shown in the picture of Clone 75, the cell density was much higher, so that confluency between the colonies can be observed.

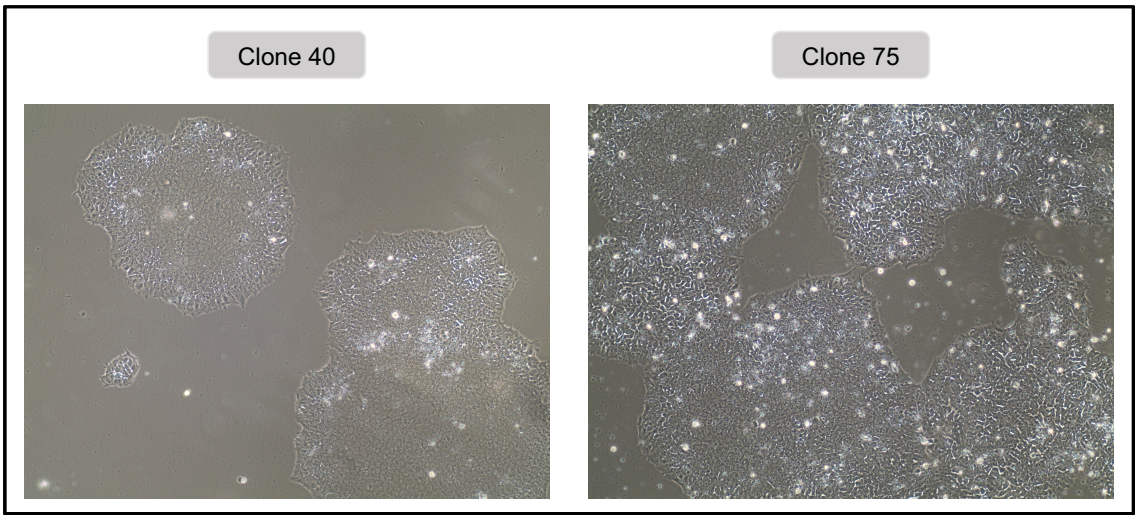

Figure 15: Cell culture images. Clone 40 and clone 75 were examined for their stem cell morphology by microscopy.

3.2.2 Clone selection

In order to generate *CSF1R* knockout lines, iPSC were transfected with sgRNA 2 and 4 simultaneously. Both sgRNAs had shown high cutting efficiency in THP-1 cells, and due to the position of their cutting sites, the combination of these guides was expected to result in the excision of a 136 bp fragment of the *CSF1R* gene including the start codon, so that transcription of the gene would be prevented. Most importantly, the excision of the gene fragment also made it possible to use PCR screening to select clones with successfully edited *CSF1R* genes. The unedited gene has an amplicon length of 734 bp, whereas the amplicon of the edited gene is only 598 bp long. Even though on protein level the knockdown efficiency of sgRNA 3 was higher than that of sgRNA 2, the removed fragment using sgRNA 3 and 4 would only be 60 bp in length; this would have impaired a PCR-based screening, as distinction between a 734 bp and a 674 bp DNA fragment via gel electrophoresis is not precise enough.

Figure 16 shows the results from the PCR screening. Two sizes of bands were seen: the upper band represents the unedited *CSF1R*, with an amplicon length of 734 bp. The lower band is shorter and represents the amplicon of the DNA where the segment between the crRNAs was cut out. This amplicon is therefore only 598 bp long.

In the PCR screening for *CSF1R*, for 10 clones only the shorter band was detected (homozygous knockout clones), 19 clones showed a double band containing both versions of *CSF1R* (heterozygous knockout clones) and 22 clones were found to only contain the longer band (wildtype clones). For 5 clones, no clear bands were detected.

Two homozygous knockout clones (clones 12 and 40) as well as two heterozygous knockout clones (clones 18 and 75) were used for further experiments.

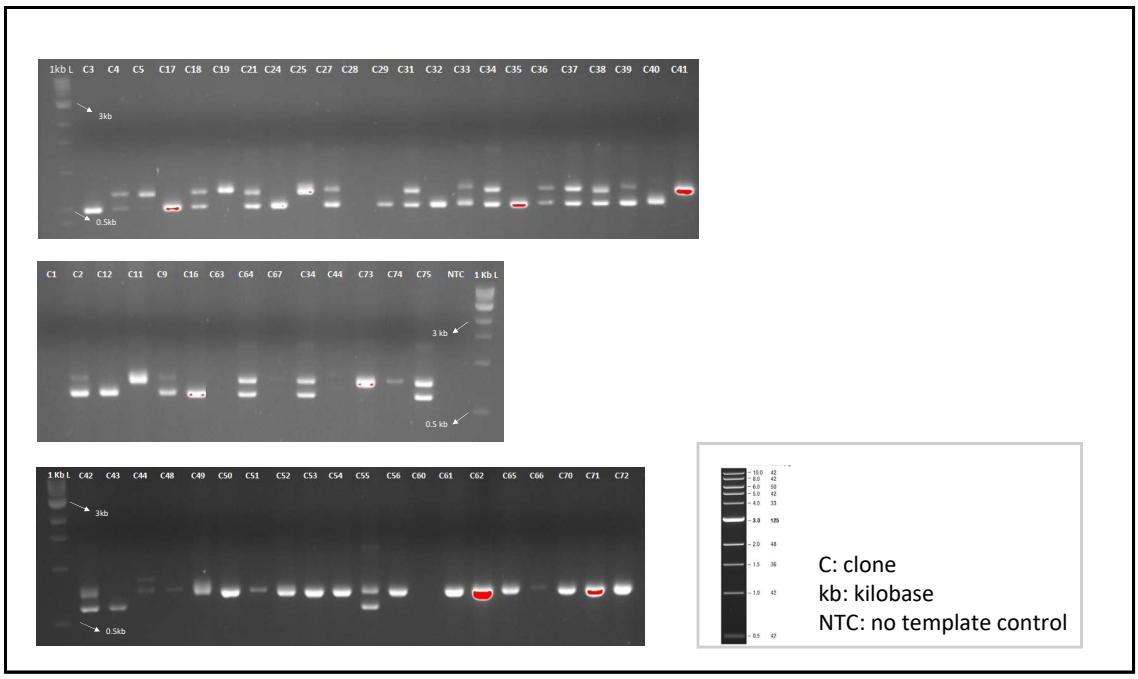

Figure 16: PCR screening for *CSF1R* of expanded iPSC clones. A PCR was performed with the transfected clones. Wildtype clones only have the longer (upper) band, homozygous knockouts only the shorter (lower) band, heterozygous clones show a double band.

Following the PCR screening, sequencing of selected homozygous and heterozygous clones was performed as described in 2.2.2.3. For the heterozygous clones, DNA from the two differently sized bands was extracted from the PCR gel to allow separate sequencing of the two bands. The sequences of the edited clones were then compared to the reference genome. The sequencing data confirmed the homozygous and heterozygous knockout states for the four chosen clones.

The sequence of the clones that were screened homozygous is shown in Figure 17. As can be seen here, the DNA sequence of the edited clones corresponded

to that of the reference genome until reaching the cutting site of sgRNA 2. The following sequence corresponded to the sequence starting at the cutting site of sgRNA 4 in the reference genome.

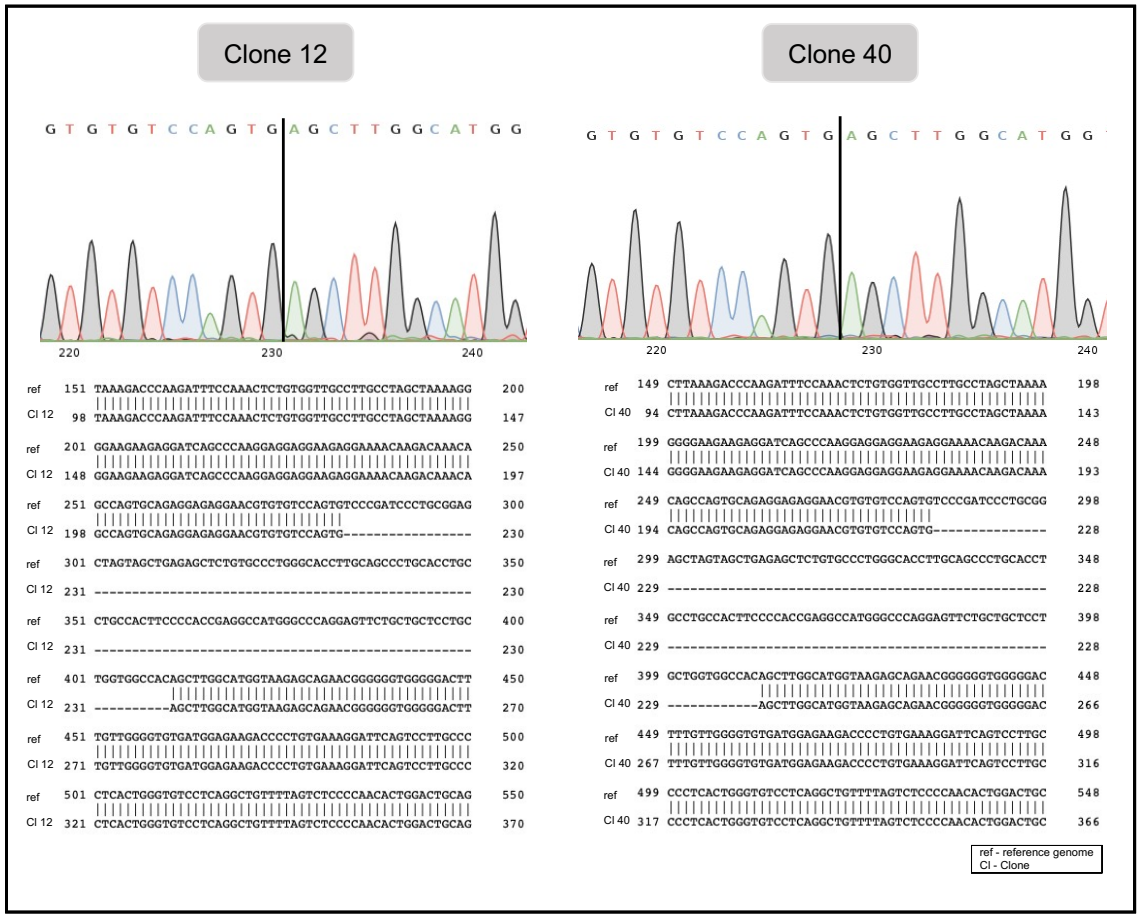

Figure 17: Sequences and alignments of homozygous knockout clones. DNA sequences of the homozygous knockout clones and alignment of DNA from the clones with the reference genome. The vertical line in the sequence trace marks the cutting site of the crRNAs, before this the sequence matches the control sequence until the cutting site of crRNA 2, afterwards it matches the control sequence from the cutting site of crRNA 4 onwards. Figure modified from own publication (Schmitz et al., 2023).

Figure 18 shows the alignment of the DNA sequences of the heterozygous clones with the reference genome. The DNA from the upper band in the gel electrophoresis aligned perfectly with the reference DNA. In contrast, for the DNA from the lower band the same effect as for the homozygous knockout clones was observed, that is, the segment between the cutting sites of sgRNA 2 and sgRNA 4 is missing.

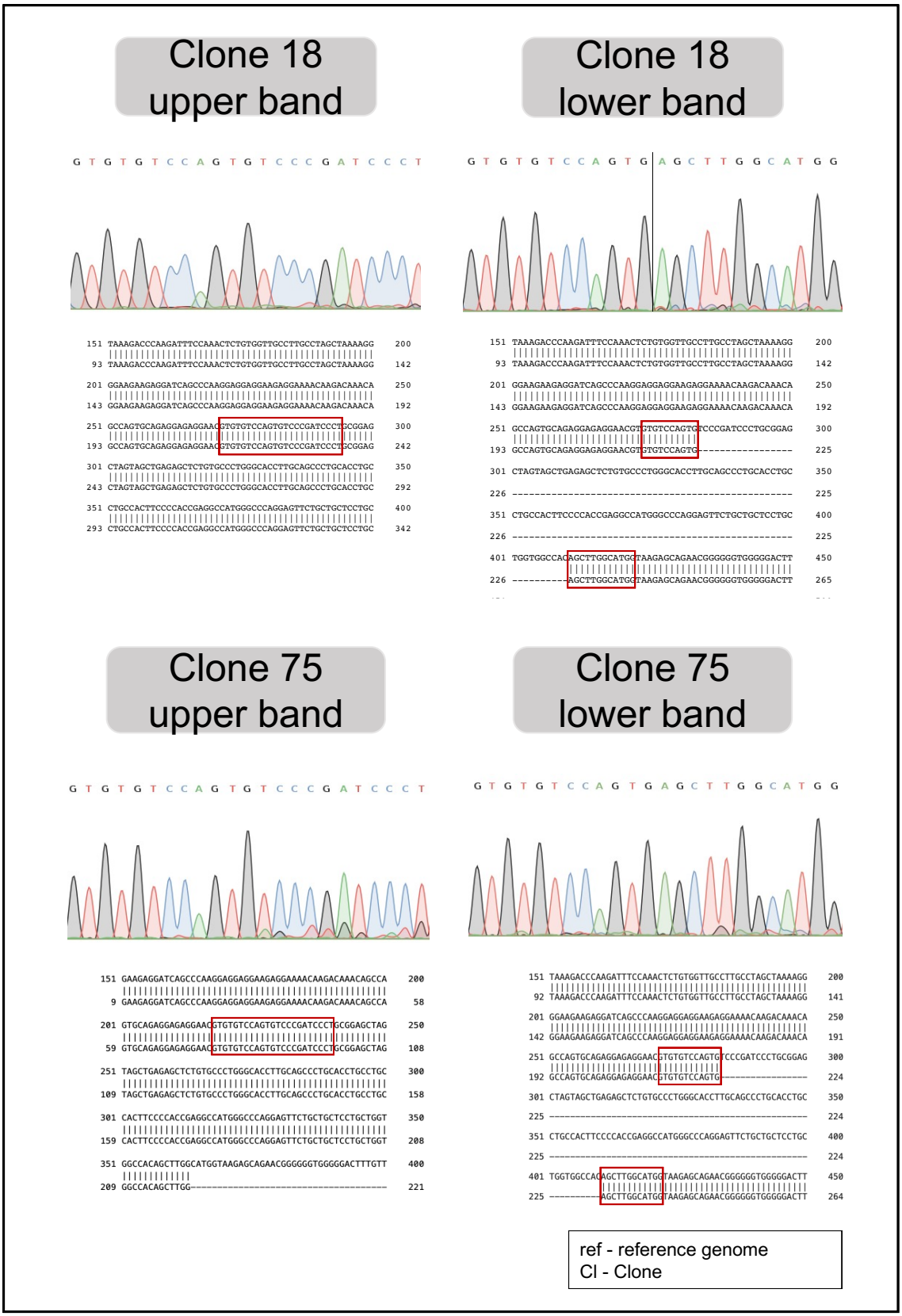

Figure 18: Sequences and alignments of heterozygous knockout clones. DNA sequences of the heterozygous knockout clones and alignment of DNA from each band from both clones with the reference genome. The depicted sequences are marked in red in the alignment. Figure modified from own publication (Schmitz et al., 2023).

3.2.3 Off-target analysis

In order to evaluate possible off-target effects of the CRISPR approach, the top 5 most probable off-targets were determined using the CRISPOR website's MIT score as described in 2.2.2.4. The identified loci were then sequenced and compared to the reference genome. The analysis did not reveal any off-target effects. Figure 19 shows representative sequencing data from Clone 12 for *SLC43A1* aligned with the reference sequence for the same target.

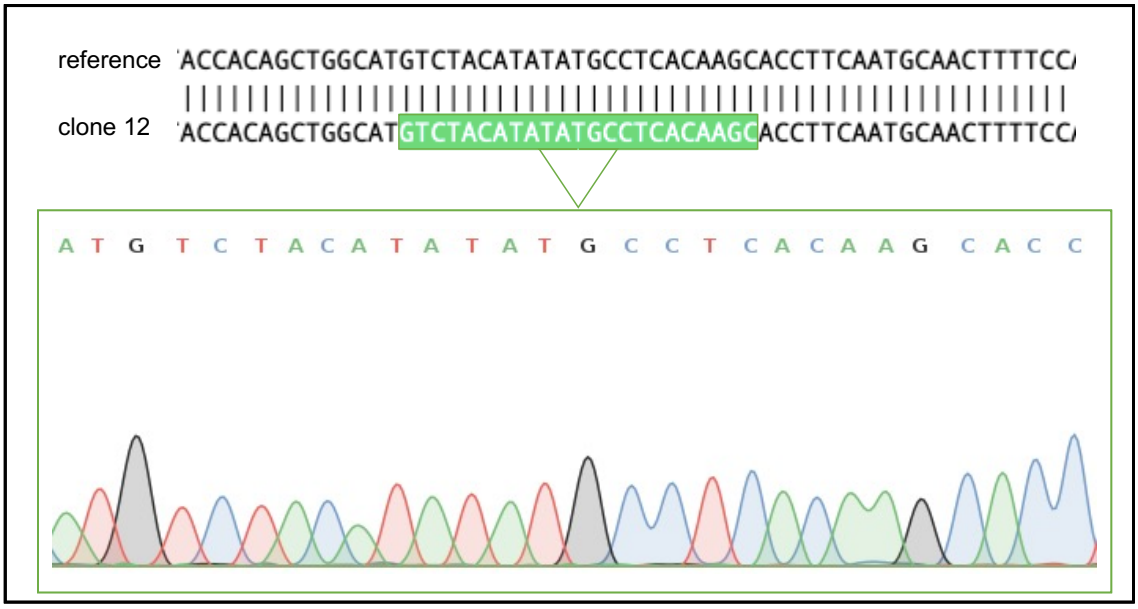

Figure 19: Off-target sequencing. Sequencing data of *SLC43A1* site in Clone 12 visualized with CRISP-ID. The sequence from the reference genome is aligned with the sequence found in the DNA from Clone 12. The off-target is marked in green in the alignment and its sequence in Clone 12 is visualized below. Figure modified from own publication (Schmitz et al., 2023).

3.2.4 Stem cell characterization

After the genetic modification, it was assessed whether the iPSC lines still exhibited pluripotent stem cell properties. For this purpose, they were characterized by evaluating their Alkaline Phosphatase (AP) expression, immunostaining of pluripotency markers, evaluation of transcriptional expression of pluripotency markers, the cells' ability to spontaneously differentiate into cells from all three germlayers and whole genome SNP genotyping. The protocols used for this characterization are described in 2.2.2.5.

3.2.4.1 Expression of Alkaline Phosphatase

AP is highly expressed in pluripotent stem cells and was therefore expected to show high activity in the iPSC. Expression was evaluated by adding Naphtol AS-MX phosphate to fixed iPSC as a substrate for AP and visualizing the enzyme's activity by adding Fast Red (see 2.2.2.5.1). As expected, all clones showed clear AP activity.

Figure 20 shows the AP staining in clones 12 (A), 40 (B), 18 (C) and 75 (D) using Fast Red substrate which produces a red reaction product in the presence of AP. In all lines, colonies were discerned and there was a distinct Fast Red signal in all wells. Clones 12 and 18 exhibited a higher cell density and a stronger Fast Red signal than the other two clones.

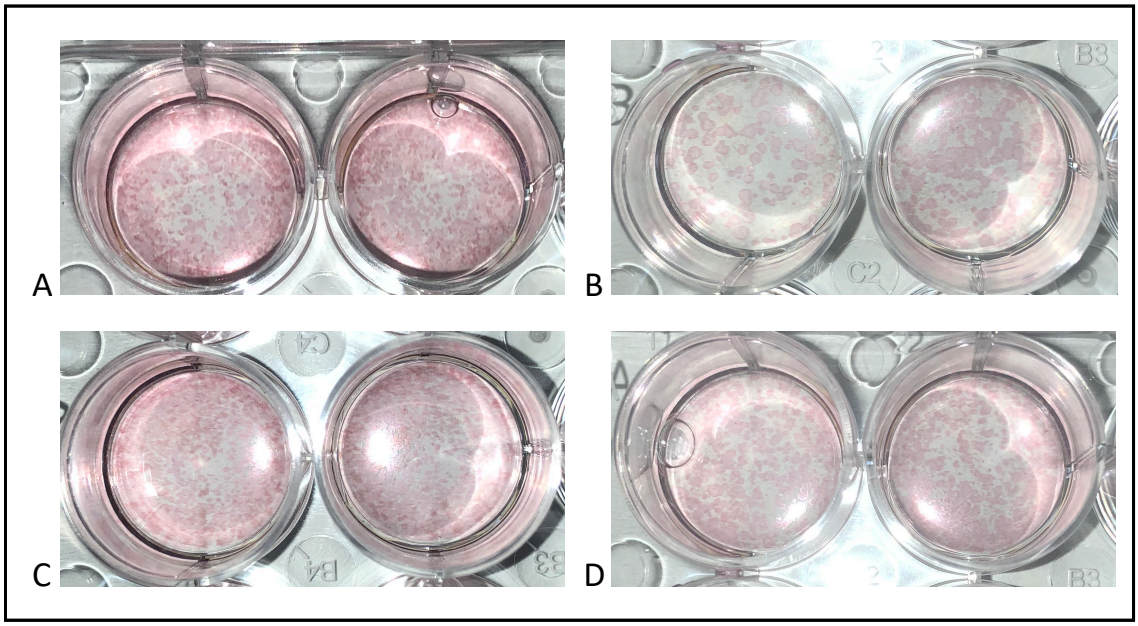

Figure 20: Alkaline Phosphatase staining. Homozygous clones 12 (A) and 40 (B) and heterozygous clones 18 (C) and 75 (D) were stained with Fast Red in order to examine AP expression. Figure modified from own publication (Schmitz et al., 2023).

3.2.4.2 Immunostaining for pluripotency markers

As pluripotent cells, the clones were expected to express Oct3/4 and Tra1-81. Expression was assessed by immunostaining as described in 2.2.2.5.2, all clones stained positive for both markers.

The results from immunostaining for Oct3/4 and Tra1-81 are shown in Figure 21 and Figure 22 respectively for all four clones.

Figure 21 shows the microscope images from the cells stained for Oct3/4. As can be seen in Figure 21 A - D, nuclei were stained with DAPI. It was observed that in the merged images of DAPI and Oct3/4 staining in Figure 21 I – L both stainings were colocalized as expected, the images for DAPI and Oct3/4 had a strong resemblance.

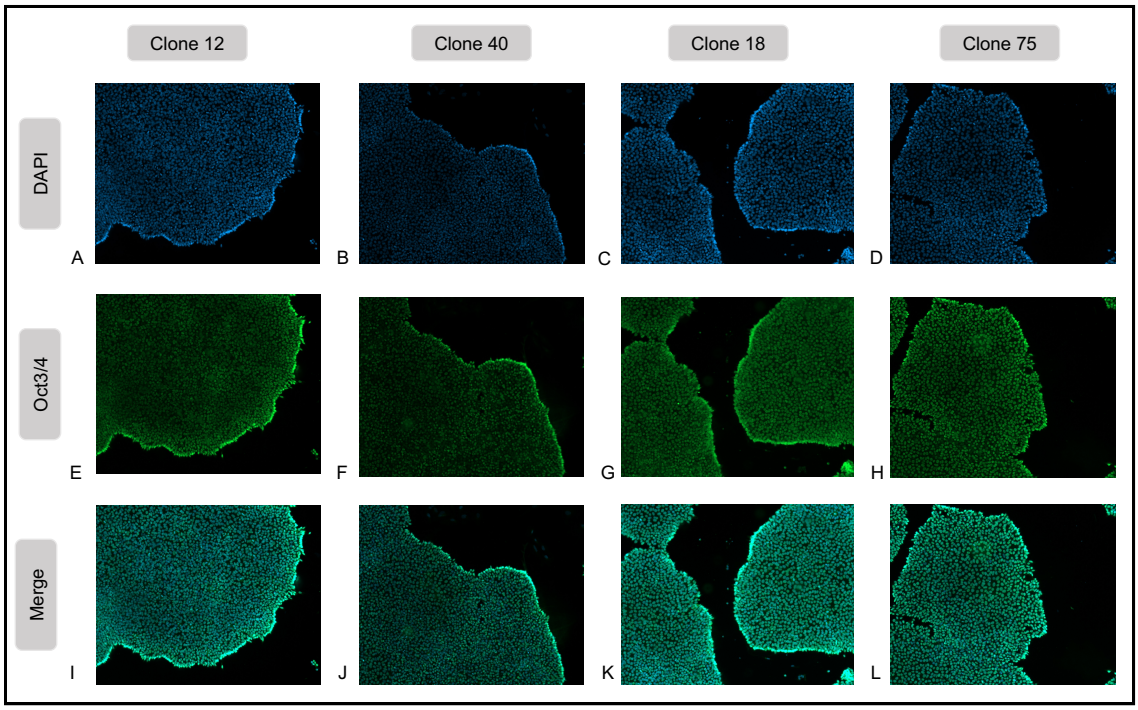

Figure 21: Oct3/4 immunocytochemistry. Clone 12 (A, E, I), 18 (B, F, J), 40 (C, G, K) and 75 (D, H, L) were stained for DAPI (A-D) and pluripotency marker Oct3/4 (E-H). Merged images of both stainings are shown in I-L. Figure modified from own publication (Schmitz et al., 2023).

Figure 22 shows the Tra1-81 staining for all four clones. DAPI was again used for nuclear staining. The merged images of both DAPI and Tra1-81 shows that cells stained positive for DAPI and Tra1-81. As Tra1-81 is a cell surface antigen, the staining pattern differed between the nuclear DAPI staining and Tra1-81 staining. The outline of the colony however remained the same.

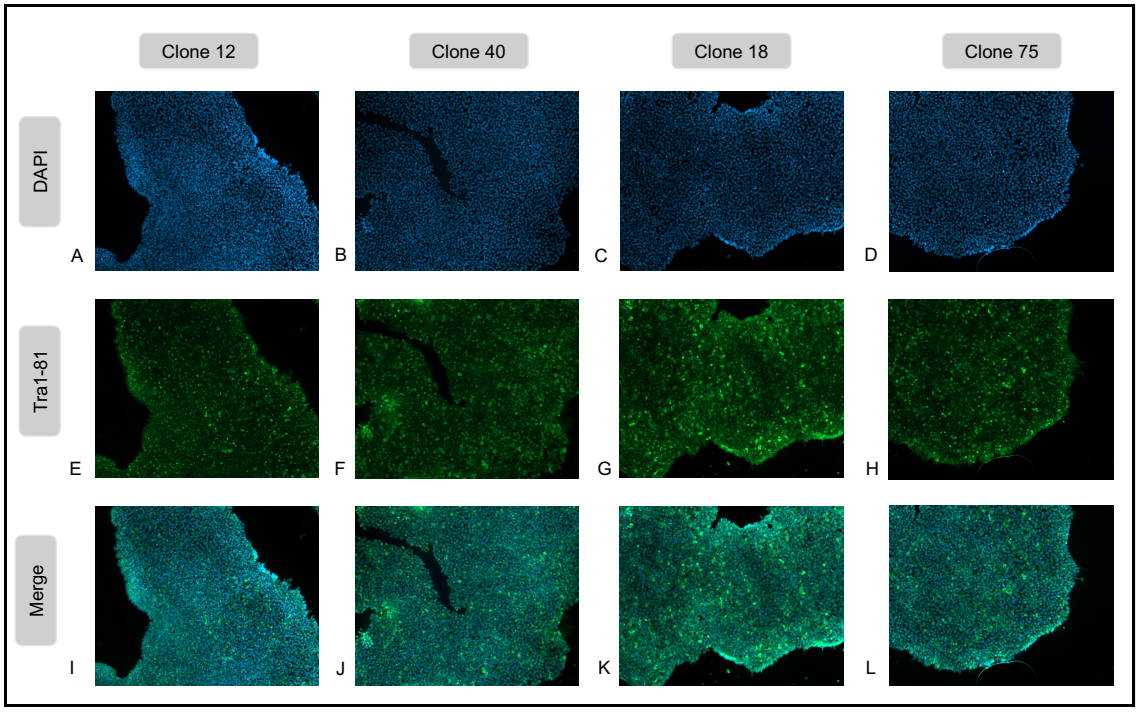

Figure 22: Tra-1-81 immunocytochemistry. Clone 12 (A, E, I), 18 (B, F, J), 40 (C, G, K) and 75 (D, H, L) were stained for DAPI (A-D)and pluripotency marker Tra1-81 (E-H). Merged images of both stainings are shown in I-L. Figure modified from own publication (Schmitz et al., 2023).

3.2.4.3 Evaluation of transcriptional expression of pluripotency markers by RT-PCR

Expression of transcripts of characteristic pluripotency genes and oncogenes was evaluated by RT-PCR and compared to human embryonic stem cells (hESC) and fibroblasts as described in 2.2.2.5.3. As expected, the iPSC's expression profile was similar to the hESC but clearly distinct from the fibroblasts.

The relative expression of pluripotency markers measured in the RT-PCR is depicted in

Figure 23. The graph demonstrates that the iPSC clones showed an elevated expression of the transcripts of pluripotency genes *Oct3/4, Sox2, Nanog, Dnmt3b* and *Tdgf1* on a similar level as hESC. The expression pattern was clearly distinct from that of the fibroblast control in which the pluripotency genes are not upregulated. As expected, the expression of oncogenes *c-Myc* and *Klf4* did not differ much between iPSC clones and the fibroblast control.

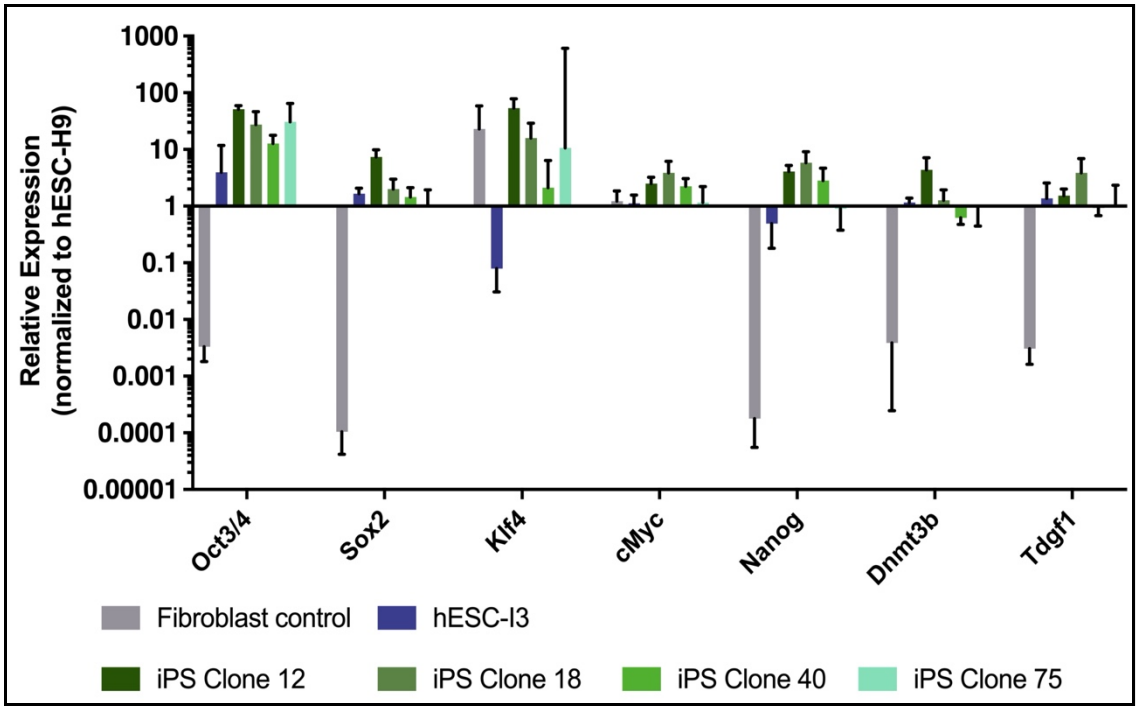

Figure 23: RT-PCR for pluripotency markers. RT-PCR was performed with cDNA from all four clones, a fibroblast control and two human embryonic stem cell (hESC) lines. Relative expression was normalized to hESC-H9 as reference and *GAPDH* as housekeeping gene. Figure modified from own publication (Schmitz et al., 2023).

3.2.4.4 Spontaneous differentiation into all three germ layers

Another characteristic feature of pluripotent stem cells is their ability to spontaneously differentiate into all three germ layers. After being cultured in the appropriate medium, the iPSC were immunostained for endodermal, mesodermal and ectodermal markers as described in 2.2.2.5.4. All four clones were able to differentiate into all three germ layers and stained positive for endodermal markers FoxA2 and Sox17, mesodermal marker SMA and ectodermal marker TUJ.

Figure 24 shows the immunostaining for endodermal markers FoxA2 (Figure 24 E-H) and Sox17 (Figure 24 I-L) for all four clones. DAPI was used for nuclear staining and a merge image with all three stainings was created (Figure 24 L-O).

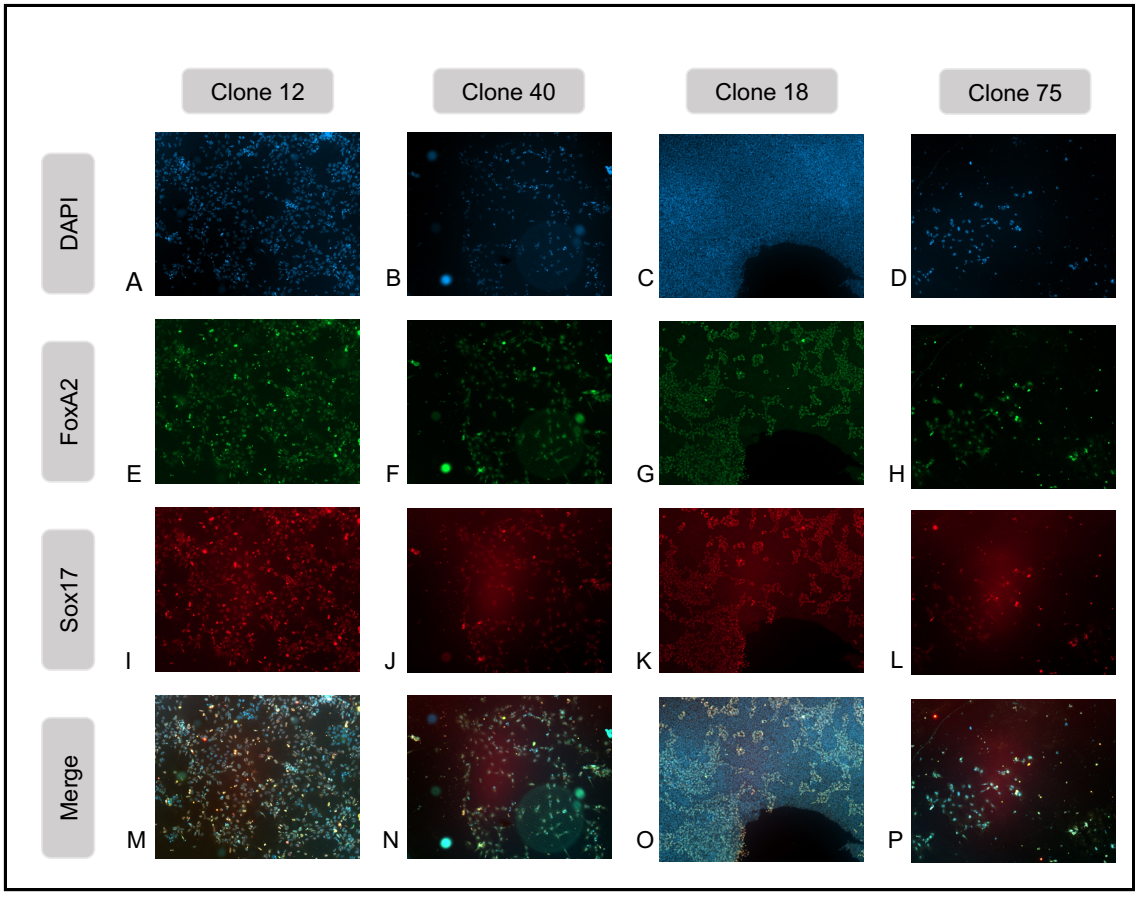

Figure 24: FoxA2 and Sox17 immunocytochemistry. Clone 12 (A, E, I, M), 40 (B, F, J, N), 18 (C, G, K, O) and 75 (D, H, L, P) were stained for DAPI (A-D) and endodermal markers FoxA2 (E-H) and Sox17 (I-L). Merged images of all stainings are shown in M-P. Figure modified from own publication (Schmitz et al., 2023).

In Figure 25, the staining for mesodermal marker SMA as well as nuclear staining with DAPI and merge images of both stainings are depicted. The merge images show that the same cells were stained positive for DAPI and SMA. However, the morphology of the structures stained positive for SMA differed from the ones positive for DAPI, they were bigger and more irregularly shaped, often with multiple branches, as SMA is expressed in the cytoplasm while DAPI is a nuclear staining.

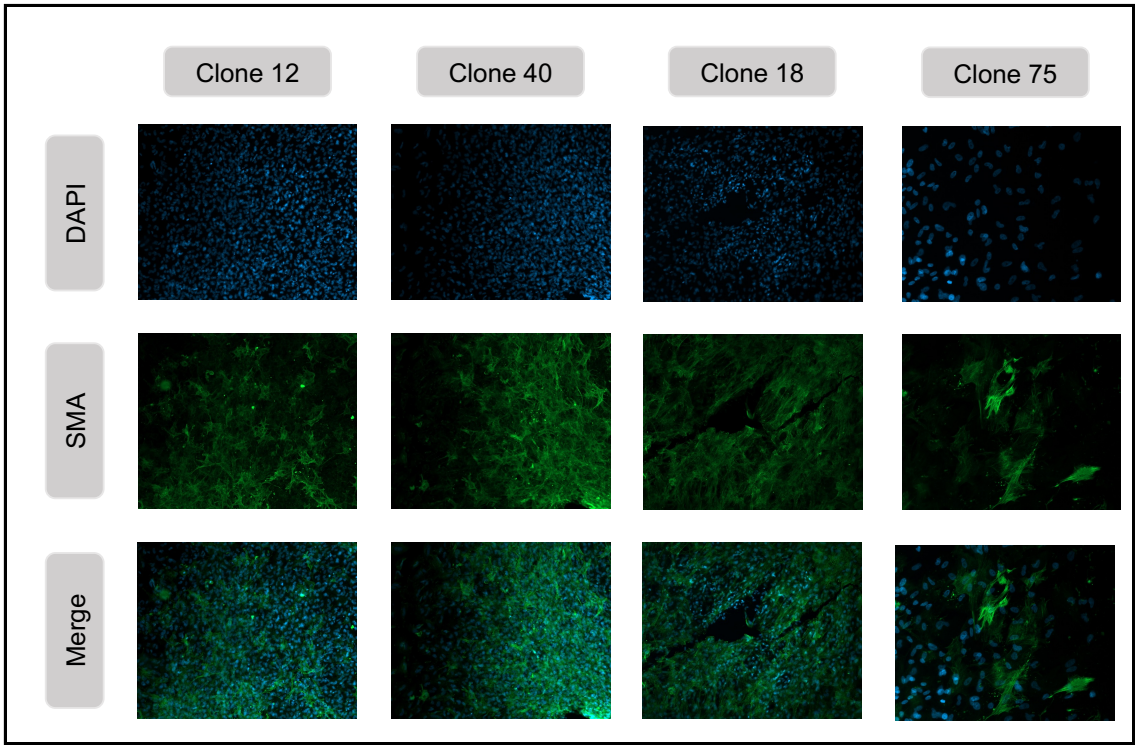

Figure 25: SMA immunocytochemistry. Clone 12 (A, E, I), 40 (B, F, J), 18 (C, G, K) and 75 (D, H, L) were stained for DAPI (A-D) and mesodermal marker SMA (E-H). Merged images of all stainings are shown in I-L. Figure modified from own publication (Schmitz et al., 2023).

Figure 26 shows the imaging of cells stained for DAPI and ectoderm marker TUJ as well as the merged images. The DAPI staining was similar as in the stainings described before. As expected, the TUJ signal showed filament-like structures in the colonies, as it represents the tubulin cytoskeleton.

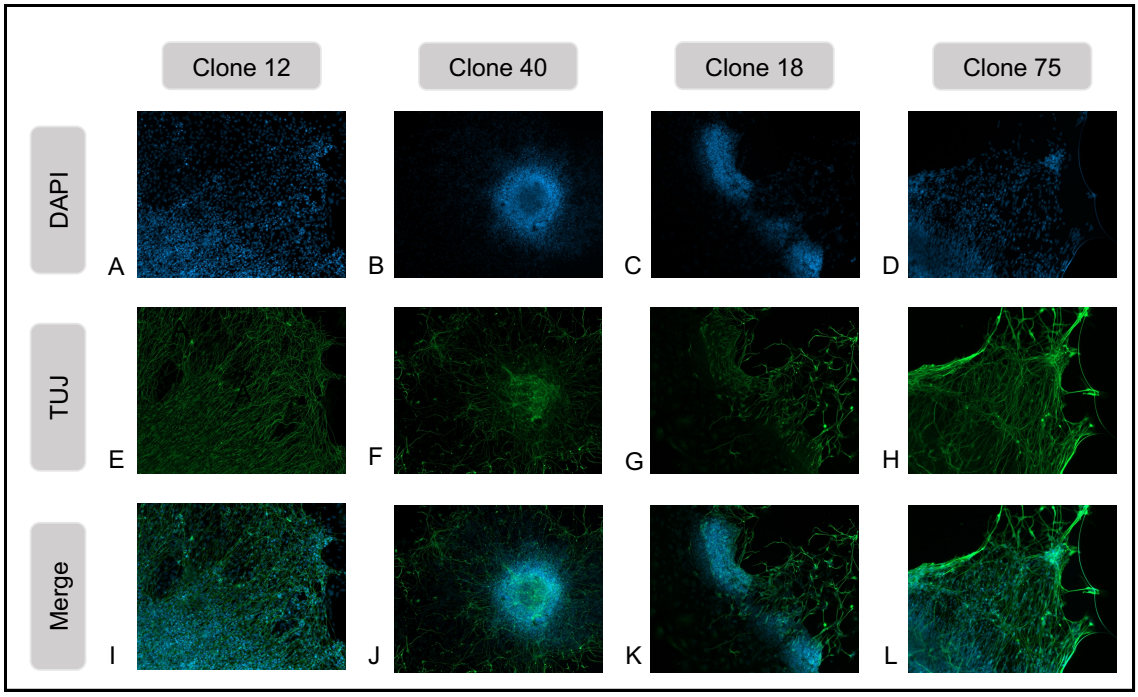

Figure 26: TUJ immunocytochemistry. Clone 12 (A, E, I), 40 (B, F, J), 18 (C, G, K) and 75 (D, H, L) were stained for DAPI (A-D) and ectodermal marker TUJ (E-H). Merged images of all stainings are shown in M-P. Figure modified from own publication (Schmitz et al., 2023).

3.2.4.5 Whole genome single nucleotide polymorphism genotyping

In order to confirm the genetic identity of the clones with the control line, whole genome single nucleotide polymorphism genotyping was performed for all clones.

In the whole genome SNP genotyping no chromosomal aberrations or copy number variations were detected in the modified clones when compared to the corresponding fibroblast and iPSC control lines. The SNP array confirmed the genetic identity of the clones with the control line. These results were generated by Life & Brain GENOMICS and are presented in Figure 27.

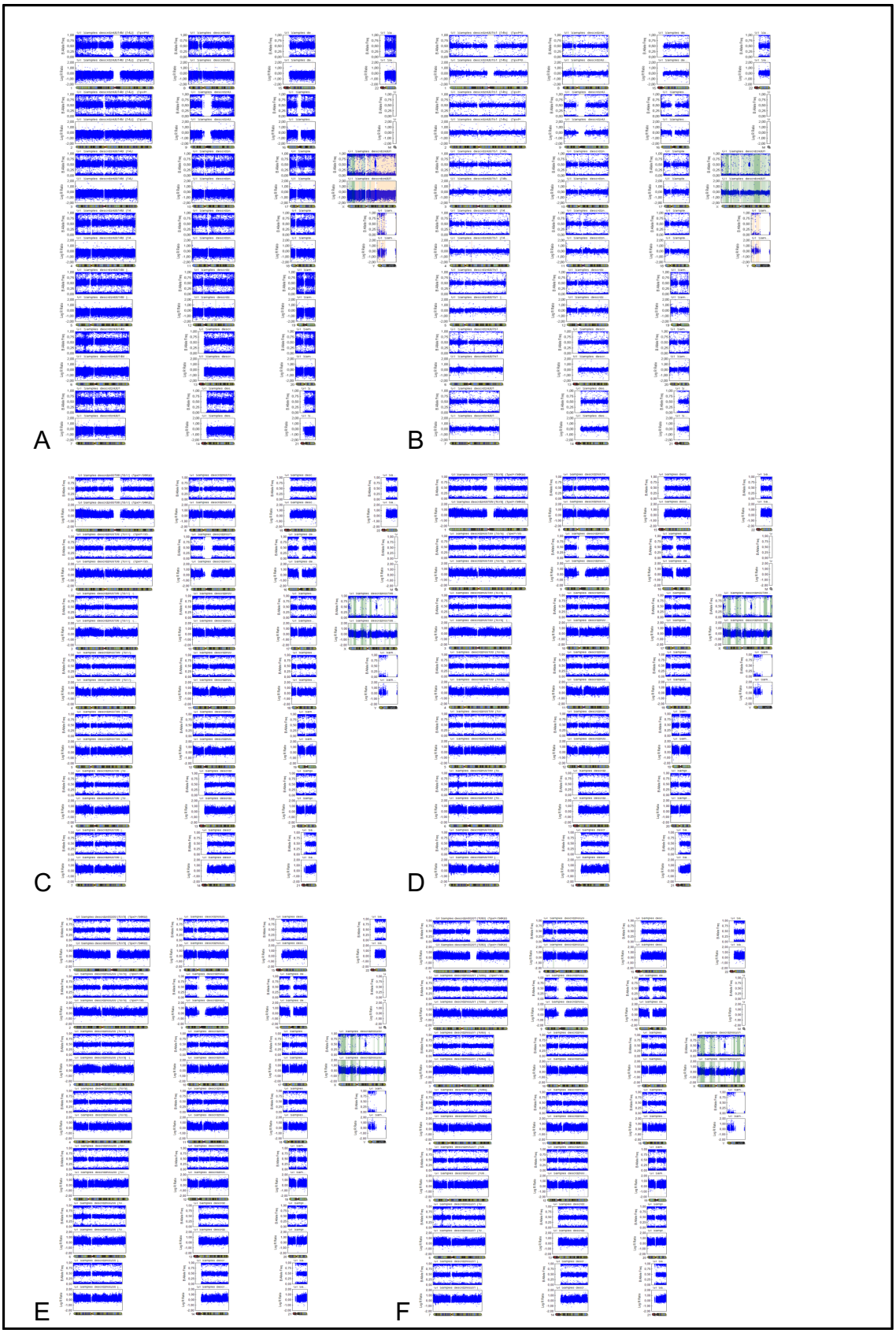

Figure 27: Karyograms. Karyograms from the fibroblast control (A), iPSC control (B), clone 12 (C), clone 40 (D), clone 18 (E) and clone 75 (F). Figure modified from own publication (Schmitz et al., 2023).

4 Discussion

4.1 Testing sgRNAs in the THP-1 cell line

4.1.1 Cell line selection and optimization of CSF1R Western Blot

Western Blots for CSF1R were performed with protein samples of the cell lines K-562 and THP-1, with varying protein amounts and antibody dilutions as well as on two different membranes, namely a Nitrocellulose and a PVDF membrane (see 3.1.2., Figure 7).

On both membranes, bands for GAPDH were detectable for all samples from both cell lines, which confirms that the Western Blot worked and protein transfer to the membrane was successful. These bands were detected at approximately the same height as the 37 kDa band of the protein standard. This is congruent with the expected size of the GAPDH subunits (Tristan et al., 2011).

Interestingly the intensity of the GAPDH bands does not match the protein amount of the samples, for instance the intensity of the band of the 40 µg THP-1 sample is considerably stronger than the one for the 60 µg sample from the same cell line. This could be explained by an incorrect assessment of the protein concentration or by inaccuracies in the Western Blotting process. Since the intensity of the CSF1R bands for THP-1 cells does increase with higher protein amounts, it seems more probable that the reason is linked to the Western Blotting process rather than the sample preparation. The fact that the bands for the samples of the K-562 cells do not form straight lines also suggests that there was a problem during gel electrophoresis, possibly pipetting errors or an inappropriate gel composition. However, since the blots were not used for quantification, the protocol was not further optimized.

CSF1R, in contrast to that, was only detected on the PVDF but not on the Nitrocellulose membrane. Furthermore, it could only be shown in THP-1 but not in K-562 samples. PVDF membranes have a higher protein binding capacity and thus a higher sensitivity for protein detection than nitrocellulose membranes (Weiss, 2012). The presented findings therefore suggest that CSF1R expression might be too low in both cell lines to be detected on a Nitrocellulose membrane.

Since CSF1R is expressed on cells of the myeloid line and as both K-562 and THP-1 cells are derived from myelogenous leukemia patients, both cell lines were expected to express CSF1R. In the Western Blots performed for this study however, CSF1R could only be detected in THP-1 cells. Although the testing data provided by the manufacturer of the antibody used in these experiments showed a detection of CSF1-R in K-562, according to the Human Protein Atlas, CSF1R is only expressed in THP-1 but not in K-562 cells (Uhlén et al., 2015). Potentially, a higher sensitivity, for example by using higher protein amounts, would make it possible to detect low CSF1R levels present in K-562 cells. However, firstly the setup of the following experiments would make it difficult to work with higher protein amounts. Secondly, the goal of this part of the study was solely to identify an appropriate cell line for further studies. For this purpose, a cell line was needed in which CSF1R can be detected so that the consequences of CRISPR edits in the *CSF1R* gene on the protein expression of the receptor can be assessed. As CSF1R expression was clearly detectable in THP-1 cells, this cell line meets that demand. It was therefore not necessary to further optimize the method in order to also show CSF1R expression in K-562 cells.

Another interesting aspect of the Western Blots is that there are two bands that are stained by the anti-CSF1R antibody, one at a size of 100 kDa and one at approximately 125 kDa. The predicted protein size of CSF1R is 108 kDa or 33 kDa for its isoform (Uhlén et al., 2015). Although a band of approximately 108 kDa has been detected in studies using Western Blots to detect CSF1R (Li et al., 2009; Zhou et al., 2021), there are also several studies in which a protein size of 150-170 kDa is reported (X. Shi et al., 2020; Tian et al., 2019). According to Wai-Mun Lee, this bigger size of the protein can be explained by posttranslational addition of oligosaccharide chains (Wai-Mun Lee, 1992). On top of that, while many Western Blots found in studies about CSF1R only show one band for CSF1R (X. Shi et al., 2020; Zhou et al., 2021), other researchers have also shown a second band of about 130 kDa that has been identified as a shorter precursor protein (Hagan et al., 2020; Wilhelmsen & Geer, 2004). It is therefore probable that the anti-CSF1R antibody used for this project binds to a part of the protein

that is present in the precursor protein as well as in the final protein with the additional oligosaccharide chains.

4.1.2 Transfection efficiency

The transfection efficiency observed in the cells transfected with eGFP was high in all three electroporations (see 3.1.3, Figure 8). This is important for the later evaluation of the sgRNAs' editing efficiency based on sequencing and Western Blot data as it shows that the editing efficiency was not limited by a low transfection efficiency.

4.1.3 CSF1R *assessment on DNA level*

The effect of the introduction of CRISPR/Cas9 complexes into the cells was evaluated on DNA level by analysis of indel percentages in Sanger sequencing data (see 3.1.4, Figure 10). Electroporation with sgRNAs 1-4 led to high indel percentages of up to 86 % with only small differences between the four guides. Interestingly, although according to the data from the eGFP flow cytometry transfection efficiency was considerably lower in the second electroporation than in the other two, a lower indel percentage in the second run could only be observed for sgRNA 1.

SgRNA 5 however did not induce any changes on DNA level, although the samples were treated the same way as for the other sgRNAs. The on-target efficiency of a specific sgRNA is affected by various factors. On the one hand, the structure of the sgRNA itself can have an effect on its activity. For instance, Moreno-Mateos et al. have shown that sgRNA activity correlates with sgRNA stability (Moreno-Mateos et al., 2016). The stability of the guide depends on the secondary structures it forms, which in turn is associated with sequence characteristics such as the guanine content (Doench et al., 2014; Moreno-Mateos et al., 2016; J. Zhang et al., 2014). This impact of the guanine content might be explained by the formation of stable structures called G-quadruplexes by guanine-rich sequences (X. Liu et al., 2016; Moreno-Mateos et al., 2016). On the other hand, features of the target site also have an impact on the efficiency of a sgRNA. For instance, Liu et al. investigated the influence of the genomic context of the target

site on CRISPR/Cas9 efficiency (X. Liu et al., 2016). Furthermore, Jensen et al. demonstrated the effect of chromatin accessibility on the editing efficiency (Jensen et al., 2017).

Interestingly, sgRNA 5 had a high efficiency prediction in the sgRNA design tools used, the Doench efficiency score on the CRISPOR website even predicted the highest efficiency out of the 5 guides for sgRNA 5. Although the algorithms of the sgRNA design tools used for this project are based on the knowledge about the impact factors described above and based on experimental data, it has previously been shown that the predictive capacity of such algorithms is limited (Labuhn et al., 2018). Furthermore, the efficiency predictions vary considerably between different algorithms which may be due to different weighting of particular features as well as the fact that they are based on datasets using experimental data from different expression systems. For example, sgRNA 5 obtained a Doench efficiency score of 70 but a Moreno efficiency score of only 35.

Nonetheless, it is surprising that despite the high ranking in various design tools, sgRNA 5 does not only have a low efficiency but does not seem to have any effect at all.

A high cleavage efficiency is an important factor for the applicability of the CRISPR/Cas9 approach for therapeutic strategies. As described above, one such strategy could be an autologous stem cell transplantation with *ex vivo* CRISPR/Cas9 based gene therapy in the hematopoietic stem cells. Especially considering the possibility that a dominant negative effect of the mutant protein might be involved in the pathomechanism of ALSP, it would be essential for a successful therapy to knock out a high percentage of the patient's receptors. If it is not possible to achieve a sufficient efficiency, a strategy for screening would need to be developed in order to select only successfully edited cells for re-transplantation. However, since hematopoietic stem cells cannot be expanded as easily as immortalized cell lines (Kumar & Geiger, 2017), this might not be feasible.

Since sgRNAs 1-4 all showed a high cleavage efficiency based on the DNA sequencing data, they all seem to be appropriate candidates for such an efficient *CSF1R* knockout. However, the results on protein level need to be considered as well.

4.1.4 CSF1R expression on protein level

The effect of the genome editing on CSF1R expression on protein level in iPSC was assessed by Western Blots following the protocol established beforehand.

Sample transfer and detection of housekeeping proteins

The Ponceau staining confirmed the successful transfer of protein onto the membrane during the Western Blot (see Figure 13). This is consistent with the presence of GAPDH or β-Actin bands for all samples except for one triplicate each for sgRNA 5 in the first run and sgRNA 4 in the second run.

In comparison to the protein standard, the bands for CSF1R and GAPDH were at the same height as in the Western Blots used for cell line selection and Western Blot optimization and thus congruent with the findings described in 4.1.1. The protein size observed for β-Actin is in line with data from the literature (Uhlén et al., 2015).

In the Western Blots, a strong variation in the intensity of the bands could be observed for CSF1R as well as GAPDH (see Figure 14). This is surprising as the protein concentration was assessed beforehand and the same protein amount was used for all samples of one blot. Therefore, the bands for GAPDH, which was used as a housekeeping control, were expected to have the same intensity in all samples. The fact that the relative intensity of the GAPDH bands matches the relative intensity of the CSF1R bands when those are present suggests that the protein amount was in fact not the same for all samples. These inaccuracies in the determination of protein concentration in the BCA might be due to the relatively low protein amount in the samples. It might therefore have been of advantage to expand the cells for a longer period of time after the electroporation in order to obtain a higher yield of protein from the pellets. Interestingly, the bands for β-Actin for the samples from the third electroporation were much more regular than the GAPDH bands in the other blots. Therefore, it might have improved the quality of the Western Blot images to have used β-Actin as control for all blots. However, as the Western Blots were only used for qualitative but not for quantitative analysis, they still present valuable information. The aim of this study was

to investigate whether CSF1R could still be detected in the cells after the CRISPR approach with each of the sgRNAs. Since this could be clearly discerned in the used Western Blots, the results attained with the protocol used for these Blots were sufficient for this study, so that this protocol was not further optimized.

CSF1R expression

The Western Blots showed important differences in the expression of CSF1R between the iPSC treated with different sgRNAs (see Figure 14).

In the control cells as well as the cells treated with sgRNA 1 and 2, the CSF1R protein was still expressed although on DNA level a high indel frequency was obtained. The targets for both sgRNA 1 and sgRNA 2 are located in the untranslated region (UTR) of exon 2 however, which explains this seeming contradiction between the sequencing and Western Blot data. Although the DNA is cut efficiently at the target site, it seems that it can still be translated.

In contrast, in none of the Western Blots CSF1R expression could be detected in cells treated with sgRNA 3 and 4, even though the bands for GAPDH clearly show that there was protein present on the membrane. This could be explained by the fact that sgRNA 3 and 4 induce cuts very close to or after the ATG so that translation and thus protein expression is prevented.

In cells treated with sgRNA 5, CSF1R could still be detected. Considering the sequencing data, it is not surprising that sgRNA 5 had no effect on protein expression since there were no changes on DNA level.

Application in further studies

Based on this data, both sgRNA 3 and 4 are suitable guides for *CSF1R* knockout strategies that may be used for CRISPR/Cas9-mediated gene therapy later-on. However, further experiments will be necessary to confirm the efficiency of these guides in hematopoietic stem cells which would be the target of the therapeutic approach. Additionally, the specificity of the guides would need to be examined in order to exclude important off-target effects. Off-target effects could cause unwanted mutations in the modified cells, which is one of the challenges of CRISPR/Cas9 based gene therapy (Qomi et al., 2019). Many researchers have

investigated the factors that affect the specificity of the CRISPR/Cas9 system. For instance, it has been shown that using Cas9 ribonucleoprotein instead of a Cas9 plasmid reduces the number of off-target effects, as the ribonucleoprotein is degraded faster (S. Kim et al., 2014; Ramakrishna et al., 2014; X. H. Zhang et al., 2015). Furthermore, the off-target activity seems to depend on the structure of the sgRNA and the target sequence. For example, mismatches in the region close to the PAM are tolerated better than mismatches more distal in the target sequence (Hsu et al., 2013; X. H. Zhang et al., 2015). Other authors have reported that using shorter sgRNAs increases the editing specificity (Fu et al., 2014). Apart from that it has been suggested to titrate the amounts of sgRNA and Cas9 to obtain the optimal balance between high on-target and low off-target activity (Hsu et al., 2013).

Several methods have been developed to assess off-target effects, including *in silico* prediction, GUIDE-seq and digenome-seq (D. Kim et al., 2015; Spitzer et al., 2014; Tsai et al., 2015; X. H. Zhang et al., 2015). These methods could also have been used to examine the modified THP-1 cells for off-target effects. However, in a study performed by Duan et al., they found that off-target effects did not overlap between different cell types which suggests that the specificity is cell type dependent (Duan et al., 2014). Therefore, it would be more useful to examine the off-target effects in the cell type that is relevant for the therapeutic approach, i. e. in hematopoietic stem cells.

Application in the establishment of *CSF1R* knockouts in iPSC

The data from experiments in THP-1 cells was used to choose the sgRNAs used for the double CRISPR approach in iPSC. SgRNA 2 and 4 both had high indel frequencies which shows their high efficiency on DNA level. On top of that, by using these two guides, the ATG is included in the segment that is cut out which should render translation to the protein impossible. Another advantage of this combination is that the two guides are the furthest away from each other which allows clearer results in the PCR screening later-on as the bands for the wildtype and mutated allele are further apart.

4.2 Establishment of CSF1R knockouts in iPSC

4.2.1 Clone selection

Two homozygous and two heterozygous knockout clones were selected from the PCR screening and the knockout state was confirmed through Sanger sequencing (see 3.2.2, Figure 17, Figure 18).

These cell lines can be used in further experiments to better understand the pathomechanism of ALSP which is still largely unknown (Guerreiro et al., 2013; Kempthorne et al., 2020). Hayer et al. have established an iPSC line using cells from an ALSP patient (Hayer et al., 2018); it would be interesting to compare the generated knockout lines to this ALSP patient iPSC line in functional assays such as their ability to differentiate into microglia. This would allow to assess whether the disease is in fact caused by haploinsufficiency or if there is a dominant-negative effect of the mutated protein. If the heterozygous knockout line presents the same phenotype as the patient-derived cells, this would suggest that the disease is caused by haploinsufficiency of the *CSF1R* gene. If, however, only the homozygous but not the heterozygous knockout line shows the same phenotype as the patient-derived cells, this would be consistent with the hypothesis that the patients' mutated receptors have a dominant-negative effect.

4.2.2 Off-target analysis

Off-target CRISPR/Cas9 activity could lead to mutations in the iPSC that might affect the results of future experiments. Therefore, it is important to assess the specificity of the CRISPR approach in the edited cell lines, although studies based on whole-genome sequencing have shown that off-target cleavage does not occur frequently in human pluripotent stem cells edited with the CRISPR/Cas9 system (Smith et al., 2014; Veres et al., 2014; X. H. Zhang et al., 2015). The factors that impact the off-target activity of the CRISPR/Cas9 system and methods that can be used to evaluate the specificity have been described above (see 4.1.4).

For this study, the CRISPOR web tool's MIT score was used to identify the top five most probable off-targets for each of the two used crRNAs (see Table 13).

These targets were then investigated by targeted Sanger sequencing which did not reveal any off-target effects in the established lines (see 3.2.3). The MIT score indicated on the CRISPOR website is a modified version of an off-target prediction score developed by Hsu et al (Hsu et al., 2013). This score ranks the probability of off-target cleavage based on the location, identity and density of mismatches within the sequence (Hsu et al., 2013). According to Haeussler et al., the modified version used for the CRISPOR website has a higher sensitivity than the original score (Haeussler et al., 2016).
Overall, the presented data confirm that the iPSC lines generated in this project can be used for further experiments as the probability of important off-target cleavage effects is low.

4.2.3 Stem cell characterization

The established cell lines were characterized for their stem cell traits in order to confirm that genome editing had not interfered with these characteristics. The results were all in the expected range and confirmed the stem cell character of both of the homozygous and the heterozygous knockout clones (see 3.2.4).
All clones showed high AP expression (see Figure 20) which is typical for pluripotent stem cells (Stefkova et al., 2015). The RT-PCR showed that the expression levels of pluripotency genes and characteristic transcription factors is similar to the expression observed in ESC but clearly distinct from the fibroblasts' expression pattern (see

Figure 23). In the immunostaining, pluripotency markers Tra1-81 and Oct3/4 were detected in all clones in the characteristic staining pattern (see Figure 21, Figure 22) (Hayer et al., 2018; Kumazaki et al., 2011). All four clones were also able to form EBs and differentiate into cells of all three germ layers which was confirmed by immunocytochemical staining of FoxA2, Sox17, TUJ and SMA respectively (see Figure 24, Figure 25, Figure 26) (Hoffman & Carpenter, 2005; Teo et al., 2011; Valadez-Barba et al., 2020). The SNP array performed by Life & Brain Genomics did not reveal any chromosomal aberrations or copy number

variations and confirmed the genetic identity of the clones with the fibroblasts and iPSC they were derived from (see Figure 27).
In summary, the cell lines established in this project have been shown to be pluripotent stem cells and can be used as such in further experiments.

4.2.4 Summary of objectives and findings

The following objectives were formulated at the beginning of this study:

I. Identification of efficient sgRNAs for knockout of human *CSF1R*
II. Generation of homozygous and heterozygous *CSF1R* iPSC knockout lines

The findings from this study showed that:

I. sgRNAs 3 and 4, designed for the purpose of this study, lead to efficient knockout of CSF1R on DNA and protein level in THP-1 cells.
II. two homozygous and two heterozygous CSF1R knockout iPSC lines could be established using a double CRISPR approach with sgRNAs 2 and 4. Stem cell characterization showed that the edited iPSC lines still possessed the characteristics of pluripotent stem cells.

5 Summary

Adult-onset leukoencephalopathy with spheroids and pigmented glia (ALSP) is a rare, early-onset neurodegenerative disease. The disease is rapidly progressive and leads to death on average six years after the manifestation of the first symptoms such as cognitive decline, psychiatric and motor disturbances. The disease is caused by mutations in colony-stimulating-factor-1 receptor (CSF1R). This receptor is expressed on cells of the myelogenous line, such as microglia, that is supposed to play a central role in the pathophysiology of ALSP. However, the exact pathophysiological mechanisms are still largely unknown. This is one of the reasons why treatment options are currently limited to symptomatic therapy. Recently, allogenic hematopoietic stem cell transplantation has been reported to have a stabilizing effect on the patients' condition in several cases. Disadvantages of allogenous transplantation include the need for a suitable donor and the necessary immunosuppression. In order to avoid these, an alternative approach might be to perform autologous stem cell transplantation combined with *ex vivo* gene therapy. For this purpose, the patients' *CSF1R* could be knocked out using the CRISPR/Cas system, a highly efficient gene editing tool that has already been applied in clinical trials for other diseases. For an efficient CRISPR/Cas-based gene knockout, appropriate single guide RNAs (sgRNAs) need to be established.

One of the objectives of this project was therefore to identify an optimal sgRNA for efficient *CSF1R* knockout. For this purpose, five sgRNAs were designed and tested in in the THP-1 cell line, which is known to express CSF1R at a high level. Their efficiency was evaluated on DNA level by Sanger sequencing and on protein level by Western Blotting. Two suitable sgRNAs with a high efficiency on DNA and protein level were identified as candidates for a therapeutic knockout strategy. Further experiments will be needed to evaluate their efficiency in hematopoietic stem cells as well as their specificity, as accidental off-target effects might lead to side effects.

Furthermore, two of the tested sgRNAs were chosen for the generation of homozygous and heterozygous *CSF1R* knockout lines in induced pluripotent stem cells (iPSC). For this approach, human iPSC of a healthy donor were treated with two

guides at the same time, so that a part of the gene was cut out. Clones were then screened by PCR and two obviously homozygous and heterozygous clones each were sequenced in order to confirm the knockout state. The five most probable off-targets for each of the sgRNAs were also sequenced in the clones and compared to the untreated iPSC control. No off-target effects were detected. Subsequently, the clones' stem cell characteristics were assessed. The cells showed the characteristic high expression of alkaline phosphatase and were stained positive for pluripotency markers. On RNA level, the expression of pluripotency-related genes was confirmed by RT-PCR. The clones were able to spontaneously differentiate into cells of all three germ layers which was verified by immunocytochemistry. Whole genome single-nucleotide polymorphism (SNP) genotyping performed by Life & Brain Genomics did not reveal any chromosomal aberrations or copy number variations and confirmed the genetic identity of the generated knockout iPSC clones with the original iPSC and fibroblasts they were derived from. The generated knockout line is ready be used in future experiments to improve the understanding of disease mechanism in ALSP.

Deutsche Zusammenfassung

Die Adulte Leukoenzephalopathie mit axonalen Sphäroiden und pigmentierter Glia (ALSP) ist eine seltene, früh einsetzende neurodegenerative Erkrankung. Sie zeigt einen raschen Progress und führt durchschnittlich innerhalb von sechs Jahren nach Auftreten der ersten Symptome zum Tode. Zu den häufigsten Symptomen zählen kognitiver Abbau, psychiatrische und motorische Störungen. Ursächlich für die Erkrankung sind Mutationen im colony-stimulating-factor-1-receptor (CSF1R), einem Rezeptor, der auf Zellen der myeloischen Linie exprimiert wird. Dieser Rezeptor wird daher auch auf Mikroglia exprimiert, der eine zentrale Rolle in der Pathophysiologie der HDLS zugeschrieben wird. Die genauen pathophysiologischen Mechanismen sind allerdings bislang nicht geklärt. Dies ist einer der Gründe, weshalb die Therapieoptionen bisher auf symptomatische Therapien beschränkt sind. In mehreren Fällen konnte jedoch durch eine allogene hämatopoetische Stamzelltransplantation eine Stabilisierung der Patienten erreicht werden. Die allogene Stamzelltransplantation geht allerdings mit Nachteilen wie der Notwendigkeit eines passenden Spenders sowie der nötigen Immunsuppression einher. Um diese zu vermeiden, bestünde ein alternativer Ansatz darin, eine autologe Stamzelltransplantation in Kombination mit einer *ex vivo* Gentherapie durchzuführen. Ein Knockout des mutierten *CSF1R*-Gens des Patienten könnte hierbei mithilfe des CRISPR/Cas-Systems vorgenommen werden. Dabei handelt es sich um ein hocheffizientes Werkzeug zur Genmodifikation, das bereits in klinischen Studien bei anderen Erkrankungen eingesetzt wird. Für ein effizientes CRISPR/Cas-basiertes Knockout werden passende single guide RNAs (sgRNAs) benötigt.

Daher bestand eines der Ziele dieses Projekts darin, eine optimale sgRNA für ein effizientes *CSF1R*-Knockout zu identifizieren. Dafür wurden fünf sgRNAs entworfen und in einer Zelllinie getestet. Die Effizienz wurde auf DNA-Ebene durch Sanger-Sequenzierung und auf Protein-Ebene durch Western Blots beurteilt. Zwei sgRNAs mit hoher Effizienz auf DNA- und Protein-Ebene wurden identifiziert, die für eine therapeutische Knockout-Strategie geeignet wären.

Außerdem wurden zwei der untersuchten sgRNAs für die Erstellung von homozygoten und heterozygoten *CSF1R* Knockout-Linien in induzierten pluripotenten

Stammzellen (iPSC) ausgewählt. Für diesen Teil des Projekts wurden iPSC mit beiden sgRNAs gleichzeitig behandelt, sodass ein Teil des *CSF1R*-Gens herausgeschnitten wurde. Daraufhin wurde ein Screening der Klone mittels Polymerase-Kettenreaktion (PCR) durchgeführt und je zwei homozygote und heterozygote Klone wurden sequenziert, um den Knockout-Status zu bestätigen. Die fünf wahrscheinlichsten Off-target-Effekte (Effekte außerhalb der gewünschten Zielsequenz) wurden ebenfalls in den Klonen und vergleichend in der unbehandelten iPSC-Kontrolle sequenziert. Dabei wurden keine Off-target-Effekte detektiert. Im Anschluss wurden die Klone auf ihre Stammzelleigenschaften untersucht. Die Zellen zeigten die für Stammzellen charakteristische hohe Expression von Alkalischer Phosphatase und positive Färbung von Pluripotenz-Markern. Auf RNA-Ebene wurde die Expression von Pluripotenz-Genen mittels Reverse-Transkriptase-PCR bestätigt. Die Fähigkeit der Klone spontan in Zellen aller drei Keimblätter zu differenzieren wurde immunhistochemisch nachgewiesen. Eine Untersuchung des gesamten Genoms auf Einzelnukleotid-Polymorphismen wurde durch Life & Brain Genomics durchgeführt, diese zeigte keine chromosomalen Aberrationen oder Kopienzahlvarianten und bestätigte die genetische Übereinstimmung der generierten Klone mit den ursprünglichen iPSC und den Fibroblasten, aus denen die iPSC erstellt wurden. Die erzeugte Knockout-Linie steht damit für Experimenten zur weiteren Erforschung der Pathomechanismen bei HDLS zur Verfügung.

6 Bibliography

Ajami, B., Bennett, J. L., Krieger, C., Tetzlaff, W., & Rossi, F. M. V. (2007). **Local self-renewal can sustain CNS microglia maintenance and function throughout adult life**. *Nature Neuroscience*, *10*(12), 1538–1543. doi: 10.1038/nn2014

Andersen, M. L., & Winter, L. M. F. (2019). **Animal models in biological and biomedical research – experimental and ethical concerns**. *An Acad Bras Cienc*, *91*. doi: 10.1590/0001-3765201720170238.1

Barrangou, R., Fremaux, C., Deveau, H., Richards, M., Boyaval, P., Moineau, S., Romero, D. A., & Horvath, P. (2007). **Against Viruses in Prokaryotes**. *Science*, *315*(March), 1709–1712. doi: 10.1126/science.1138140

Barriga, F., Ramírez, P., Wietstruck, A., & Rojas, N. (2012). **Hematopoietic stem cell transplantation : clinical use and perspectives**. *Biological Research*, *45*(3), 307–316. doi: 10.4067/S0716-97602012000300012

Bender, B., Klose, U., Lindig, T., Biskup, S., Nägele, T., Schöls, L., & Karle, K. N. (2014). **Imaging features in conventional MRI, spectroscopy and diffusion weighted images of hereditary diffuse leukoencephalopathy with axonal spheroids (HDLS)**. *Journal of Neurology*, *261*(12), 2351–2359. doi: 10.1007/s00415-014-7509-2

Benveniste, E. N., Nguyen, V. T., & O'Keefe, G. M. (2001). **Immunological aspects of microglia: Relevance to Alzheimer's disease**. *Neurochemistry International*, *39*(5–6), 381–391. doi: 10.1016/S0197-0186(01)00045-6

Bergner, C. G., Schäfer, L., Vucinic, V., Schetschorke, B., Lier, J., Scherlach, C., Rullmann, M., Sabri, O., Classen, J., Platzbecker, U., Kühl, J.-S., Barthel, H., Köhler, W., & Franke, G.-N. (2023). **Case report : Treatment of advanced CSF1-receptor associated leukoencephalopathy with hematopoietic stem cell transplant**. *Frontiers in Neurology*, *14*(May). doi: 10.3389/fneur.2023.1163107

Blinzinger, K., & Kreutzberg, G. (1968). **Displacement of synaptic terminals from regenerating motoneurons by microglial cells**. *Z Zellforsch Mikrosk Anat*, *85*, 145–157.

Boillée, S., & Cleveland, D. W. (2008). **Revisiting oxidative damage in ALS: Microglia, Nox, and mutant SOD1**. *Journal of Clinical Investigation*, *118*(2), 474–478. doi: 10.1172/JCI34613

Brouns, S. J. J., Jore, M. M., Lundgren, M., Westra, E. R., Rik, J. H., Snijders, A. P. L., Dickman, M. J., Makarova, K. S., Koonin, E. V., & Oost, J. van der. (2008). **Small CRISPR RNAs Guide Antiviral Defense in Prokaryotes**. *Science*, *321*(5891), 960–964. doi: 10.1126/science.1159689.Small

Calderó, J., Brunet, N., Ciutat, D., Hereu, M., & Esquerda, J. E. (2009). **Development of microglia in the chick embryo spinal cord: Implications in the regulation of motoneuronal survival and death**. *Journal of Neuroscience Research*, *87*(11), 2447–2466. doi: 10.1002/jnr.22084

Carroll, D. (2017). **Genome editing: Past, present, and future**. *Yale Journal of Biology and Medicine*, *90*(4), 653–659.

Chan, W. Y., Kohsaka, S., & Rezaie, P. (2007). **The origin and cell lineage of microglia-New concepts**. *Brain Research Reviews*, *53*(2), 344–354. doi: 10.1016/j.brainresrev.2006.11.002

Chapman, J. R., Taylor, M. R. G., & Boulton, S. J. (2012). **Playing the End Game : DNA Double-Strand Break Repair Pathway Choice**. *Molecular Cell*, *47*(4), 497–510. doi: 10.1016/j.molcel.2012.07.029

Concordet, J., & Haeussler, M. (2018). *CRISPOR : intuitive guide selection for CRISPR / Cas9 genome editing experiments and screens*. *46*(May), 242–245. doi: 10.1093/nar/gky354

Cox, D. B. T., Platt, R. J., & Zhang, F. (2015). **Therapeutic Genome Editing: Prospects and Challenges**. *Nat Med*, *21*(2), 121–131. doi: 10.1038/nm.3793.Therapeutic

Cui, Y., Xu, J., Cheng, M., Liao, X., & Peng, S. (2018). **Review of CRISPR/Cas9 sgRNA Design Tools**. *Interdisciplinary Sciences: Computational Life Sciences*, *10*(2), 455–465. doi: 10.1007/s12539-018-0298-z

Doench, J. G., Fusi, N., Sullender, M., Hegde, M., Vaimberg, E. W., Donovan, K. F., Smith, I., Tothova, Z., Wilen, C., Orchard, R., Virgin, H. W., Listgarten, J., & Root, D. E. (2016). **Optimized sgRNA design to maximize activity and minimize off-target effects of CRISPR-Cas9**. *Nature Biotechnology*, *34*(2). doi: 10.1038/nbt.3437

Doench, J. G., Hartenian, E., Graham, D. B., Tothova, Z., Hegde, M., Smith, I., Sullender, M., Ebert, B. L., Xavier, R. J., & Root, D. E. (2014). **Rational design of highly active sgRNAs for CRISPR-Cas9 – mediated gene inactivation**. *Nature Biotechnology*, *32*(12). doi: 10.1038/nbt.3026

Duan, J., Lu, G., Xie, Z., Lou, M., Luo, J., Guo, L., & Zhang, Y. (2014). **Genome-wide identification of CRISPR / Cas9 off-targets in human genome**. *Cell Research*, *24*, 1009–1012. doi: 10.1038/cr.2014.87

Dulski, J., Heckman, M. G., White, L. J., Zur-Wyrozumska, K., Lund, T. C., & Wszolek, Z. K. (2022). **Hematopoietic Stem Cell Transplantation in CSF1R -Related Leukoencephalopathy : Retrospective Study on Predictors of Outcomes**. *Pharmaceutics*, *14*(2778), 1–10. doi: https://doi.org/10.3390/pharmaceutics14122778

Eglitis, M. A., & Mezey, É. (1997). **Hematopoietic cells differentiate into both microglia and macroglia in the brains of adult mice**. *Proceedings of the National Academy of Sciences of the United States of America*, *94*(8), 4080–4085. doi: 10.1073/pnas.94.8.4080

Eichler, F. S., Li, J., Guo, Y., Caruso, P. A., Bjonnes, A. C., Pan, J., Booker, J. K., Lane, J. M., Tare, A., Vlasac, I., Hakonarson, H., Gusella, J. F., Zhang, J., Keating, B. J., & Saxena, R. (2016). **CSF1R mosaicism in a family with hereditary diffuse leukoencephalopathy with spheroids**. *Brain*, *139*(6), 1666–1672. doi: 10.1093/brain/aww066

Elitt, M. S., Barbar, L., & Tesar, P. J. (2018). **Drug screening for human genetic diseases using iPSC models**. *Human Molecular Genetics*, *27*(R2), 89–98. doi: 10.1093/hmg/ddy186

Flgel, A., Bradl, M., Kreutzberg, G. W., & Graeber, M. B. (2001). **Transformation of donor-derived bone marrow precursors into host microglia during autoimmune CNS inflammation and during the retrograde response to axotomy**. *Journal of Neuroscience Research*, *66*(1), 74–82. doi: 10.1002/jnr.1198

Frade, J. M., & Barde, Y. A. (1998). **Microglia-derived nerve growth factor causes cell death in the developing retina**. *Neuron*, *20*(1), 35–41. doi:

10.1016/S0896-6273(00)80432-8
Fu, Y., Sander, J. D., Reyon, D., Cascio, V. M., & Joung, J. K. (2014). *Improving CRISPR-Cas nuclease specificity using truncated guide RNAs*. *32*(3). doi: 10.1038/nbt.2808
Galanello, R., & Origa, R. (2010). **Beta-thalassemia**. *Orphanet Journal of Rare Diseases*, *5*(11), 1–15. doi: 10.1186/1750-1172-5-11
Gelfand, J. M., Greenfield, A. L., Barkovich, M., Mendelsohn, B. A., Haren, K. Van, Hess, C. P., & Mannis, G. N. (2019). **Allogeneic HSCT for adult-onset leukoencephalopathy with spheroids and pigmented glia Case descriptions**. *Brain*, 1–9. doi: 10.1093/brain/awz390
Ginhoux, F., Greter, M., Leboeuf, M., Nandi, S., See, P., Gokhan, S., Mehler, M. F., Conway, S. J., Ng, L. G., Stanley, E. R., Samokhvalov, I. M., & Merad, M. (2010). **Fate Mapping Analysis Reveals That Adult Microglia Derive from Primitive Macrophages**. *Science*, *701*(November), 841–845. doi: 10.1126/science.1194637
Ginhoux, F., Lim, S., Hoeffel, G., Low, D., & Huber, T. (2013). **Origin and differentiation of microglia**. *Frontiers in Cellular Neuroscience*, *7*(MAR), 1–14. doi: 10.3389/fncel.2013.00045
Gowing, G., Philips, T., Van Wijmeersch, B., Audet, J. N., Dewil, M., Van Den Bosch, L., Billiau, A. D., Robberecht, W., & Julien, J. P. (2008). **Ablation of proliferating microglia does not affect motor neuron degeneration in amyotrophic lateral sclerosis caused by mutant superoxide dismutase**. *Journal of Neuroscience*, *28*(41), 10234–10244. doi: 10.1523/JNEUROSCI.3494-08.2008
Graeber, M. B., & Streit, W. J. (2010). **Microglia: Biology and pathology**. *Acta Neuropathologica*, *119*(1), 89–105. doi: 10.1007/s00401-009-0622-0
Guerreiro, R., Kara, E., Le Ber, I., Bras, J., Rohrer, J. D., Taipa, R., Lashley, T., Hannequin, D., Sedel, F., Depienne, C., Golfier, V., Boisguéheneuc, F. Du, Fox, N. C., Beck, J., Mead, S., Martin, N., Hardy, J., Revesz, T., Brice, A., & Houlden, H. (2013). **Genetic Analysis of Inherited Leukodystrophies : Genotype-Phenotype Correlations in the CSF1R Gene**. *JAMA Neurology*, *70*(7), 875–882. doi: 10.1001/jamaneurol.2013.698.
Haeussler, M., Schönig, K., Eckert, H., Eschstruth, A., Mianné, J., Renaud, J., Schneider-maunoury, S., Shkumatava, A., Teboul, L., Kent, J., & Joly, J. (2016). **Evaluation of off-target and on-target scoring algorithms and integration into the guide RNA selection tool CRISPOR**. *Genome Biology*, 1–12. doi: 10.1186/s13059-016-1012-2
Hagan, N., Kane, J. L., Grover, D., Woodworth, L., Madore, C., Saleh, J., Sancho, J., Liu, J., Li, Y., Proto, J., Zelic, M., Mahan, A., Kothe, M., Scholte, A. A., Fitzgerald, M., Gisevius, B., Haghikia, A., Butovsky, O., & Ofengeim, D. (2020). **CSF1R signaling is a regulator of pathogenesis in progressive MS**. *Cell Death and Disease*, *11*(904). doi: 10.1038/s41419-020-03084-7
Hatton, C. F., & Duncan, C. J. A. (2019). **Microglia Are Essential to Protective Antiviral Immunity: Lessons From Mouse Models of Viral Encephalitis**. *Frontiers in Immunology*, *10*(November). doi: 10.3389/fimmu.2019.02656
Hayer, S. N., Schelling, Y., Höflinger, P., Hauser, S., & Schöls, L. (2018). **Generation of an induced pluripotent stem cell line from a patient with adult-onset leukoencephalopathy with axonal spheroids and**

pigmented glia (ALSP): HIHCNi003-A. *Stem Cell Research*, *30*(June), 206–209. doi: 10.1016/j.scr.2018.06.011

Hoffman, L. M., & Carpenter, M. K. (2005). **Characterization and culture of human embryonic stem cells**. *Nature Biotechnology*, *23*(6), 699–708. doi: 10.1038/nbt1102

Hsu, P. D., Scott, D. A., Weinstein, J. A., Ran, F. A., Konermann, S., Agarwala, V., Li, Y., Fine, E. J., Wu, X., Shalem, O., Cradick, T. J., Marraffini, L. A., Bao, G., & Zhang, F. (2013). **DNA targeting specificity of RNA-guided Cas9 nucleases**. *Nature Biotechnology*, *31*(9). doi: 10.1038/nbt.2647

Im, W., Moon, J., & Kim, M. (2016). **Applications of CRISPR/Cas9 for Gene Editing in Hereditary Movement Disorders**. *Journal of Movement Disorders*, *9*(3), 136–143. doi: 10.14802/jmd.16029

Inoue, K., & Tsuda, M. (2018). **Microglia in neuropathic pain: Cellular and molecular mechanisms and therapeutic potential**. *Nature Reviews Neuroscience*, *19*(3), 138–152. doi: 10.1038/nrn.2018.2

Ishino, Y., Shinagawa, H., Makino, K., Amemura, M., & Nakata, A. (1987). **Nucleotide Sequence of the iap Gene , Responsible for Alkaline Phosphatase Isozyme Conversion in Escherichia coli , and Identification of the Gene Product**. *Journal of Baceteriology*, *169*(12), 5429–5433.

Jansen, R., Van Embden, J. D. A., Gaastra, W., & Schouls, L. M. (2002). **Identification of genes that are associated with DNA repeats in prokaryotes**. *Molecular Microbiology*, *43*(6), 1565–1575. doi: 10.1046/j.1365-2958.2002.02839.x

Jensen, K. T., Fløe, L., Petersen, T. S., Huang, J., Xu, F., Bolund, L., Luo, Y., & Lin, L. (2017). *Chromatin accessibility and guide sequence secondary structure affect CRISPR-Cas9 gene editing efficiency*. *591*, 1892–1901. doi: 10.1002/1873-3468.12707

Jinek, M., Chylinski, K., Fonfara, I., Hauer, M., Jennifer, A., & Charpentier, E. (2012). **A programmable dual RNA-guided DNA endonuclease in adaptive bacterial immunity**. *Science*, *337*(6096), 816–821. doi: 10.1126/science.1225829

Karle, K. N., Biskup, S., Schüle, R., Schweitzer, K. J., Krüger, R., Bauer, P., Bender, B., Nägele, T., & Schöls, L. (2013). **De novo mutations in hereditary diffuse leukoencephalopathy with axonal spheroids (HDLS)**. *Neurology*.

Kaur, G., & Dufour, J. M. (2012). **Cell lines - Valuable tools or useless artifacts**. *Spermatogenesis*, *2*(1), 1–5.

Kempthorne, L., Yoon, H., Madore, C., Smith, S., Wszolek, Z. K., Rademakers, R., Kim, J., Butovsky, O., & Dickson, D. W. (2020). **Loss of homeostatic microglial phenotype in CSF1R- related Leukoencephalopathy**. *Acta Neuropathologica*, *8*(72), 1–15. doi: 10.1186/s40478-020-00947-0

Kim, D., Bae, S., Park, J., Kim, E., Kim, S., Yu, H. R., Hwang, J., Kim, J., & Kim, J. (2015). **Digenome-seq : genome-wide profiling of CRISPR-Cas9 off-target effects in human cells**. *Nat Methods*, *12*(3), 237–244. doi: 10.1038/nmeth.3284

Kim, S. I., Jeon, B., Bae, J., Won, J. K., Kim, H. J., Yim, J., Kim, Y. J., & Park, S. H. (2019). **An autopsy proven case of CSF1R-mutant adult-onset**

leukoencephalopathy with axonal spheroids and pigmented glia (ALSP) with premature ovarian failure. *Experimental Neurobiology*, *28*(1), 119–129. doi: 10.5607/en.2019.28.1.119

Kim, S., Kim, D., Cho, S. W., Kim, J., & Kim, J. (2014). *Highly efficient RNA-guided genome editing in human cells via delivery of purified Cas9 ribonucleoproteins*. 1012–1019. doi: 10.1101/gr.171322.113.Freely

Konno, T., Yoshida, K., Mizuno, T., Kawarai, T., Tada, M., Nozaki, H., Ikeda, S. I., Nishizawa, M., Onodera, O., Wszolek, Z. K., & Ikeuchi, T. (2017). **Clinical and genetic characterization of adult-onset leukoencephalopathy with axonal spheroids and pigmented glia associated with CSF1R mutation**. *European Journal of Neurology*, *24*(1), 37–45. doi: 10.1111/ene.13125

Konno, T., Yoshida, K., Mizuta, I., Mizuno, T., Kawarai, T., Tada, M., Nozaki, H., Ikeda, S. I., Onodera, O., Wszolek, Z. K., & Ikeuchi, T. (2018). **Diagnostic criteria for adult-onset leukoencephalopathy with axonal spheroids and pigmented glia due to CSF1R mutation**. *European Journal of Neurology*, *25*(1), 142–147. doi: 10.1111/ene.13464

Kumar, S., & Geiger, H. (2017). **HSC Niche Biology and HSC Expansion Ex Vivo**. *Trends in Molecular Medicine*, *23*(9), 799–819. doi: 10.1016/j.molmed.2017.07.003

Kumazaki, T., Kurata, S., Matsuo, T., Mitsui, Y., & Takahashi, T. (2011). **Establishment of human induced pluripotent stem cell lines from normal fibroblast TIG-1**. *Human Cell*, *24*, 96–103. doi: 10.1007/s13577-011-0016-1

Labuhn, M., Adams, F. F., Ng, M., Knoess, S., Schambach, A., Charpentier, E. M., Schwarzer, A., Mateo, J. L., Klusmann, J., & Heckl, D. (2018). *Refined sgRNA efficacy prediction improves large- and small-scale CRISPR – Cas9 applications*. *46*(3), 1375–1385. doi: 10.1093/nar/gkx1268

Labun, K., Montague, T. G., Krause, M., Cleuren, Y. N. T., Tjeldnes, H., & Valen, E. (2019). **CHOPCHOP v3 : expanding the CRISPR web toolbox beyond genome editing**. *Nucleic Acids Research*, *47*(May), 171–174. doi: 10.1093/nar/gkz365

Landry, J. J. M., Pyl, P. T., Rausch, T., Zichner, T., Tekkedil, M. M., Stütz, A. M., Jauch, A., Aiyar, R. S., Pau, G., Delhomme, N., Gagneur, J., Korbel, J. O., Huber, W., & Steinmetz, L. M. (2013). *The Genomic and Transcriptomic Landscape of a HeLa Cell Line*. *3*(August), 1213–1224. doi: 10.1534/g3.113.005777

Lawson, L. J., Perry, V. H., & Gordon, S. (1992). **Turnover of resident microglia in the normal adult mouse brain**. *Neuroscience*, *48*, 405–415. doi: 10.1002/glia.20535

Li, N. F., Kocher, H. M., Salako, M. A., Obermueller, E., Sandle, J., & Balkwill, F. (2009). **A novel function of colony-stimulating factor 1 receptor in hTERT immortalization of human epithelial cells**. *Oncogene*, *28*, 773–780. doi: 10.1038/onc.2008.412

Lieber, M. R. (2010). **The Mechanism of Double-Strand DNA Break Repair by the Nonhomologous DNA End Joining Pathway**. *Annual Review of Biochemistry*, *79*, 181–211. doi: 10.1146/annurev.biochem.052308.093131.The

Lieber, M. R., Ma, Y., Pannicke, U., & Schwarz, K. (2003). **Mechanism and**

regulation of human non-homologous DNA end-joining. *Nat Rev Moll Cell Biol*, *4*, 712–720. doi: 10.1038/nrm1202

Lino, C. A., Harper, J. C., Carney, J. P., Timlin, J. A., Lino, C. A., Harper, J. C., Carney, J. P., Timlin, J. A., Lino, C. A., Harper, J. C., Carney, J. P., & Timlin, J. A. (2018). **Delivering CRISPR : a review of the challenges and approaches**. *Drug Delivery*, *25*(1), 1234–1257. doi: 10.1080/10717544.2018.1474964

Liu, B., Wang, K., Gao, H. M., Mandavilli, B., Wang, J. Y., & Hong, J. S. (2001). **Molecular consequences of activated microglia in the brain: Overactivation induces apoptosis**. *Journal of Neurochemistry*, *77*(1), 182–189. doi: 10.1046/j.1471-4159.2001.t01-1-00216.x

Liu, X., Homma, A., Say, J., Yang, S., Ohashi, J., & Takumi, T. (2016). **Sequence features associated with the cleavage efficiency of CRISPR / Cas9 system**. *Nature Publishing Group*, 1–9. doi: 10.1038/srep19675

Loiseau, P., Busson, M., Balere, M., Dormoy, A., Bignon, J., Gagne, K., Gebuhrer, L., Jollet, I., Bois, M., Perrier, P., Masson, D., Reviron, D., Lepage, V., Tamouza, R., Toubert, A., Marry, E., Chir, Z., Jouet, J., Blaise, D., … Raffoux, C. (2007). **HLA Association with Hematopoietic Stem Cell Transplantation Outcome : The Number of Mismatches at HLA-A , -B , -C , -DRB1 , or -DQB1 Is Strongly Associated with Overall Survival**. *Biology of Blood and Marrow Transplantation*, *13*, 965–974. doi: 10.1016/j.bbmt.2007.04.010

Lozzio, C. B., & Lozzio, B. B. (1975). **Human Chronic Myelogenous Leukemia Cell-Line With Positive Philadelphia Chromosome**. *Blood Advances*, *45*(3), 321–334. doi: 10.1182/blood.V45.3.321.321

Lünemann, A., Ullrich, O., Diestel, A., Jöns, T., Ninnemann, O., Kovac, A., Pohl, E. E., Hass, R., Nitsch, R., & Hendrix, S. (2006). **Macrophage/microglia activation factor expression is restricted to lesion-associated microglial cells after brain trauma**. In *Glia* (Vol. 53, Issue 4, pp. 412–419). http://ovidsp.ovid.com/ovidweb.cgi?T=JS&PAGE=reference&D=emed7&NEWS=N&AN=2006096923

Luo, J., Elwood, F., Britschgi, M., Villeda, S., Zhang, H., Ding, Z., Zhu, L., Alabsi, H., Getachew, R., Narasimhan, R., Wabl, R., Fainberg, N., James, M. L., Wong, G., Relton, J., Gambhir, S. S., Pollard, J. W., & Wyss-Coray, T. (2013). **Colony-stimulating factor 1 receptor (CSF1R) signaling in injured neurons facilitates protection and survival**. *Journal of Experimental Medicine*, *210*(1), 157–172. doi: 10.1084/jem.20120412

Luther, D.C., P., Lee, Y.W., P., Nagaraj, H., Scaletti, F., & Rotello, V. M. (2018). **Delivery Approaches for CRISPR/Cas9 Therapeutics In Vivo: Advances and Challenges**. *Expert Opinion on Drug Delivery*, *15*(9), 905–913. doi: 10.1080/17425247.2018.1517746

Lynch, D. S., Jaunmuktane, Z., Sheerin, U. M., Phadke, R., Brandner, S., Milonas, I., Dean, A., Bajaj, N., McNicholas, N., Costello, D., Cronin, S., McGuigan, C., Rossor, M., Fox, N., Murphy, E., Chataway, J., & Houlden, H. (2016). **Hereditary leukoencephalopathy with axonal spheroids: A spectrum of phenotypes from CNS vasculitis to parkinsonism in an adult onset leukodystrophy series**. *Journal of Neurology, Neurosurgery and Psychiatry*, *87*(5), 512–519. doi: 10.1136/jnnp-2015-310788

Maeder, M. L., & Gersbach, C. A. (2016). **Genome-editing technologies for gene and cell therapy**. *Molecular Therapy*, *24*(3), 430–446. doi: 10.1038/mt.2016.10

Manno, C. S., Pierce, G. F., Arruda, V. R., Glader, B., Ragni, M., Rasko, J. J. E., Ozelo, M. C., Hoots, K., Blatt, P., Konkle, B., Dake, M., Kaye, R., Razavi, M., Zajko, A., Zehnder, J., Rustagi, P. K., Nakai, H., Sommer, M., Tigges, M., … Kay, M. A. (2006). **Successful transduction of liver in hemophilia by AAV-Factor IX and limitations imposed by the host immune response**. *Nature Medicine*, *12*(3), 342–348. doi: 10.1038/nm1358

Maqsood, M. I., Matin, M. M., Bahrami, A. R., & Ghasroldasht, M. M. (2013). **Immortality of cell lines : challenges and advantages of establishment**. *Cell Biology International*, *37*, 1038–1045. doi: 10.1002/cbin.10137

Mildner, A., Schmidt, H., Nitsche, M., Merkler, D., Hanisch, U. K., Mack, M., Heikenwalder, M., Brück, W., Priller, J., & Prinz, M. (2007). **Microglia in the adult brain arise from Ly-6ChiCCR2+ monocytes only under defined host conditions**. *Nature Neuroscience*, *10*(12), 1544–1553. doi: 10.1038/nn2015

Mochel, F., Delorme, C., Czernecki, V., Froger, J., Cormier, F., Ellie, E., Fegueux, N., Lehéricy, S., Lumbroso, S., Schiffmann, R., Aubourg, P., Roze, E., Labauge, P., & Nguyen, S. (2019). **Haematopoietic stem cell transplantation in CSF1R-related adult-onset leukoencephalopathy with axonal spheroids and pigmented glia**. *Journal of Neurology, Neurosurgery and Psychiatry*, 1–2. doi: 10.1136/jnnp-2019-320701

Mojica, F. J. M., Díez-Villaseñor, C., García-Martínez, J., & Soria, E. (2005). **Intervening sequences of regularly spaced prokaryotic repeats derive from foreign genetic elements**. *Journal of Molecular Evolution*, *60*(2), 174–182. doi: 10.1007/s00239-004-0046-3

Mojica, F. J. M., Ferrer, C., Juez, G., & Rodríguez-Valera, F. (1995). **Long stretches of short tandem repeats are present in the largest replicons of the Archaea Haloferax mediterranei and Haloferax volcanii and could be involved in replicon partitioning**. *Molecular Microbiology*, *17*(1), 85–93. doi: 10.1111/j.1365-2958.1995.mmi_17010085.x

Moreno-Mateos, M. A., Vejnar, C. E., Beaudoin, J., Juan, P., Mis, E. K., Khokha, M. K., Giraldez, A. J., Haven, N., Haven, N., & Haven, N. (2016). **CRISPRscan: designing highly efficient sgRNAs for CRISPR/Cas9 targeting in vivo**. *Nat Methods*, *12*(10), 982–988. doi: 10.1038/nmeth.3543.CRISPRscan

Nakade, S., Yamamoto, T., & Sakuma, T. (2017). **Cas9 , Cpf1 and C2c1 / 2 / 3 ¡ What ' s next ?** *Bioengineered*, *8*(3), 265–273. doi: https://doi.org/10.1080/21655979.2017.1282018 COMMENTARY

Naldini, L. (2015). **Gene therapy returns to centre stage**. *Nature*, *526*(7573), 351–360. doi: 10.1038/nature15818

Nayak, D., Roth, T. L., & McGavern, D. B. (2014). **Microglia Development and Function**. *Annual Review of Immunology*, *32*(1), 367–402. doi: 10.1146/annurev-immunol-032713-120240

Okita, K., Matsumura, Y., Sato, Y., Okada, A., Morizane, A., Okamoto, S., & Hong, H. (2011). **A more efficient method to generate integration-free human iPS cells**. *Nat Methods*, *8*, 409–412.

Ousterout, D. G., Perez-pinera, P., Thakore, P. I., Kabadi, A. M., Brown, M. T., Qin, X., Fedrigo, O., Mouly, V., Tremblay, J. P., & Gersbach, C. A. (2013). **Reading Frame Correction by Targeted Genome Editing Restores Dystrophin Expression in Cells From Duchenne Muscular Dystrophy Patients**. *Molecular Therapy*, *21*(9), 1718–1726. doi: 10.1038/mt.2013.111

Papapetropoulos, S., Pontius, A., Finger, E., & Karrenbauer, V. (2022). **Adult-Onset Leukoencephalopathy With Axonal Spheroids and Pigmented Glia : Review of Clinical Manifestations as Foundations for Therapeutic Development**. *Frontiers in Neurology*, *12*(February), 1–20. doi: 10.3389/fneur.2021.788168

Patil, K. R., Mahajan, U. B., Unger, B. S., Goyal, S. N., Belemkar, S., Surana, S. J., Ojha, S., & Patil, C. R. (2019). **Animal Models of Inflammation for Screening of Anti-inflammatory Drugs : Implications for the Discovery and Development of Phytopharmaceuticals**. *International Journal of Molecular Sciences*, *20*(18). doi: 10.3390/ijms20184367

Perrin, A., Dujon, B., & Nicolas, J.-F. (1995). **Induction of Homologous Recombination in Mammalian Chromosomes by Using the I- Sce I System of Saccharomyces cerevisiae**. *Molecular and Cellular Biology*, *15*(4), 1968–1973. doi: doi:10.1128/MCB.15.4.1968

Pridans, C., Sauter, K. A., Baer, K., Kissel, H., & Hume, D. A. (2013). **CSF1R mutations in hereditary diffuse leukoencephalopathy with spheroids are loss of function**. *Scientific Reports*, *3*, 1–5. doi: 10.1038/srep03013

Qomi, S. B., Asghari, A., & Mojarrad, M. (2019). **An Overview of the CRISPR-Based Genomic- and Epigenome- Editing System : Function , Applications , and Challenges**. *Advanced Biomedical Research*, *8*(49). doi: 10.4103/abr.abr

Rademakers, R., Baker, M., Nicholson, A. M., Rutherford, N. J., Finch, N., Soto-Ortolaza, A., Lash, J., Wider, C., Wojtas, A., Dejesus-Hernandez, M., Adamson, J., Kouri, N., Sundal, C., Shuster, E. A., Aasly, J., MacKenzie, J., Roeber, S., Kretzschmar, H. A., Boeve, B. F., … Wszolek, Z. K. (2012). **Mutations in the colony stimulating factor 1 receptor (CSF1R) gene cause hereditary diffuse leukoencephalopathy with spheroids**. *Nature Genetics*, *44*(2), 200–205. doi: 10.1038/ng.1027

Ramakrishna, S., Dad, A. K., Beloor, J., Gopalappa, R., Lee, S., & Kim, H. (2014). *Gene disruption by cell-penetrating peptide-mediated delivery of Cas9 protein and guide RNA*. 1020–1027. doi: 10.1101/gr.171264.113.Freely

Sahin, U., Toprak, S. K., Atilla, P. A., Atilla, E., & Demirer, T. (2016). **An overview of infectious complications after allogeneic hematopoietic stem cell transplantation**. *Journal of Infection and Chemotherapy*, *22*(8), 505–514. doi: 10.1016/j.jiac.2016.05.006

Sasaki, A. (2017). **Microglia and brain macrophages: An update**. *Neuropathology*, *37*(5), 452–464. doi: 10.1111/neup.12354

Schmitz, A. S., Korneck, M., Raju, J., Daniel-Moreno, A., Antony, J. S., Mezger, M., Schöls, L., Hauser, S., & Hayer, S. N. (2023). **Generation of a heterozygous and a homozygous CSF1R knockout line from iPSC using CRISPR / Cas9**. *Stem Cell Research*, *69*. doi: 10.1016/j.scr.2023.103066

Shi, X., Kaller, M., Rokavec, M., Kirchner, T., & Horst, D. (2020).

Characterization of a p53/miR-34a/CSF1R/STAT3 Feedback Loop in Colorectal Cancer. *Cellular and Molecular Gastroenterology and Hepatology*, *10*(2), 391–418. doi: 10.1016/j.jcmgh.2020.04.002

Shi, Y., Inoue, H., Wu, J. C., Yamanaka, S., Biology, S. C., & Francisco, S. (2017). **Induced pluripotent stem cell technology: a decade of progress**. *Nat Rev Drug Discov*, *16*(2), 115–130. doi: 10.1038/nrd.2016.245.Induced

Smith, C., Gore, A., Yan, W., Abalde-atristain, L., Li, Z., He, C., & Wang, Y. (2014). **Whole-Genome Sequencing Analysis Reveals High Specificity of CRISPR / Cas9 and TALEN-Based Genome Editing in Human iPSCs**. *Stem Cell*, *15*(1), 12–13. doi: 10.1016/j.stem.2014.06.011

Somera-Molina, K. C., Nair, S., Van Eldik, L. J., Watterson, D. M., & Wainwright, M. S. (2009). **Enhanced microglial activation and proinflammatory cytokine upregulation are linked to increased susceptibility to seizures and neurologic injury in a "two-hit" seizure model**. *Brain Research*, *1282*(51), 162–172. doi: 10.1016/j.brainres.2009.05.073

Spitzer, M., Wildenhain, J., Rappsilber, J., & Tyers, M. (2014). **E-CRISP : fast CRISPR target site identification**. *Nature Methods*, *11*(2), 122–123. doi: 10.1038/nmeth.2812

Stanley, E. R., & Chitu, V. (2014). **CSF-1 receptor signaling in myeloid cells**. *Cold Spring Harbor Perspectives in Biology*, *6*(6), 1–21. doi: 10.1101/cshperspect.a021857

Stefkova, K., Prochazkova, J., & Pachernik, J. (2015). *Alkaline Phosphatase in Stem Cells*. *2015: 6283*. doi: 10.1155/2015/628368

Sundal, C., Lash, J., Aasly, J., Øygarden, S., Roeber, S., Kretzschman, H., Garbern, J. Y., Tselis, A., Rademakers, R., Dickson, D. W., Broderick, D., & Wszolek, Z. K. (2012). **Hereditary diffuse leukoencephalopathy with axonal spheroids (HDLS): A misdiagnosed disease entity**. *Journal of the Neurological Sciences*, *314*(1–2), 130–137. doi: 10.1016/j.jns.2011.10.006

Takahashi, K., Tanabe, K., Ohnuki, M., Narita, M., Ichisaka, T., & Tomoda, K. (2007). **Induction of Pluripotent Stem Cells from Adult Human Fibroblasts by Defined Factors**. *Cell*, *131*, 861–872. doi: 10.1016/j.cell.2007.11.019

Takahashi, K., & Yamanaka, S. (2006). **Induction of Pluripotent Stem Cells from Mouse Embryonic and Adult Fibroblast Cultures by Defined Factors**. *Cell*, *126*, 663–676. doi: 10.1016/j.cell.2006.07.024

Teo, A. K. K., Arnold, S. J., Trotter, M. W. B., Brown, S., Ang, L. T., Chng, Z., Robertson, E. J., Dunn, N. R., & Vallier, L. (2011). **Pluripotency factors regulate definitive endoderm specification through eomesodermin**. *Genes & Development*, *25*(3), 238–250. doi: 10.1101/gad.607311.allocation

Terada, S., Ishizu, H., Yokota, O., Ishihara, T., Nakashima, H., Kugo, A., Tanaka, Y., Nakashima, T., Nakashima, Y., & Kuroda, S. (2004). **An autopsy case of hereditary diffuse leukoencephalopathy with spheroids, clinically suspected of Alzheimer's disease**. *Acta Neuropathologica*, *108*(6), 538–545. doi: 10.1007/s00401-004-0920-5

Thompson, A. A., Walters, M. C., Kwiatkowski, J., Rasko, J. E. J., Ribeil, J.-A., Hongeng, S., Magrin, E., Schiller, G. J., Payen, E., Semeraro, M., Moshous, D., Lefrere, F., Puy, H., Bourget, P., Magnani, A., Caccavelli, L., Diana, J.-S., Suarez, F., Monpoux, F., … Cavazzana, M. (2018). **Gene Therapy in**

Patients with Transfusion-Dependent ß-Thalassemia. *New England Journal of Medicine*, *378*(16), 1479–1493. doi: 10.1056/NEJMoa1705342

Tian, W. T., Zhan, F. X., Liu, Q., Luan, X. H., Zhang, C., Shang, L., Zhang, B. Y., Pan, S. J., Miao, F., Hu, J., Zhong, P., Liu, S. H., Zhu, Z. Y., Zhou, H. Y., Sun, S., Liu, X. L., Huang, X. J., Jiang, J. W., Ma, J. F., … Cao, L. (2019). **Clinicopathologic characterization and abnormal autophagy of CSF1R-related leukoencephalopathy**. *Translational Neurodegeneration*, *8*(1), 1–13. doi: 10.1186/s40035-019-0171-y

Tipton, P. W., Kenney-Jung, D., Rush, B. K., Middlebrooks, E. H., Nascene, D., Singh, B., Holtan, S., Ayala, E., Broderick, D. F., Lund, T., & Wszolek, Z. K. (2021). **Treatment of CSF1R-Related Leukoencephalopathy : Breaking New Ground**. *Movement Disorders*, *36*(12), 2901–2909. doi: 10.1002/mds.28734

Tristan, C., Shahani, N., Sedlak, T. W., & Sawa, A. (2011). **The diverse functions of GAPDH: views from different subcellular compartments**. *Cell Signal*, *23*(2), 317–323. doi: 10.1016/j.cellsig.2010.08.003.The

Tsai, S. Q., Zheng, Z., Nguyen, N. T., Liebers, M., Topkar, V. V., Thapar, V., Wyvekens, N., Khayter, C., Iafrate, A. J., Le, L. P., Aryee, M. J., & Joung, J. K. (2015). **GUIDE-seq enables genome-wide profiling of off-target cleavage by CRISPR-Cas nucleases**. *Nature Biotechnology*, *33*(2), 187–198. doi: 10.1038/nbt.3117

Tsuchiya, S., Yamabe, M., Yamaguchi, Y., Kobayashi, Y., Konno, T., & Tada, K. (1980). **Establishment and characterization of a human acute monocytic leukemia cell line (THP-1)**. *Int J CAncer*, *26*, 171–176. doi: 10.1002/ijc.2910260208

Tushinski, R. J., & Stanley, E. R. (1983). **The regulation of macrophage protein turnover by a colony stimulating factor (CSF-1)**. *Journal of Cellular Physiology*, *116*(1), 67–75. doi: 10.1002/jcp.1041160111

Uhl, E. W., & Warner, N. J. (2015). **Mouse Models as Predictors of Human Responses : Evolutionary Medicine**. *Current Pathobiology Reports*, *3*, 219–223. doi: 10.1007/s40139-015-0086-y

Uhlén, M., Fagerberg, L., Hallström, B., Lindskog, C., Oksvold, P., Mardinoglu, A., Sivertsson, Å., Kampf, C., Sjöstedt, E., Asplund, A., Olsson, I., Edlund, K., Lundberg, E., Navani, S., Szigyarto, C., Odeberg, J., Djureinovic, D., Takanen, J., Hober, S., … F., P. (2015). **Proteomics. Tissue-based map of the human proteome**. *Science*, *347*(6220).

Valadez-Barba, V., Cota-Coronado, A., Hernández-Pérez, O. R., Lugo-Fabres, P. H., Padilla-Camberos, E., Díaz, N. F., & Díaz-Martínez, N. E. (2020). **iPSC for modeling neurodegenerative disorders**. *Regenerative Therapy*, *15*, 332–339. doi: 10.1016/j.reth.2020.11.006

Veres, A., Gosis, B. S., Ding, Q., Collins, R., Ragavendran, A., Brand, H., & Erdin, S. (2014). **Low Incidence of Off-Target Mutations in Individual CRISPR-Cas9 and TALEN Targeted Human Stem Cell Clones Detected by Whole-Genome Sequencing**. *Cell Stem Cell*, *15*, 27–30. doi: 10.1016/j.stem.2014.04.020

Volarevic, V., Markovic, B. S., Gazdic, M., Volarevic, A., & Jovicic, N. (2018). *Ethical and Safety Issues of Stem Cell-Based Therapy*. *15*. doi: 10.7150/ijms.21666

Wai-Mun Lee, A. (1992). **Signal Transduction by the Colony-Stimulating Factor-1 Receptor ; Comparison to Other Receptor Tyrosine Kinases**. In *Current Topics in Cellular Regulation* (Vol. 32). ACADEMIC PRESS, INC. doi: 10.1016/B978-0-12-152832-4.50005-7

Weiss, A. J. (2012). **Overview of Membranes and Membrane Plates Used in Research and Diagnostic ELISPOT Assays**. In A. E. Kalyuzhny (Ed.), *Handbook of ELISPOT: Methods and Protocols, Methods in Molecular Biology, vol. 792* (Second Edi, pp. 243–256). doi: 10.1007/978-1-61779-325-7_19

Wilhelmsen, K., & Geer, P. Van Der. (2004). *Phorbol 12-Myristate 13-Acetate-Induced Release of the Colony-Stimulating Factor 1 Receptor Cytoplasmic Domain into the Cytosol Involves Two Separate Cleavage Events*. *24*(1), 454–464. doi: 10.1128/MCB.24.1.454

Yu, J., Hu, K., Smuga-Otto, K., Tian, S., Stewart, R., Igor, I., & Thomson, J. A. (2009). *Human Induced Pluripotent Stem Cells Free of Vector and Transgene Sequences*. *324*(5928), 797–801. doi: 10.1126/science.1172482.Human

Yu, W., Chen, J., Xiong, Y., Pixley, F. J., Yeung, Y. G., & Stanley, E. R. (2012). **Macrophage proliferation is regulated through CSF-1 receptor tyrosines 544, 559, and 807**. *Journal of Biological Chemistry*, *287*(17), 13694–13704. doi: 10.1074/jbc.M112.355610

Zhang, J., Adikaram, P., Pandey, M., Genis, A., & Simonds, F. (2016). **Optimization of genome editing through CRISPR- Cas9 engineering**. *Bioengineered*, *7*(3), 166–174. doi: 10.1080/21655979.2016.1189039

Zhang, J., Pandey, M., Kahler, J. F., Loshakov, A., Harris, B., Dagur, P. K., Mo, Y., & Simonds, W. F. (2014). **Improving the specificity and efficacy of CRISPR / CAS9 and gRNA through target specific DNA reporter**. *Journal of Biotechnology*, *189*, 1–8. doi: 10.1016/j.jbiotec.2014.08.033

Zhang, X. H., Tee, L. Y., Wang, X. G., Huang, Q. S., & Yang, S. H. (2015). **Off-target effects in CRISPR/Cas9-mediated genome engineering**. *Molecular Therapy - Nucleic Acids*, *4*(11), e264. doi: 10.1038/mtna.2015.37

Zhou, Y., Zeng, J., Tu, Y., Li, L., Du, S., Zhu, L., Cang, X., Lu, J., Zhu, M., & Liu, X. (2021). **CSF1/CSF1R-mediated Crosstalk Between Choroidal Vascular Endothelial Cells and Macrophages Promotes Choroidal Neovascularization**. *Investigative Ophthalmology and Visual Science*, *62*(3), 1–10.

Figures 1 and 5 of this dissertation were created with BioRender.com

7 Statement of originality

This doctoral thesis was conducted in the Hertie-Institut für Klinische Hirnforschung and Deutsches Zentrum für Neurodegenerative Erkrankungen under the supervision of Prof. Dr. Ludger Schöls.

The study was designed in association with Dr. Stefanie Hayer. All experiments and statistical analyses, except those listed below, were conducted by myself after initial training by Dr. Stefanie Hayer and the research group of the Schöls Lab.

Whole genome single nucleotide polymorphism genotyping was performed by Life & Brain GENOMICS.

I confirm that I have written the dissertation autonomously and have not used any sources other than those indicated.

8 Publications

Parts of this study have been published beforehand in the following paper:

Generation of a heterozygous and a homozygous CSF1R knockout line from iPSC using CRISPR/Cas9 (Schmitz et al., 2023).

This publication is based in parts on the results presented in chapter 3.2 of this dissertation. My contribution to the publication consisted of the execution, analysis and evaluation of the experiments described in this thesis (see chapters 2.2.2, 3.2, 4.2) as well as the composition of the manuscript draft and figures.

Acknowledgements

I would like to thank Prof. Dr. Ludger Schöls for the opportunity to work on this project as well as for his support and feedback throughout.

Special thanks go to Dr. Stefanie Hayer for her guidance and encouragement in every step of the project. Thank you for your constant presence despite the work-load in research and the hospital.

I am very grateful to my research group as well as the other colleagues at the DZNE, Hertie Institute and the Children's Hospital for the helpful advice and tips as well as for making me feel welcome and part of their great teams. I'd like to especially thank Dr. Dr. Markus Mezger and Dr. Stefan Hauser for the helpful discussions and feedback on this project, Milena Korneck for the introduction to iPSC culture and for always being willing to lend a helping hand, Andrés Lamsfus-Calle for the introduction to electroporation, Melanie Kraft for all her practical tips, and Janani Raju for the great collaboration on our projects.

Finally, I would like to thank my parents for their support and all the opportunities they have afforded me. Thank you to my mother and sister for proofreading this dissertation.